MEASUREMENT OF THE LAMB SHIFT IN MUONIUM

by

CHARLES ALAN FRY

A THESIS SUBMITTED IN PARTIAL FULFILMENT OF

THE REQUIREMENTS FOR THE DEGREE OF

DOCTOR OF PHILOSOPHY

in

THE FACULTY OF GRADUATE STUDIES

Department of Physics

We accept this thesis as conforming

to the required standard

THE UNIVERSITY OF BRITISH COLUMBIA

August, 1985

© Charles Alan Fry, 1985

22

In presenting this thesis in partial fulfilment of the requirements for an advanced degree at the University of British Columbia, I agree that the Library shall make it freely available for reference and study. I further agree that permission for extensive copying of this thesis for scholarly purposes may be granted by the head of my department or by his or her representatives. It is understood that copying or publication of this thesis for financial gain shall not be allowed without my written permission.

Department of Physics

The University of British Columbia
1956 Main Mall
Vancouver, Canada
V6T 1Y3

Date August 27, 1985

Abstract

This thesis describes the first measurement of the Lamb shift in n=2 muonium. The muonium atom is a hydrogen-like bound state of two leptons (μ^+e^-), both of which are believed to be point-like particles. The point-like nature of the constituent particles simplifies and reduces the uncertainty of the application of quantum electrodynamics (QED) to the calculation of the Lamb shift in the muonium atom. Measurements of the Lamb shift in hydrogen disagree with the predictions of theory by a few standard deviations; however, theoretical predictions also disagree with each other, partly because of difficulties associated with the treatment of the proton structure. Thus a measurement in the muonium system of similar precision to those already made in the hydrogen system will be a valuable test of QED. The present experiment is not intended to test QED. It is an investigation of the methods and techniques necessary to surmount the difficulties presented by the nature of muonium. The available number of muonium atoms is about 10^{+10} times less than that of hydrogen used by Lamb in his first measurement. The value obtained for the n=2 muonium Lamb shift 1070^{+12}_{-15} MHz. The uncertainty quoted is statistical at the 68% confidence level. Systematic effects were found to contribute a further 2 MHz uncertainty.

ADVISOR

Table of Contents

1. Introduction 1

1.1 The Muonium Atom 1

1.2 Historical Perspective 3

1.2.1 Lamb's Experiments 6

1.2.2 The Race between Theory and Experiment 8

1.3 Present Status of the Lamb Shift Calculation and Experiment 9

1.4 Outline of the Thesis 12

2. The Muonium Energy Levels 15

2.1 Symmetry 15

2.2 The Eigenstates of F, m_F, J, and L 16

2.3 Separation of the Center of Mass Motion 17

2.4 Non-radiative Corrections 19

2.4.1 Corrections to the Fine structure 19

2.4.2 Corrections to the Hyperfine structure 21

2.4.3 Recoil Corrections 22

2.5 Radiative Corrections 25

2.5.1 Self-energy 25

2.5.2 Magnetic Moment 28

2.5.3 Vacuum Polarization 28

2.5.4 Higher Order Binding Corrections 29

2.6 Summary of the Lamb Shift Calculations 32

3. The Formation of 2s Muonium 35

3.1 General Considerations 35

3.2 Methods of Forming Muonium 35

3.3 The Beam Foil Interaction 37

3.4 Slowing Muons 40

3.5 The Statistical Properties of a Degrader 50

3.5.1 Momentum Straggling 50

3.5.2 Multiple Scattering 51

3.6 Monte Carlo Simulation of Moderation of the Muon Beam 52

3.7 Summary 58

4. Radio-frequency Excitation of the Lamb shift Transition 59

4.1 The Time Dependent Schrödinger Equation 59

4.2 Approximate Solution 61

4.2.1 DC Stark effect 64

4.2.2 AC Stark Shift 64

4.2.3 Effect of the $2p_{3/2}$ state 65

5. Description of the Apparatus and Experimental Procedure 66

5.1 Vacuum System 66

5.2 Scintillation Counters 66

5.3 Neutral Production Foil 68

5.4 RF Region 70

5.5 The Quench Region and Microchannel Plates 73

5.6 Data Acquisition and Event Trigger 76

5.7 Beam Parameters and Experimental Rates 78

6. Data Reduction and Analysis 82

6.1 Timing 82

6.2 Normalization 92

6.3 Form of the Resonance Curve 92

6.4 The Fitting Procedure 95

6.5 Systematic Uncertainties in the Lamb Shift Measurement 96

6.5.1 RF Power Uncertainty 96

6.5.2 Non-linearity of the RF Power Level 103

6.5.3 Alignment of the RF Region and the Beam ..103

6.5.4 Velocity Distribution 104

6.5.5 Normalization Uncertainty 104

6.6 Other Effects 105

6.6.1 Transverse Doppler Shift (Time Dilation) .105

6.6.2 RF Stark shift 105

6.6.3 Magnetic Fields 106

6.7 Summary of Uncertainties and Systematic Effects 106

7. Conclusion 108

7.1 Comparison with the Other Lamb Shift Measurement 108

7.2 Limitations of the Present Technique 110

7.3 New Methods for a Muonium Lamb Shift Measurement 112

7.4 Possible Measurement of the n=2 Lamb Shift in Pionium 115

7.5 Summary of Results 116

REFERENCES 118

APPENDIX A: THE MAXIMUM LIKELIHOOD TECHNIQUE FOR A POISSON PROCESS 123

List of Figures

page

Figure 1.1: Schematic of the Muonium Energy Levels. 2

Figure 1.2: Schematic of the apparatus used in Lamb's first experiments. 7

Figure 1.3: The Layout of the Experimental Areas at TRIUMF. 13

Figure 2.1: Some Feynman diagrams which contribute to the Lamb shift. 26

Figure 3.1: The neutral fraction and relative population in various states for a beam of positively charged particles emerging from a foil as a function of velocity. 38

Figure 3.2: dp/dx for aluminum as calculated using equation 3.5. 43

Figure 3.3: Muon velocity as a function of path length in an aluminum degrader. 45

Figure 3.4: Proton velocity as a function of path length in an aluminum degrader. 46

Figure 3.5: Number of particles available from the M13 beam line at TRIUMF as a function of momentum per μA of primary proton current at 500 MeV. 48

Figure 3.6: Monte Carlo results for the fraction of a muon beam stopping in an aluminum degrader and the neutral fraction as a function of incident momentum. 54

Figure 3.7: Monte Carlo results for the fraction of the beam emerging from the degrader with momentum less than 2 MeV/c as a function of the incident muon momentum. ...55

Figure 3.8: Comparison of the Monte Carlo results with experiment for the number of particles emerging from the foil with momentum less than 2 MeV/c as a function of incident momentum. 57

Figure 5.1: A schematic diagram of the apparatus. 67

Figure 5.2: The RF transmission line arrangement. 71

Figure 5.3: The RF system. 72

Figure 5.4: The electric field in the quench region. View is from the side at the vertical midplane. 74

Figure 5.5: Efficiency of channel electron multipliers as a function of wave length. 75

Figure 5.6: Typical circuit used to run a micro-channel plate. Specific values of the resistances and capacitances depend on the size and kind of micro-channel plates. 77

Figure 5.7: Simplified diagram of the electronic logic for data acquisition. 79

Figure 5.8: The M13 beam line at TRIUMF. 80

Figure 6.1: A typical time-of-flight histogram for particles travelling between the incident scintillator and MCP B. 84

Figure 6.2: Events as a function of time-of-flight and time of detection of a Lyman-α photon. See text for meanings of a, b, c. 85

Figure 6.3: The timing cuts on the events of Figure 6.2 (see text). 86

Figure 6.4: Events as a function of $1/\beta$ and time in the quench region (i.e. time of detection of the Lyman-α photon less the time of entry into the quench region). 88

Figure 6.5: 2s muonium detected as a function of velocity. The effect of timing criteria for entry into the quench region is illustrated. 89

Figure 6.6: 2s muonium detected as a function of time from entry into the quench region to emit a Lyman-α photon. The effect of velocity requirements is illustrated. ..90

Figure 6.7: The data points and best fit resonance curve as a function of applied RF power and frequency. 97

Figure 6.8: The best fit resonance curve shown for the three power levels at which data was acquired. The open circles are an independent test of the normalization (see text). 98

Figure 6.9: χ^2 contours for variation of the Lamb shift S and the signal intensity, a. 100

Figure 6.10: χ^2 contours for variation of the signal intensity, a and background intensity, b. 101

Figure 7.1: The data obtained by Baderstacher *et al.* for the Lamb shift transition and a schematic of the apparatus used. 109

List of Tables

page

Table 2.1: Various contributions to the Lamb shift in hydrogen and muonium. 33

Table 2.2: Lamb shift calculation results from Table 2.1..34

Table 5.1: Summary of materials present in the path of the muon beam. 69

Table 6.1: The observed numbers of counts and normalized signals used to determine the Lamb shift. 91

Table 6.2: The results of various fits to the resonance data, in which different parameters have been allowed to vary. Line III is the the quoted result for the Lamb shift. 100

Table 6.3: Summary of the various contributions to the systematic uncertainty of the Lamb shift. 103

Acknowledgements

This experiment and thesis could not have been successful without the assistance of a great many people. I wish to thank my collaborators who helped provide the manpower necessary to run the experiments over the many weeks of data-taking. I owe many thanks to Rob Kiefl for his careful attention to detail in the final design of the apparatus. The encouragement and assistance of John Warren, from the very inception of the experimental program to measure the Lamb shift, was in large part reponsible for the success of the experiment. I also learned, received much encouragement, and gained insight from conversations with John Bailey, Gord Giles, Glen Marshall, and Art Olin for which I am very grateful. Tim Miles deserves thanks for his assistance, above and beyond the call of duty, with the data acquisition system. I very much appreciate the many corrections and suggestions of Jess Brewer incorporated in the final draft of the thesis, as well as his generosity, enthusiasm, and effort over the past few years as one of the co-supervisors of my work. Finally, I wish to express my most heartfelt thanks to Chris Oram, with whom I worked most closely over the course of the experimental program, for his guidance, assistance, and friendship.

1. INTRODUCTION

1.1 THE MUONIUM ATOM

The muonium atom is a bound system of two particles. It is very much like the hydrogen atom in which the proton, being some 1836 times more massive than the electron, acts as an almost stationary nucleus around which the electron orbits. In the case of muonium the nucleus is a positive muon of approximately 207 times the mass of the orbital electron. Since the charge of the μ^+ is identical to that of the proton, the atom is electrostatically almost identical to the hydrogen atom. Most of the differences can be explained as arising from differences in the reduced mass between hydrogen and muonium and relative magnitudes of the magnetic moments, approximately a factor of three. Figure 1.1 shows the energy level diagram for the ground and first excited state (n=2) of muonium. The energy difference between the average energy of the $2s_{1/2}$ and the average energy of the $2p_{1/2}$ states is called the Lamb shift. The value of the Lamb shift is denoted by S, following Lamb's notation.

The muon is a point-like particle, unlike the proton, which is known to be spread out over a radius of about 1 fm; this simplifies the mathematical treatment of muonium and circumvents the unknowns of proton structure. On the other hand, because the muon is 1836/207 times less massive than the proton, more attention must be paid to the calculation of effects of the motion of the muon (nucleus) in a

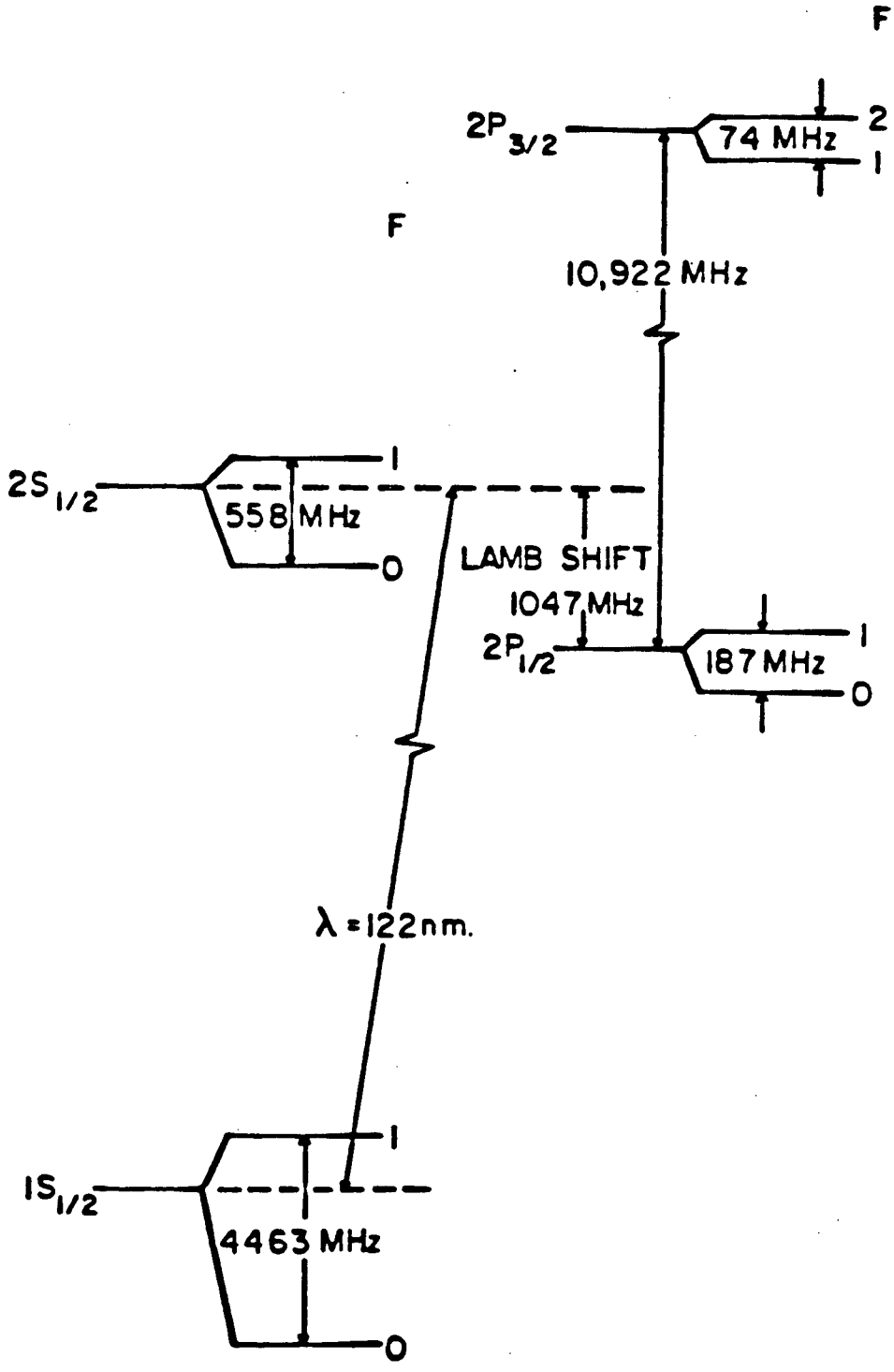

Figure 1.1: Schematic of the Muonium Energy Levels

description of the muonium atom.

1.2 HISTORICAL PERSPECTIVE

In the latter part of the nineteenth century, spectroscopy of hydrogen atoms, both solar and in the laboratory, had revealed the Balmer series. The first successful explanation of the observations was that of Bohr (Bohr, 1913, 1914). He proposed that an electron orbiting in a Coulomb field did not radiate if the product of its momentum and the length of the orbit equaled an integral number times Planck's constant, h. The orbits satisfying Bohr's criteria should have energies and radii

$$E_n^{Bohr} = -\frac{(Z\alpha)^2}{2n^2} mc^2 \; ; \; a_n = \frac{n^2}{Z} a_0 \qquad \ldots(1.1)$$

relative to the energy of a free electron at rest, where α = 1/137.03604(11) and m = .5110034(14) MeV/c^2 are the accepted values of the fine structure constant and electron mass today (Particle Data Group, 1984). The number n takes on all integer values greater than zero, labelling the infinitely many Bohr orbits. Taking the free electron at rest as the zero of energy, the absolute value of the Bohr energy for n=1 is known as the infinite mass Rydberg or R_0, where the subscript zero indicates that the free electron mass, m, is used rather than the reduced mass[1]. The first Bohr radius (n=1) using the infinite mass Rydberg is denoted by a_0. It

[1] $R_0 = e^2/2a_0hc = \alpha/4\pi a_0$ =13.6058 eV or $3.28985 \cdot 10^9$ MHz

is large compared to the proton size, being of the order of 50000 fm. The Bohr energy differences were in agreement with the observed wavelengths of the Balmer series to within a few parts in 10,000.

Schrödinger (Schrödinger, 1926) next placed the Bohr energy relation (1.1) on a firmer basis, deriving it from the solution of a differential equation for the motion of the electron in a Coulomb field. This naturally led to the assumptions that Bohr had made to "quantize" the energy levels of the atom. Schrödinger's solution also naturally included the three dimensional nature of the real problem and showed that for each value of the principal quantum number n, there should be n states, differing in orbital angular momentum $l\hbar$, where the "orbital" quantum number l ranges through integers 0,1,2,...(n-1). The energies of the n states associated with each value of n still exhibited no dependence on l although it was expected that a relativistic treatment of the problem should break the n-fold degeneracy. It was also known by this time that the electron possessed "spin" and had a magnetic moment associated with the spin. Attempts to find a relativistic equation failed until Dirac (Dirac, 1927) proposed the famous "Dirac equation" which explained the presence of the spin of the electron and successfully predicted the previously observed "splittings" or "fine structure" of the Balmer series as consequences of the electron spin magnetic moment and of relativistic effects. The electron spin angular momentum $s\hbar = \hbar/2$ should

combine with the orbital angular momentum to give a single total angular momentum $j\hbar$ where the allowed values of j are given by $|l \pm s|$. One of the most dramatic predictions of the Dirac theory was that the spin magnetic moment has exactly twice the value it would have if the charge and mass of the electron were distributed identically in a classical model. This means that angular motion associated with the electron spin is orbital in nature and therefore behaves magnetically like orbital angular momentum with $l=1$ of the electron as a whole so that the energy of a state with $j=1/2$ should be identical for the two cases: $j=l+s=0+1/2$ for the $2s_{1/2}$ state and $j=l-s=1-1/2$ for the $2p_{1/2}$ state.

By the early 1930's atomic spectroscopy was able to measure the fine structure of hydrogen with enough resolution to observe that the intervals were slightly less than those predicted by the Dirac equation. Pasternack (Pasternack,1938) proposed that the observations could be explained if the binding energy of the $2s_{1/2}$ state were reduced by about 10% of the fine structure interval relative to the $2p_{1/2}$ state. Only in the $2s_{1/2}$ state do the electronic and nuclear wavefunctions have significant overlap; therefore the proposed reduction could occur if the Coulomb potential were modified [reduced] at short distances. Ühling (Ühling, 1935) had already proposed the polarization of the Dirac vacuum around a charge, but the effect was of the wrong sign and of too small a magnitude to explain the required shift. In 1947 Lamb (Lamb, 1947)

explain the required shift. In 1947 Lamb (Lamb, 1947) reported his observation of an energy difference of "about 1000 MHz" using a microwave technique. On the way home from the same meeting, Bethe (Bethe, 1947) made the first successful calculation of the $2s_{1/2}$ - $2p_{1/2}$ energy difference, obtaining a shift of the $2s_{1/2}$ state of about 1040 MHz due to the interaction of the electron with the vacuum field.

1.2.1 LAMB'S EXPERIMENTS

Briefly, the principle of the Lamb experiments was as follows (see Figure 1.2). Hydrogen was prepared in an oven. The hot atoms were allowed to escape in a stream from the oven through a small hole. Travelling with thermal velocities on the order of 10^4 m/s they were bombarded with a beam of electrons which was adjusted so as to maximize the probability of exciting atoms from the ground state to the first excited state (n=2). This would populate the 2s-states as well as the 2p-states. The p-states however were not stable as they could rapidly (τ about 1.6 ns) return to the ground state by emission of a Lyman-α photon (122 nm) via an electric dipole transition. The 2s states, on the other hand, were metastable, the dominant de-excitation process being the emission of two photons (τ about 1/7 of a second). The stream of atoms passed through a microwave interaction region and finally struck a detector which registered the

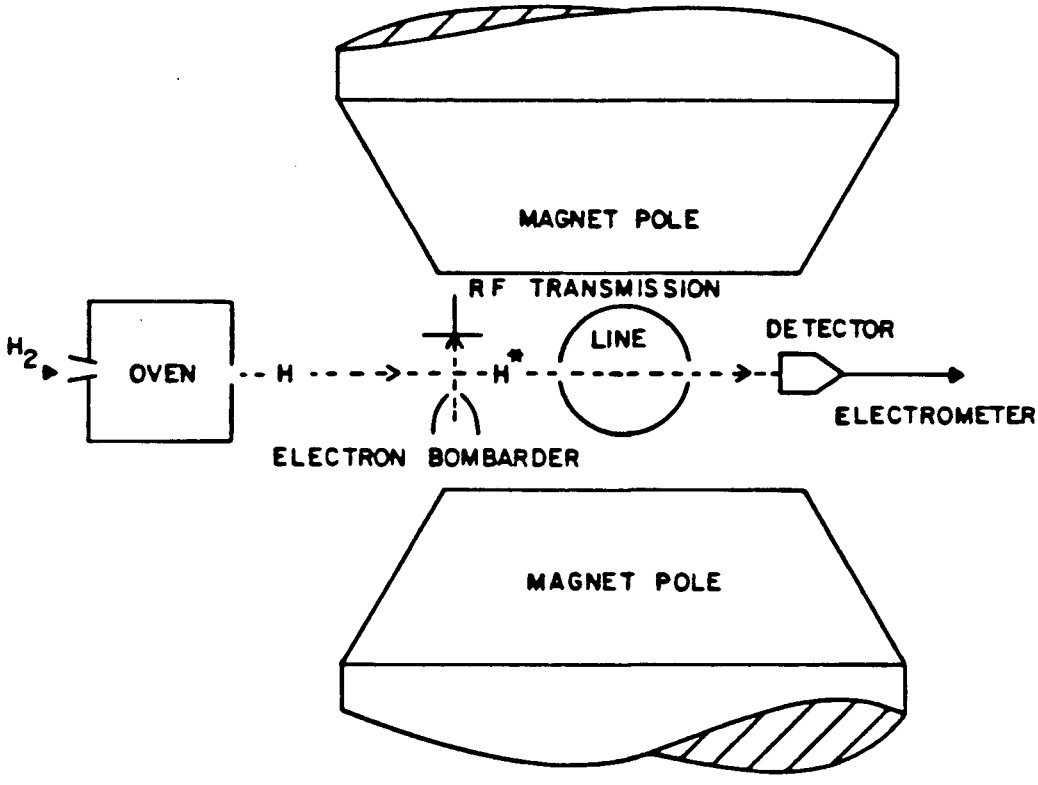

Figure 1.2: Schematic of the apparatus used in Lamb's first experiments.

current of atoms in excited states[1], consisting mainly of atoms in the 2s state. If the microwaves were of the correct frequency to excite transitions between the $2s_{1/2}$ and $2p_{1/2}$ levels, and were of sufficient power density, the metastable 2s atoms would be transferred to the short-lived 2p-levels and de-excite before striking the detector. The current registered by the detector would be reduced.

At that time, generating microwaves of the frequency required (approximately 1000 MHz) was not difficult but it was difficult to generate a variable frequency while maintaining a constant level of power required for the experiment. Lamb and his co-workers solved the problem by placing the microwave region in a magnetic field which could be varied so as to sweep the $2s_{1/2}$-$2p_{1/2}$ energy difference through the applied microwave frequency, thus observing a reduction in the n=2 signal as a function of magnetic field. By performing measurements of several resonances at several frequencies it was possible to extrapolate, using the Breit-Rabi relation, to the energy difference for zero-field.

1.2.2 THE RACE BETWEEN THEORY AND EXPERIMENT

Attempts to employ Bethe's method (Bethe, 1947) to calculate the anomalous electron magnetic moment failed (Welton, 1949; Koba, 1949), even yielding the wrong sign for

[1]The detector was a copper plate. The work function for the emission of electrons from the surface was such that only atoms in excited states could cause them to be ejected, and hence a current in an electrometer connected to the plate.

g-2. Kroll and others (Kroll, 1949) were refining Bethe's preliminary calculation when Lamb reported his next determination of the Lamb shift S = 1062±5 MHz at the meeting of the American Physical Society in 1949 (Lamb, 1949) and subsequently in a series of papers[1]. Lamb's value was significantly higher than the theoretical value at that time, which was about 1052 MHz. This prompted further thought on the part of theoreticians to find and calculate effects to bring their values back into line with experiment. Karplus, Klein and Schwinger (Karplus, 1951a,b) as well as Baranger, Bethe, and Feynman (Baranger, 1953) obtained a correction of about 7 MHz which brought the theoretical value back into line with experiment (In 1952 Lamb reported S = 1057.77±0.10 MHz [3 s.d.]) and to within a fraction of a megahertz of where it lies today.

1.3 PRESENT STATUS OF THE LAMB SHIFT CALCULATION AND EXPERIMENT

Quantum electrodynamics has been with us for more than 30 years now. Although cumbersome, QED has been an eminently successful theory. Since the first successful Lamb shift calculation by Hans Bethe in 1949, QED has been formulated in renormalizable form by Feynman, Schwinger, and many others. The principal statements of the theory have been clear but the actual calculations were fraught with numerous

[1](Lamb, 1950, 1951, 1952)
(Triebwasser, 1953)
(Dayhoff, 1953)

errors because of the sheer complexity of the method of calculation. The current formulation of QED does not lend itself well to calculation in closed form but demands an approach of successive approximation and expansion.

The greatest success of the theory is unquestionably the prediction of the electron and muon g-factors to 8 digit precision in agreement with experiment. The g-factor predictions are the result of calculations of the self-energy processes for a point-like fermion in vacuum. The same terms amount to only 7% of the Lamb shift in hydrogen, where other self-energy contributions dominate. The vacuum polarization or "photon structure" as calculated from QED is also small, reducing the Lamb shift by about 3 % in hydrogen and muonium[1].

In the usual treatment of the Lamb shift one uses QED perturbatively, begining with a free electron plane wave. A Coulomb wave-function is not ever a plane wave, not even asymptotically. The idea of approximating the interaction of an electron bound in a Coulomb field as that of a free electron before and after interaction is intuitively unappealing, but necessary from the point of view of computation. The bound state solutions of the Coulomb problem must be added from outside the QED formalism to calculate the radiative corrections. The Lamb shift, because it is inherently a bound-state problem, is a testing ground

---

[1] Vacuum polarization in muonic atoms is the dominant effect, where it is of sufficient magnitude to reverse the sign of the Lamb shift.

for QED, upon which the development of new and more powerful methods may be forced to occur.

Current calculations of the Lamb shift in hydrogen are still the subject of some controversy. Although few would dispute the success of QED in predicting the effect, the difficulties involved in the calculation of higher order QED effects are enormous. For example, the calculation of the sixth order correction to the electronic g-factor required several months of computer time (Borie,1980). The current problems in the hydrogen Lamb shift calculation are discussed in greater detail in Chapter 2. Briefly, there are at present two calculations which disagree slightly, but by much more than their uncertainties, in the estimation of the higher order self energy QED corrections for the electron (Mohr, 1975; Erickson, 1977). Neither value agrees with the current experimental value, both predicting S greater than that of experiment by a few standard deviations. Edith Borie (Borie, 1981) has proposed a correction that includes the effects of the finite size of the proton at the level of the QED calculations instead of as an additive correction separate from QED which lessens the disagreement of theory and experiment, but as yet this correction is not widely accepted by the physics community (Lepage, 1981)

An experimental measurement of the Lamb shift in muonium of sufficient accuracy would differentiate between the calculations by Mohr and Erickson without the complicating factor of the structure of the proton. It would

also give a better understanding of the reduced mass effects which are too small to be tested by hydrogen measurements and as yet are untested in the positronium system.

1.4 OUTLINE OF THE THESIS

The experiment described in this thesis is the latest in a series of experiments which began in late 1980 at the TRIUMF cyclotron, situated south of the University of British Columbia campus. The layout of the experimental areas of TRIUMF is shown in Figure 1.2. The experiments were performed using the M13 secondary channel.

The first of these experiments confirmed the production of neutral muonium in the beam-foil interaction (Oram, 1981a). The result was subsequently confirmed by others at the Los Alamos Meson Facility (Bolton, 1981). The next step in the experimental program was to attempt to learn more about tuning the M13 secondary channel for 'sub-surface' muons and to produce epithermal muonium in excited states. Detection of Lyman-alpha photons from the Stark quenching of the n=2 state of muonium was consistent with a Lamb shift of about 1000 MHz (Oram, 1981c). The design and construction of the apparatus to measure the Lamb shift to an accuracy of a few percent was aided by the knowledge gained from this preliminary work.

The apparatus described in Chapter 3 was tested in a Stark configuration in the fall of 1982; i.e, the RF region was replaced by a region of electric field. This experiment

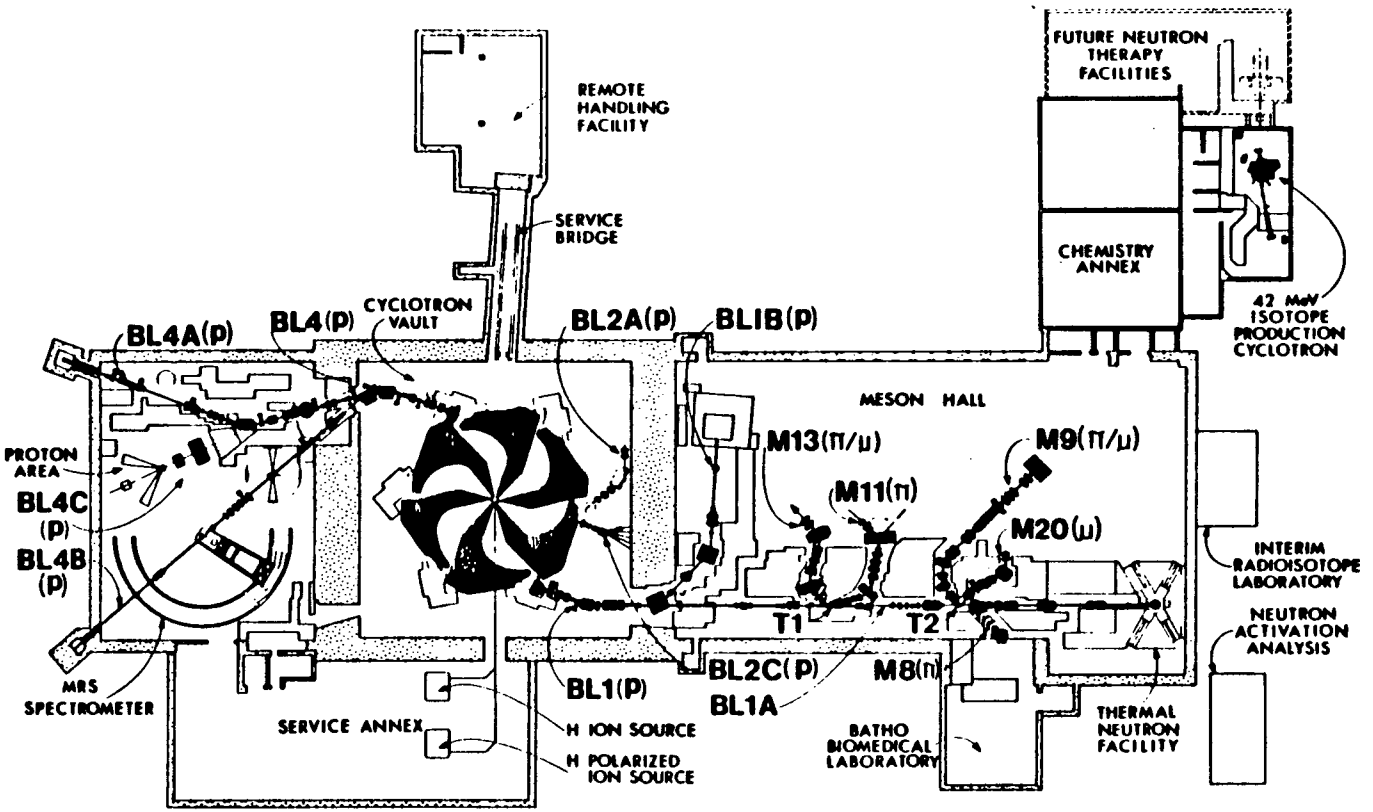

Figure 1.3: The Layout of the Experimental Areas at TRIUMF.

(Fry, 1984) confirmed that the beam-foil interaction was similar for protons and muons of the same velocity. It also confirmed that micro-channel plates could be used to detect epithermal muonium and that a coating of CsI on the front surface of the plates could increase the efficiency for detection of Lyman-alpha photons to more than 10%. The experiment described in the following chapters was performed in June of 1983.

The theory of the muonium atom energy levels is outlined in Chapter 2. Chapter 3 describes the beam-foil production of epithermal muonium and the tuning of the secondary channel to optimize the production. The behaviour of muonium in electric fields (Stark effect) and the excitation of the Lamb shift transitions are examined in Chapter 4. Chapter 5 describes the apparatus and the experimental procedure used to acquire the data over a two week period. The analysis and reduction of the data to extract the experimental value of the Lamb shift is described in Chapter 6. Finally Chapter 7 summarizes the results and suggestions for future experiments are examined.

2. THE MUONIUM ENERGY LEVELS

In this chapter the basic theory of the energy levels of hydrogen-like atoms is discussed. Of course, particular emphasis is given to the n=2 level and to the muonium atom. Wherever possible, an intuitive understanding is preferred to more rigorous derivation. The reader desiring the latter is referred to the extensive literature[1]. Historically it has been the case that experiment has shown errors in the application of theory in this field. Without experimental results the theoretical predictions of the Lamb shift and of the muon g-factor might well be quite different (and wrong). The careful reader will realize that the intuitive treatment which follows relies heavily on prior knowledge of the correct results. The approach is aimed at the calculations necessary for the design and interpretation of an experiment to measure the n=2 muonium atom Lamb shift at the few percent level of accuracy.

2.1 SYMMETRY

Consider an isolated muonium atom. The total angular momentum $\bar{F}$ is the sum of the intrinsic angular momentum (spin) $\bar{I}$ of the muon, the spin $\bar{S}$ of the electron and the orbital angular momentum $\bar{L}$ of the two particle system. In the reference frame in which the atom is at rest, $\bar{F}$ is independent of the point with respect to which it is defined and is a constant of the motion because of the isotropy of

[1]See for example the following reviews: Drake, 1983
Erickson, 1977

space. Therefore the energy levels cannot depend upon the orientation of $\bar{F}$.

Using the commutation properties of the total angular momentum F one deduces that there are 2F+1 different values for the projection of $\bar{F}$ along a particular axis. These will be labelled by m_F. Since the energy must not depend on the orientation of the atom, there will be 2F+1 degenerate eigenstates belonging to the eigenvalue associated with each value of F. This limits the number of distinct energy levels for the n=2 atom, reducing the sixteen possible eigenvalues belonging to the sixteen eigenstates to at most six distinct values. Thus at most five independent energy differences or intervals exist between the eigenstates of the n=2 level of an isolated muonium atom.

2.2 THE EIGENSTATES OF F, m_F, J, AND L

Before proceeding it is prudent at this point to construct eigenstates of F and m_F and at the same time establish some of the notation. There are several ways in which one might do this.

One method is to combine the spins $\bar{S}$ and $\bar{I}$, using the usual rules for combining angular momenta, to form the vector $\bar{K} = \bar{I}+\bar{S}$. Next, one adds the orbital angular momentum $\bar{L}$ forming $\bar{F} = \bar{L}+\bar{K}$. The resulting eigenstates, $|F,m_F,K,L\rangle$ would be appropriate in the treatment of positronium or more generally in the system of two particles of identical mass and spin (Owen, 1984).

In the case of atoms in which one particle is much more massive than the other ($m_\mu/m_e \simeq 207$) the heavier particle behaves as the 'nucleus' of the atom. It is more appropriate to combine $\bar{S}$ and $\bar{L}$ to form $\bar{J} = \bar{S}+\bar{L}$, and then to add $\bar{J}$ and $\bar{I}$ to form $\bar{F}$ obtaining the eigenstates $|F,m_F,J,L\rangle$. The Hamiltonian of the isolated n=2 muonium atom is very nearly diagonal with respect to the 16 eigenstates thus formed.

2.3 SEPARATION OF THE CENTER OF MASS MOTION

The Dirac and Klein-Gordon equations can be solved analytically and exactly for the motion of a point-like particle in a fixed Coulomb field. By "fixed" one means the field is immovable, being produced by a ficticious infinitely massive charged particle with zero spin. The energy levels E_n for an orbiting particle of mass m and opposite charge -e are then given by:

$$E_n = mc^2 \{ [1 + (Z\alpha/[n-\epsilon+\sqrt{\epsilon^2-(Z\alpha)^2}])^2]^{-1/2} - 1 \} \qquad ...(2.1)$$

where $\epsilon = j + 1/2$ for the solution of the Dirac equation, yielding E_n^D, describing for example the motion of an electron, and $\epsilon = l + 1/2$ for the solution of the Klein-Gordon equation, yielding E_n^{KG}, describing the motion of a spinless particle, for example that of a pion.

The energy levels given by 2.1 must be modified because a real atom is not infinitely massive nor is the field of the nucleus purely Coulomb. The nucleus may be a particle of finite extent (such as a proton) and possess a magnetic

moment contibuting a non-central component to the net potential.

The corrections for finite mass are largely accounted for by introduction of the reduced mass μ in 2.1. However, this is a non-relativistic limit of the relativistic defintions below: In relativistic mechanics the point with radius vector

$$\bar{R} = \frac{\Sigma E \bar{r}}{\Sigma E} \qquad \ldots(2.2)$$

moves with uniform velocity

$$\bar{V} = c^2 \frac{\Sigma \bar{p}}{\Sigma E} \qquad \ldots(2.3)$$

where the summation is over all particles and fields, and $\bar{p}$ and E are the momentum and energy at each point. The non-relativistic limit gives $E \simeq mc^2$ thus 2.2 and 2.3 become

$$\bar{R} = \frac{\Sigma m \bar{r}}{\Sigma m} \; ; \; \bar{V} = \frac{\Sigma \bar{p}}{\Sigma m} \qquad \ldots(2.4)$$

The center of mass motion is then separated, for a system of two particles of mass m and M, by defining

$$\mu = \frac{mM}{m + M} \qquad \ldots(2.5)$$

As already stated, using μ in 2.1 takes care of most of the effects of finite nuclear mass, but it is not the result of

any correct or relativistic treatment of the two body system. It is, however, a starting point after which one can derive *corrections* which will fall into two classes: those of radiative origin and those of non-radiative origin.

2.4 NON-RADIATIVE CORRECTIONS

2.4.1 CORRECTIONS TO THE FINE STRUCTURE

The differences between the energy levels given by 2.1 and those predicted by the Schrödinger equation for the motion of an electron are known as *fine structure*. The relativistic energy E_n and non-relativistic energy E_n^{NR} are related by:

$$\frac{E_n}{E_n^{NR}} = 1 + \frac{(Z\alpha)^2}{n^2}\left[\frac{n}{\epsilon} - \frac{3}{4}\right] + O((Z\alpha)^4); \quad E_n^{NR} = -\frac{(Z\alpha)^2}{2n^2}mc^2 \qquad \ldots(2.6)$$

The difference $E_n^{KG}-E_n^{NR}$ shows relativistic effects while the difference $E_n^{D}-E_n^{KG}$ isolates the effects of spin. One has:

$$E_n^{D} - E_n^{KG} = 2mc^2\,\frac{(Z\alpha)^4}{n^3}\cdot\frac{j-l}{(2j+1)(2l+1)} \qquad \ldots(2.7)$$

One notes that 2.1 predicts that the muonium energy levels depend on j and not on l and hence the $2p_{1/2}$ and $2s_{1/2}$ levels are degenerate. This can be interpreted as a statement that the electron g-factor is exactly 2 and therefore that orbital and spin angular momenta are

indistinguishable. However, it is well known that the electron g-factor differs slightly from 2 (as can be calculated extremely accurately) and hence we must correct 2.1 for this. Barker and Glover (Barker, 1955) obtained corrections to the fine structure from reduction of a relativistic two-body Breit equation. The corrections are proportional to $E_n^D - E_n^{KG}$.

(i) Correction for the anomalous moment of the electron

$$\frac{g_e - 2}{2} \cdot 2mc^2 \frac{(Z\alpha)^4}{n^3} \cdot \frac{j - l}{(2j+1)(2l+1)} \cdot \left[\frac{\mu}{m}\right]^{3-l} \qquad \ldots(2.8)$$

(ii) Correction for the anomalous moment of the muon for s-states:

$$\frac{g_\mu - 2}{2} \cdot 2Mc^2 \frac{(Z\alpha)^4}{n^3} \cdot \frac{j - l}{(2j+1)(2l+1)} \cdot \left[\frac{\mu}{M}\right]^{3} \delta_{0l} \qquad \ldots(2.9)$$

(ii) is ignored in the hydrogen Lamb shift calculation where it would amount to 0.023 MHz in the 2S state (Foldy, 1951; Salpeter, 1953) because it is claimed that proton size already accounts for this.

(iii) Correction for the Dirac moment of the muon for p-states:

$$-2\mu c^2 \frac{(Z\alpha)^4}{n^3} \cdot \frac{j - l}{(2j+1)(2l+1)} \cdot \left[\frac{\mu}{M}\right]^{2} \delta_{1l} \qquad \ldots(2.10)$$

This correction, while very small in hydrogen, where it decreases the Lamb shift by about 0.002 MHz, is proportional

to $(m/M)^2$ and so is about 100 times larger for muonium, where it reduces the Lamb shift by 0.171 MHz. The values of g_e and g_μ may be inserted phenomenologically from experimental results or from calculation.

2.4.2 CORRECTIONS TO THE HYPERFINE STRUCTURE

The muon is much lighter than the proton so its magnetic moment is much larger than that of a proton and consequently the hyperfine structure of muonium is larger as well. On the other hand, by the same token the hyperfine structure of muonium is much smaller than that of positronium.

The muon magnetic moment $\bar{\mu}_\mu$ introduces a non-central component to the net potential. The magnetic moment is

$$\bar{\mu}_\mu = g_\mu \mu_0 m_e / m_\mu \, \bar{I} \qquad \ldots(2.11)$$

and interacts with the spin and orbital magnetic moments of the electron, $\bar{\mu}_S$ and $\bar{\mu}_L$, thus contributing to the hyperfine splitting ΔE_{HF}

$$\Delta E_{HF} = \bar{\mu}_\mu (a_1 \bar{\mu}_S + a_2 \bar{\mu}_L) \qquad \ldots(2.12)$$

Without going into too much detail (see for example Tinkham) one can appeal to the isotropy of space, demanding that ΔE_{HF} be a scalar to obtain:

$$\Delta E_{HF} = a \bar{I} \cdot \bar{J} \qquad \ldots(2.13)$$

where a is an l and j dependent constant. Barker and Glover

(Barker, 1955) obtained

$$\Delta E_{2s_{1/2}} = \frac{4}{3} \cdot \frac{\mu^3 Z^3 \alpha^4}{mMn^3} \frac{g_\mu g_e}{4} 2\, \bar{I}\cdot\bar{J}$$

$$\Delta E_{2p_{1/2}} = \frac{4\mu^3 Z^3 \alpha^4}{9mMn^3} \left[\frac{g_\mu g_e}{4} + \frac{g_\mu}{2} + \frac{g_e m}{2M} + \frac{(g_e-2)m}{2M} \right] \bar{I}\cdot\bar{J}$$

$$\Delta E_{2p_{3/2}} = \frac{4\mu^3 Z^3 \alpha^4}{18mMn^3} \left[\frac{g_\mu g_e}{20} + \frac{g_\mu}{2} + \frac{g_e m}{2M} + \frac{(g_e-2)m}{2M} \right] \bar{I}\cdot\bar{J}$$

...(2.14)

The operator $\bar{I}\cdot\bar{J}$ is traceless as can be seen by writing

$$\bar{I}\cdot\bar{J} = 1/2\ \{f(f+1) - j(j+1) - i(i+1)\}$$

...(2.15)

to evaluate $\bar{I}\cdot\bar{J}$ for each of 16 eigenstates of the n=2 atom. The mean energies of the $2s_{1/2}$, $2p_{1/2}$, and $2p_{3/2}$ states are not shifted so that the Lamb shift is unaffected by ΔE_{HF}. In an actual experiment, however, a knowledge of ΔE_{HF} is required in order to extract the Lamb shift since, in practice, only one or two energy differences may be measured. The agreement between experiment and theory for ΔE_{HF} in the ground state of muonium is excellent (Casperson, 1975; Cleland, 1972; Kinoshita, 1984). The accuracy required in the present experiment allows us to scale from this result by $1/n^3$ to predict the result for n=2, although there are small deviations from $1/n^3$ scaling not included in 2.13.

2.4.3 RECOIL CORRECTIONS

Recoil corrections are larger in muonium than in hydrogen because they are proportional to the ratio m/M. The

emission and absorption of photons (and therefore recoil) is external to the Dirac theory.

The following example illustrates the nature of recoil corrections. The energy change E_n from a just unbound state to the nth bound state is given to sufficient accuracy by

$$E_n^{NR} = -\frac{(Z\alpha)^2}{2n^2}\mu c^2 \qquad \ldots(2.16)$$

Now, recombination proceeds by emission of a photon of energy E_n and consequently of momentum E_n/c. Conservation of momentum requires that an equal and opposite recoil momentum be imparted to the atom. The kinetic energy associated with the recoil is easily seen to be [1]

$$\Delta E_R = \frac{E_n^{NR_2}}{2(m+M)c^2} = \frac{(Z\alpha)^4\mu^2c^2}{8n^4(m+M)^2} \qquad \ldots(2.17)$$

The total energy of the transition is increased by ΔE_n^R which amounts to shifting all the n=2 levels by -1.5 MHz, -13.3 MHz, and -342 MHz in hydrogen, muonium and positronium respectively. In principle this effect would contribute to the Lamb shift; however S is a small fraction of E_n^{NR} and the effect is seen to be negligible. Measurements of the energy difference between the ground and first excited states in positronium (Chu, 1982) are not yet of sufficient accuracy to see this effect.

---

[1]This result was first derived by Barker and Glover from treatment of a relativistic two-body Breit equation, however their result contains a typographical error showing ΔE_n^R proportional to $1/n^3$ instead of $1/n^4$.

The dominant recoil effect which does contribute to the Lamb shift enters indirectly from considerations of the effect of recoil when calculating radiative effects. The magnitude of this effect can be estimated very roughly as follows: the Lamb shift S decreases the kinetic energy of the electron in the $2s_{1/2}$ state; therefore the momentum is decreased as well and the associated recoil of the muon is is also lessened so that the binding energy of the 2s level is reduced by mS/M. The exact result is (Erickson, 1977)

$$\frac{\mu^3}{mM}\frac{4(Z\alpha)^5c^2}{3\pi n^3}\Bigg[2\,\{[-2\ln(Z\alpha)+11/24]\,\delta_{l0}+\ln[K_0(n,l)]\}+$$

$$-7/2\{[\ln(n/2Z\alpha)-\sum_{i=1}^{n} i^{-1}+1/(2n)-1]\delta_{l0}+\frac{1-\delta_{l0}}{2l(2l+1)(l+1)}\}$$

$$\delta_{l0}+\frac{2-7/2}{M^2-m^2}\{M^2\ln(m/M)-m^2\ln(M/m)\}\delta_{l0}\Bigg]$$

...(2.18)

where the Bethe logarithm $\ln[K_0(n,l)]$ will be defined later. This was first obtained by Salpeter (Salpeter, 1952) for the n=2 level of hydrogen-like atoms and then for arbitrary m and M in the n=2 state by Fulton and Martin (Fulton, 1954). Erickson generalized it to arbitrary n (Erickson, 1965) and Grotch and Yennie have verified it using a different approach (Grotch, 1969).

This effect has been seen in both the 2s positronium (Mills, 1975) and 2s hydrogen Lamb shift measurements (Lundeen, 1981; Pal'chikov, 1983). In muonium it amounts to

3.19 MHz.

2.5 RADIATIVE CORRECTIONS

2.5.1 SELF-ENERGY

The electron self-energy or "electron structure" in the Coulomb field is the dominant radiative contribution to the Lamb shift. Figure 2.1a shows the lowest order Feynman diagrams contributing to the electron structure. The self-energy mainly affects the s-states for which the electron and nucleus approach each other closely. It can be understood qualitatively following the treatment of Welton (Welton, 1948) as the interaction of the electron with the zero point fluctuations of the vacuum. These can be seen to cause the position of the electron to fluctuate rapidly (an effect closely related to the *zitterbewegung*). The variance $(\Delta r)^2$ of the fluctuation of the separation of the electron and the nucleus is of the order of (see Bjorken and Drell, p. 59)

$$2\alpha^3 a^2/\pi \qquad \ldots(2.19)$$

The average potential V seen by the electron is modified such that

$$\Delta V \simeq (1/6)(\Delta r)^2 \langle \nabla^2 V \rangle \qquad \ldots(2.20)$$

Now, since $\nabla^2 V = 4\pi Z e^2 \delta^3(\bar{r})$ we can evaluate the energy shift using non-relativistic wave functions for which

SELF ENERGY MAGNETIC MOMENT

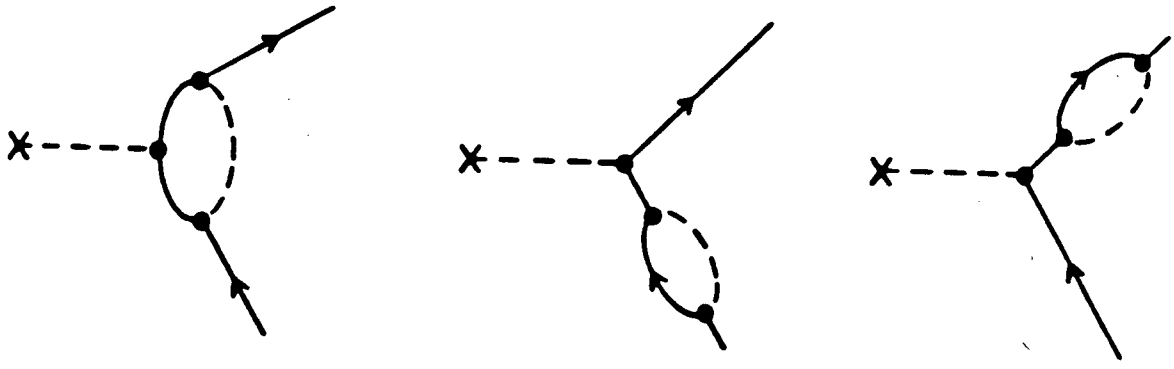

VACUUM POLARIZATION

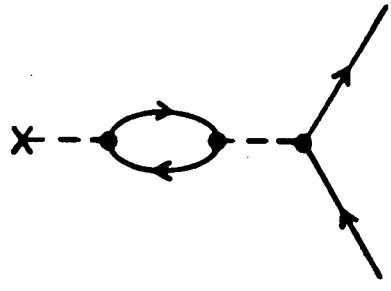

Figure 2.1: Some Feynman diagrams which contribute to the Lamb shift.

$$|\psi_{nl}(0)|^2 = \frac{Z^3}{\pi n^3 a^3}\delta_{l0} \qquad ...(2.21)$$

obtaining

$$\Delta E_n^S \simeq \frac{4(Z\alpha)^4}{3\pi n^3} mc^2 \ln(Z\alpha)^{-1} \qquad ...(2.22)$$

The preceding argument shows clearly that the self-energy interaction should reduce the binding energy of s-states. The self-energy correction (to terms of second order in $Z\alpha$), in units of $[4(Z\alpha)^4 \alpha mc^2]/(3\pi n^3)$, affects both p and s-states

$$\{[\ln(Z\alpha)^{-2}+\ln(m/\mu)+11/24]\delta_{l0} + \ln[K_0(n,l)]\}\{\mu/m\}^3 \qquad ...(2.23)$$

where $\ln[K_0(n,l)]$ is the logarithmic average of the excitation energy of the state to all other bound and continuum states. $\ln[K_0(n,l)]$, the so called *Bethe logarithm* (Bethe, 1947), has been evaluated by numerous authors; the values for the $2s_{1/2}$ and $2p_{1/2}$ states are +2.9841285559(3) and +0.0300167089(3) respectively (Erickson, 1977).

The fourth order correction to self-energy is (Lautrup, 1972)

$$[3\alpha/\pi]\ \{-4819/5184-45\pi^2/432+(\pi^2/2)\ln 2-(3/4)\zeta(3)\} \qquad ...(2.24)$$

which affects only s-states. The neglect of reduced mass factors at this order is the rule in the literature since no one seems to know what the correct ones are (Erickson, 1977)[1]. Higher order corrections to the self-energy are

[1] The usual rule is to use three reduced mass factors for terms which depend on the volume integral of the wave

discussed later.

2.5.2 MAGNETIC MOMENT

The value of the anomalous electron g-factor can be calculated with extreme accuracy, through terms of sixth order in α. The result is

$$\alpha/(2\pi)-(\alpha/\pi)^2\{197/144+\pi^2/12-(\pi^2/2)\ln 2+(3/4)\zeta(3)\}+ \\ +(\alpha/\pi)^3\{1.285\pm 0.057\} \qquad ...(2.25)$$

where ζ is the Riemann zeta function. It contains the highest order term calculated in QED today and tested by experiment $g_e-2 = 2\cdot 1159656.7(3.5)\cdot 10^{-9}$ (Particle Data Group, 1984). The values of g_e and g_μ can be inserted in equations 2.8 and 2.9. However, many authors use the reduced mass factors only on the second order correction to g/2 and not on the higher order terms.

2.5.3 VACUUM POLARIZATION

Vacuum polarization or "photon structure" (see Figure 2.1b) increases the binding energy of s-states. The coupling constant e in the coulomb potential e/r can be thought of as depending on r such that as r decreases (at small values of r), $e^2(r)$ increases. The bare electronic charge is screened by polarization of the vacuum (Uhling, 1935) so that at long

[1](cont'd) function at the origin and to ignore them elsewhere. However, as is the case in calculations involving pionic atoms, when the wave function vanishes at the origin then the divergence of the wave function may be seen to contribute thus giving two reduced mass factors for some interactions involving p-states.

distances the observed charge is e but at short distances the apparent charge increases. The effect on the energy levels from the lowest order diagrams is, to terms of order $(Z\alpha)^2$,

$$-1/5(\mu/m)^3 \qquad \ldots(2.26)$$

The next order vacuum polarization diagrams give (Baranger, 1952)

$$-(\alpha/\pi)(41/54) \qquad \ldots(2.27)$$

Presumably, since this is a short range interaction, the reduced mass factor $(\mu/m)^3$ should also multiply this term; however, since the effect is small and for consistency with the literature they are ignored here. Vacuum polarization due to production of other pairs of particles (like $\mu^+ \mu^-$) is negligible in this case.

2.5.4 HIGHER ORDER BINDING CORRECTIONS

Historically there was about a 7 MHz discrepancy between calculation and experiment when the hydrogen Lamb shift was first measured. Theoreticians reacted quickly by realizing they had forgotten to calculate relativistic corrections to the binding of the hydrogen atom which arise as a result of the radiative corrections. Baranger(Baranger,1953) and Karplus (Karplus, 1951) both obtained, to second order in $(Z\alpha)$

$$(Z\alpha)(3\pi)\{1+11/128-(1/2)\ln 2+5/192\}$$

...(2.28)

restoring agreement between the theory and experiment. Baranger uses one reduced mass factor in his result, commenting, "At the present time, the ,most logical course is to use [the reduced mass] in $|\psi(0)|^2$ and [the electron mass] everywhere else."

Still higher order corrections are the source of discussion today (Drake, 1983). These take the form of expansions. (Here we take only the difference contributing to the n=2 Lamb shift for simplicity). Following the notation of Mohr, they are:

$$(Z\alpha)^2\{G(z\alpha)-(3/4)\ln 2-(55/48+4\ln 2)\ln(Z\alpha)^2\}$$

...(2.29)

where $G(Z\alpha) = G^{WK}+G^{U}+G^{SE}$ and

$$G^{U} = -0.557\pm 0.003 + 0.221(Z\alpha)\ln(Z\alpha)^{-2}$$

$$G^{WK} = 0.04251 - 0.10305(Z\alpha) + \ldots$$

...(2.30)

are higher order corrections to the vacuum polarization calculated by Wichmann and Kroll (WK) (Wichman, 1956). G^{U} has been calculated numerically by Mohr (Mohr, 1975) by fitting the assumed dependence on $Z\alpha$ (as in 2.26) for various values of Z and extrapolating to Z=1. It is an estimate of the effect of including all orders of $Z\alpha$ in the calculation of the diagrams in Figure 2.1b.

The last term G^{SE} is a point of disagreement between the Erickson and Mohr calculations. It is an estimation of the higher order terms in $Z\alpha$ for the lowest order self-energy diagrams (see Figure 2.1a). Mohr (Mohr, 1975) performed calculations for atoms of higher Z and then extrapolated to Z=1 by fitting the parametrization

$$G^{SE} \simeq a_1 + a_2(Z\alpha)\ln(Z\alpha)^{-2} + a_3(Z\alpha) \qquad ...(2.31)$$

to his numerical results for Z=10,20, and 30, thus obtaining

$$a_1 = -24.064;\ a_2 = 7.3071;\ a_3 = 15.6609 \qquad ...(2.32)$$

Erickson, on the other hand, finds (Erickson, 1977)

$$G^{SE} \simeq -17.246 + 19.760(Z\alpha) \qquad ...(2.33)$$

Another calculation of G^{SE} for the ground state of hydrogen by Sapirstein (Sapirstein, 1981) obtained -24.9±0.9 for the first term ($Z\alpha$=0) which, since the n dependence is small, supports the Mohr result.

Borie (Borie, 1981) has pointed out that the inclusion of the finite size of the proton separately from the radiative calculations is incorrect because the self-energy calculation is affected by consideration of the finite extent of the charge distribution. The dominant contribution can be seen to enter in equation 2.20, where $\nabla^2 V$ no longer can be simply evaluated by replacing it with $4\pi Z e^2 \delta^3(\bar{r})$. She obtains a correction in the case of hydrogen which decreases the Lamb shift by 0.042 MHz; thus the total net effect of

the finite size of the proton for $\sqrt{<r_p^2>}$ = 0.862(12) fm (Simon, 1980) is to increase the Lamb shift by 0.102 MHz, according to Borie.

2.6 SUMMARY OF THE LAMB SHIFT CALCULATIONS

Table 2.1 shows various terms contributing to the Lamb shifts in hydrogen and muonium. Table 2.2 shows the resulting Lamb shift values. The current experimental results for the Lamb shift in hydrogen are in agreement with each other. Lundeen (1981) obtains S = 1057.845(9) MHz by measuring the $2s_{1/2}$ F=0 to $2p_{1/2}$ F=1 transition energy using a separated oscillatory field technique from which he deduced the value of S from the already measured values of the hyperfine splittings. Pal'chikov (1983) used a much different technique, relying on a theoretical calculation of the lifetime of the $2p_{1/2}$ state to obtain S = 1057.8514(19) MHz.

Mohr's (1976) result for hydrogen used an incorrect value of the r.m.s. charge radius of the proton. Correcting his result for the currently accepted value of 0.862(9) fm one obtains S = 1057.88(1) MHz, which disagrees with both of the experimental results by a few standard deviations. If we include Borie's correction, Mohr's result is S = 1057.84(1) MHz, which is in agreement with experiment. Erickson (1977) obtains S = 1057.93(1) MHz, which disagrees with experiment even more than Mohr's calculation. Including Borie's correction here gives S = 1057.89(1) MHz, which is still

EFFECT	HYDROGEN (MHz)	MUONIUM (MHz)
SELF ENERGY		
Second order (2.23)	1009.924	997.611
Fourth order (2.24)	0.444	0.444
g_e-2 (2.8) AND (2.25)		
Second order	67.720	66.928
Fourth order	-0.103	-0.103
VACUUM POLARIZATION		
Second order (2.26)	-27.084	-26.739
Fourth order (2.27)	-0.239	-0.239
RELATIVISTIC EFFECTS (2.28)	7.140	7.140
NUCLEUS DIRAC		
MOMENT (2.10)	-0.002	-0.171
HIGHER ORDER EFFECTS (2.29)		
Erickson	-0.372	-0.372
Mohr	-0.424	-0.424
RECOIL (2.18)	0.359	3.188
Owen (Coulomb recoil)	-0.074	-0.656
FINITE SIZE	0.145	0.000
Borie (finite size correction)	-0.042	0.000

Table 2.1: Various Contributions to the Lamb Shift in Hydrogen and Muonium.

higher than experiment by a couple of standard deviations.

Owen has calculated the Lamb shift in muonium from first principles, obtaining 1047.03 MHz (Owen, 1973). In his calculation, however, he obtained incorrect values for the hyperfine structure of the muonium atom which he later corrected (Owen, 1984) without affecting the Lamb shift result. Owen's result appears to differ from the value one obtains for the muonium Lamb shift using the Erickson method of calculation by a single term amounting to -0.65 MHz (which he calls "Coulomb recoil"). Including this term in the hydrogen Lamb shift calculation of Erickson reduces the result by 0.074 MHz to 1057.86(1) MHz thus giving good agreement between theory and experiment. Applying Mohr's method to the Lamb shift in muonium gives S = 1047.64 MHz. The correction for the anomalous moment of the muon (equation 2.9) is seen to be negligible.

Table 2.2: Lamb shift calculation results from Table 2.1

TOTAL LAMB SHIFT (MHz)	HYDROGEN	MUONIUM
Erickson	1057.93	1047.69
Mohr	1057.88	1047.64
Erickson and Borie	1057.89	1047.69
Erickson and Owen	1057.86	1047.03
Mohr and Borie	1057.84	1047.64

3. THE FORMATION OF 2S MUONIUM

3.1 GENERAL CONSIDERATIONS

A Lamb shift measurement requires muonium in the n=2 excited state (recall the level diagram of Figure 1.1). The mean lifetime, 1.6 ns, of the 2p level corresponds to a level width of about 100 MHz. In order to de-excite the n=2 levels it is therefore necessary to observe the n=2 muonium for times significantly longer than the level lifetime. The n=2 muonium must remain in the apparatus and be free of interaction with the walls and gas molecules for times at least of the order of 10 ns. Hence the experiment must be performed in a vacuum such that the probablity of interaction over the flight path of the atom is low. This generally means vacuums of better than 10^{-5} Torr; otherwise the muonium is rapidly de-excited by collisional processes. This is also the case in the production of muonium in powder samples (such as SiO_2) where, although the energies are thermal, the mean collision time is very short.

3.2 METHODS OF FORMING MUONIUM

We now examine various methods to form muonium with a view to the considerations discussed above. The most copious sources of muons available today are those of the secondary beam lines of the meson factories. Typically 10^6 μ^+ per second can be delivered to an experiment by these beam lines. Within the time structure of the proton beam which

produces the muons, instantaneous rates may be much greater.

The positively charged muon flux delivered must be converted to a neutral muonium beam. Most methods of conversion work well at low velocities ($v < c/100$) and their efficiency is highly dependent on the velocity. They require the velocity of the charged beam to be "tuned" to optimize the conversion. This is even more critical if one wishes to preferentially populate an excited state. Unfortunately, the available μ^+ flux from secondary beam lines is of rather high velocity, $v \simeq 0.3c$. Hence, one finds that the more usual methods of neutralizing charged beams, such as those used in ion sources (e.g., charge exchange in Cæsium vapour), are ineffective.

Various alternatives have been suggested. Neutralization proceeding by Coulomb recombination of the muons with an intense electron beam has been investigated (Mezzorani, 1982) and could be relatively efficient even at higher velocities, but in order to keep the apparatus down to a reasonable size, the muonium thus produced would still have to be slowed down. Phase space compression methods have also been proposed (Taqqu, 1984) which potentially could improve the brightness and decrease momentum spread of low momentum beams.

3.3 THE BEAM FOIL INTERACTION

The beam-foil interaction (neutralization by passing a charged beam through a foil) has been studied by many authors. It has been verified experimentally that the behaviours of p and d (Lee, 1985) and of μ^+ (Fry, 1984) in the beam-foil neutralization process are essentially the same for projectiles of the same velocity . This is also expected from the theories of Coulomb recombination, and energy loss in matter, and experiments using various ion beams which measure the range and energy loss of ions as functions of incident projectile charge, mass, and energy. Hence, one expects a positive muon to behave very much as a positive proton of the same velocity. The beam-foil interaction has been employed in recent measurements of the Lamb shift in hydrogen using fast proton beams (Lundeen, 1981). The experimentally measured neutral fractions emerging from various foils as functions of the emerging particle's velocity are reviewed by S.K. Allison (Allison, 1958) and are found to be, within experimental systematic uncertainty, independent of the elemental composition for metallic foils. The neutral fraction predicted on this basis for muonium is shown in Figure 3.1.

Figure 3.1 also shows the relative cross sections for populating excited states. These were calculated using the theory of Coulomb recombination for a muon of velocity $v = \beta c$ interacting with an electron at rest. The cross section for recombination into the 1s state, σ_{1s}, is given by Bethe

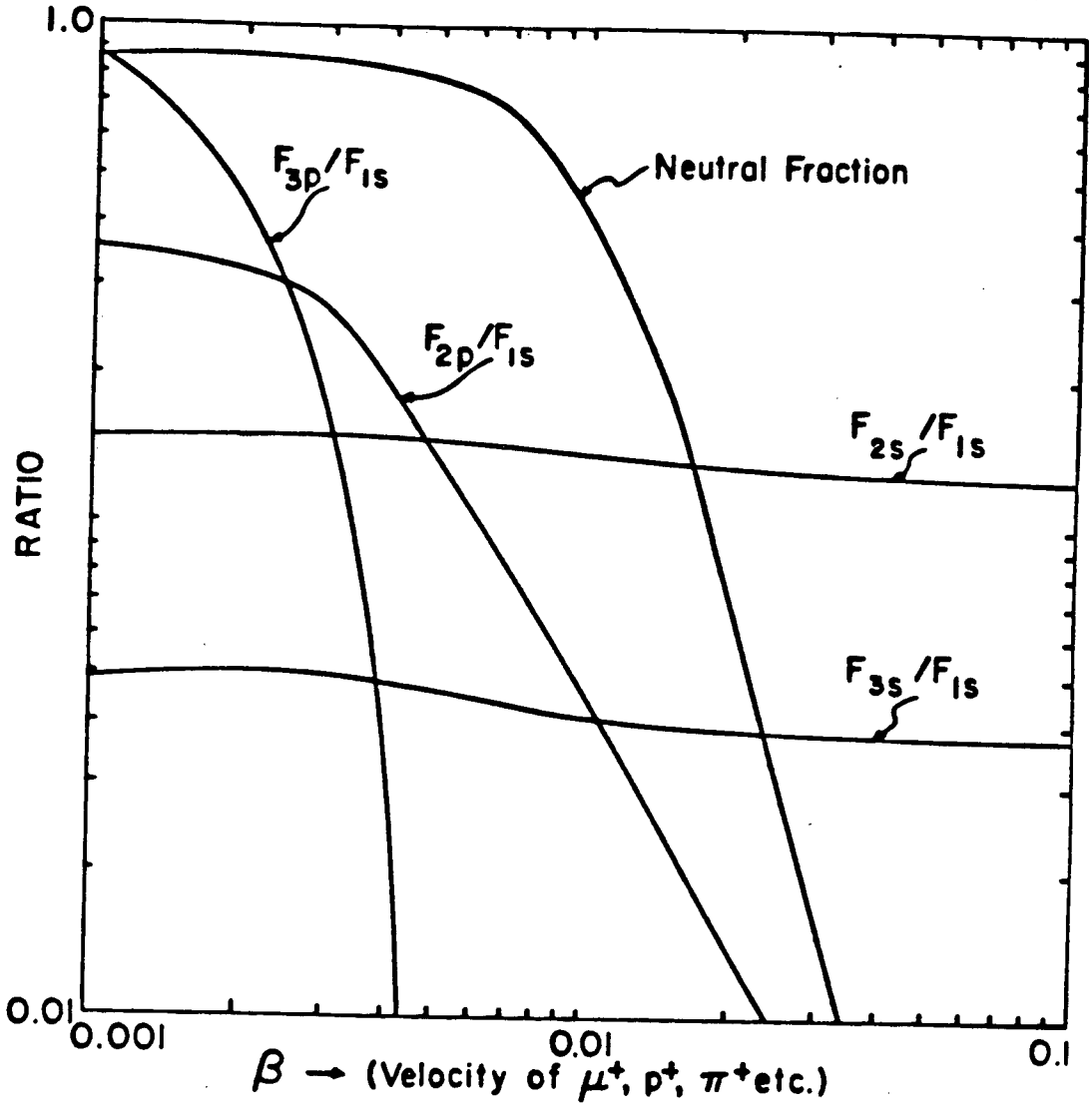

Figure 3.1: The neutral fraction and fraction in various states of a beam of positively charge particles emerging from a foil as a function of velocity.

(Bethe, 1977):

$$\sigma_{1s} = \frac{2^8 \hbar e}{3m^2c^3} \frac{\gamma^6}{(\gamma^2+1)^2} \frac{e^{-4\gamma\cot^{-1}\gamma}}{1 - e^{-2\pi\gamma}} \qquad \ldots(3.1)$$

which is the result of calculating the matrix element of $\bar{r}$ between continuum states and the ground state (γ is defined below). More generally we may calculate analytically the result for an arbitrary bound state (Miller, 1980). The result depends only on the angular momentum l and principal quantum number n of the final state. Explicitly, the ratio F of the excited state cross section to the ground state cross section (3.1) is

$$F_{n,l} = \frac{2^{-8}}{n^2} \frac{(n+l)!}{(n-l-1)!(2l+1)!^2} \chi\ (1+1/\gamma^2)^2(1+n^2/\gamma^2)\ \cdot$$

$$\cdot\{l\ J(l-1)\left[\sum_{j=0}^{n-l-1} \frac{(1+l-n)_j}{j!(2l+1)_j} Q(l-1,j+3)\right]^2 +$$

$$+\ (l+1)\ J(l+1)\left[\sum_{j=0}^{n-l-1} \frac{(1+l-n)_j}{j!(2l+1)_j} Q(l+1,j+1)\right]^2\} \qquad \ldots(3.2)$$

where:

E = energy of the electron in the rest frame of the μ^+ in Rydbergs. $(a)_j = \Gamma(a+j)/\Gamma(a)$

$\gamma = 1/\sqrt{E}$

$\chi = \exp\{-4\gamma[\cot^{-1}(\gamma/n)-\cot^{-1}\gamma]\}$

$$J(L) = \{4n/(1+n^2E)\}^{2L}\prod_{k=0}^{L}(1+k^2E)$$

Q is defined recursively by

$$Q(L,M) = 1 \text{ for all } M \leq 0$$

$$(1+n^2E)Q(L,M) =$$

$$4(M+L-n)Q(L,M-1) - 4(M-1)(M+2L)Q(L,M-2)$$

Equation 3.1 shows that σ_{1s} is proportional to velocity at low velocities and inversely proportional to the fifth power of velocity at higher velocities. Clearly, one requires projectile velocities on the order of c/100. Lower velocities tend to populate higher angular momentum states while higher velocities suffer from a rapidly decreasing neutral cross section, although the relative probability of populating the ns state is constant. Coherent superpositions of states (for example np and ns) are also populated in the beam foil interaction; however, as long as the velocity is not too low the s-state cross section will dominate.

3.4 SLOWING MUONS

The results of the previous section regarding the beam foil interaction indicate the need for a slow muon beam if the beam foil interaction is to be employed to create 2s muonium. Muons are produced by the decay of positive pions at rest in the production target of a secondary beam line. They are all born with the same momentum, 29.86 MeV/c, dictated by the kinematics of the pion decay. Depending on where the pion is in the production target, the momenta of muons emerging from the target will range from 29.86 MeV/c for decays at the surface (surface muons) down to zero for

decays at a depth inside the target corresponding to the range of a surface muon. Depending on the momentum setting of the secondary beam line viewing the production target, any of these muons may be collected and delivered to an experiment, however the flux delivered will be a function of the momentum.

We examine the process of slowing projectiles by passage through matter, called degradation. For simplicity, we consider the passage of muons through aluminum[1]. The differential energy loss for protons in aluminum, dE/dx, is a function of velocity that is well approximated by the empirical formula:

$$\frac{dE}{dx} \propto \begin{cases} v \; ; & c/100 \gg v \\ v^{-3/2} \; ; & c/2 > v > c/50 \end{cases} \qquad \ldots(3.3)$$

The two behaviours of dE/dx can be combined according to the prescription of Varelas and Biersack (Varelas,1970):

$$(dE/dx)^{-1} \simeq (dE/dx)^{-1}_{\text{low } v} + (dE/dx)^{-1}_{\text{high } v} \qquad \ldots(3.4)$$

Converting to momentum one has

[1] Properties of other degrader materials can be obtained by scaling since dE/dx is roughly proportional to the density of electrons in the material.

$$\frac{dp}{dx} = -\frac{a}{(v/b)^{5/2} + 1}$$

...(3.5)

where a and b are constants to be determined. The data (Anderson and Ziegler, 1977) indicate the values $a = 62500$ MeV/(c g/cm^2) and $b = 0.0158c$ for aluminum. Figure 3.2 shows dp/dx for aluminum using these values in equation 3.5. The value of b seems to vary slightly for different degraders but is not well determined because the experimental data for many materials are sparse. Nevertheless, in the future it may be found that careful choice of the degrader material can be important if a particular value of b is preferred. The constant a, on the other hand, exhibits a simple dependence upon the density of electrons in the material (Z/A). The following limits apply to equation 3.5:

(i) $dp/dx \simeq a$ for $v < c/200$

(ii) $dp/dx \simeq a(v/b)^{-5/2}$ for $v > c/50$

Integration of equation 3.5 gives the trajectory of the projectile (mass M) inside the degrader as a function of its velocity v:

$$(M/a)\{[(2/7)/b^{5/2}][v_0^{7/2}-v^{7/2}] + [v_0-v]\} = x$$

$$\text{range} \simeq x(v=0) \simeq \frac{2Mv_0^{7/2}}{7ab^{5/2}}$$

...(3.6)

where v_0 is the velocity of the projectile when it strikes

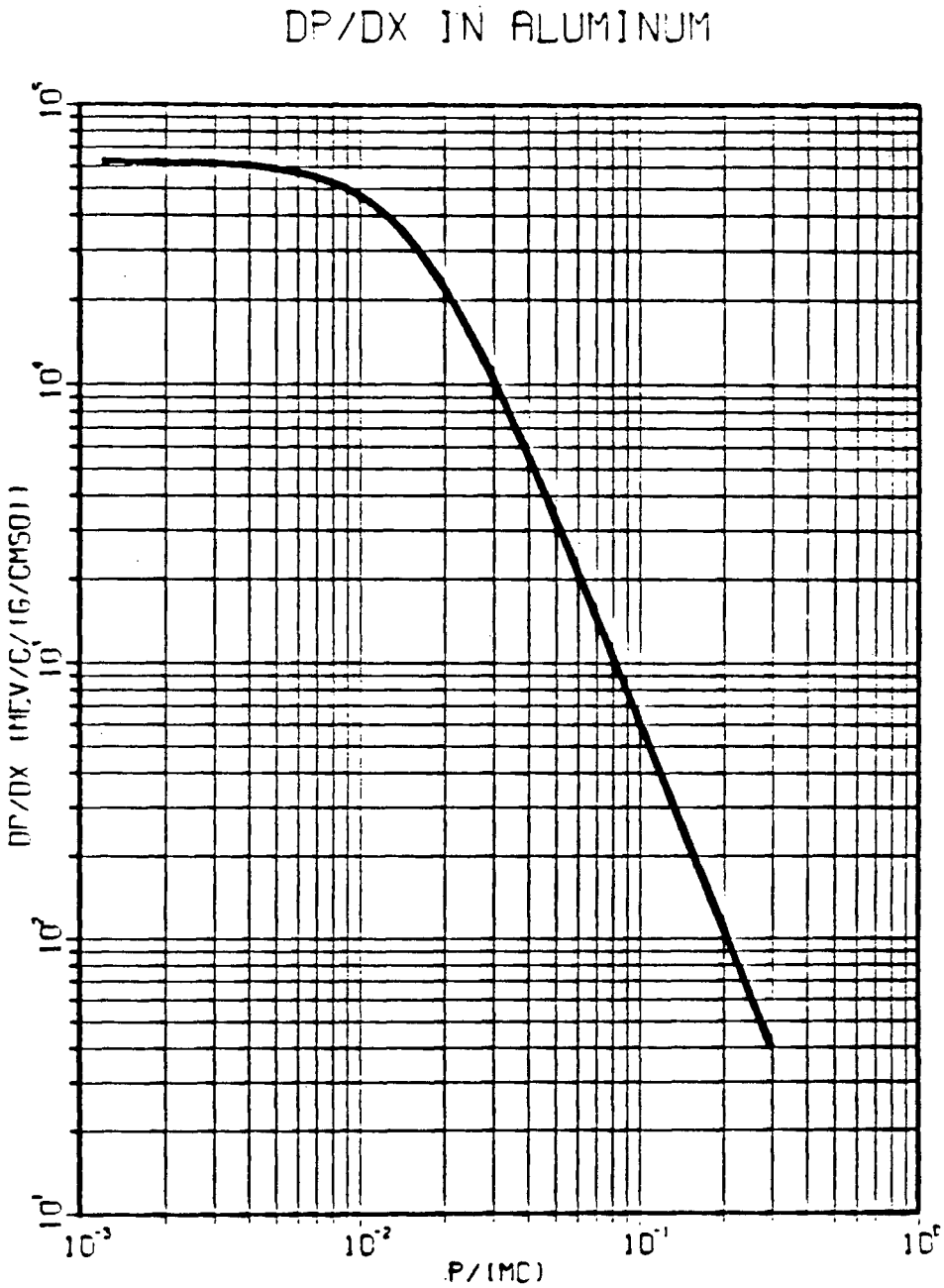

Figure 3.2: dp/dx for aluminum as calculated using equation 3.5.

the degrader (x=0).[1] Figures 3.3 and 3.4 show the "positions" of muons and protons respectively as a functions of velocity, for various initial velocities.

Variation of equation 3.6 for a fixed degrader thickness gives

$$\frac{\Delta v_0}{\Delta v} = \frac{(v/b)^{5/2} + 1}{(v_0/b)^{5/2} + 1} \qquad \ldots(3.7)$$

hence for v >> b we have the law

$$\Delta p_0/\Delta p \simeq (p/p_0)^{5/2} \qquad \ldots(3.8)$$

which determines the number of particles per unit momentum, ρ_x in the degrader as a function of the number of particles per unit incident momentum, ρ_0. One has

$$\rho_x(p)dp = \rho_0(p_0)dp_0$$

$$\rho_x(v) = \rho_0(v_0)\,\frac{(v/b)^{5/2+1}}{(v_0/b)^{5/2+1}} \qquad \ldots(3.9)$$

Equation 3.9 shows that the number of particles per unit momentum falls rapidly as the velocity is reduced and that for uniform production of particles throughout a degrader of momentum p_0, the number of particles emerging from the degrader will have the following shape:

---

[1] One notes that in general path length is greater than the linear depth of penetration because of multiple scattering.

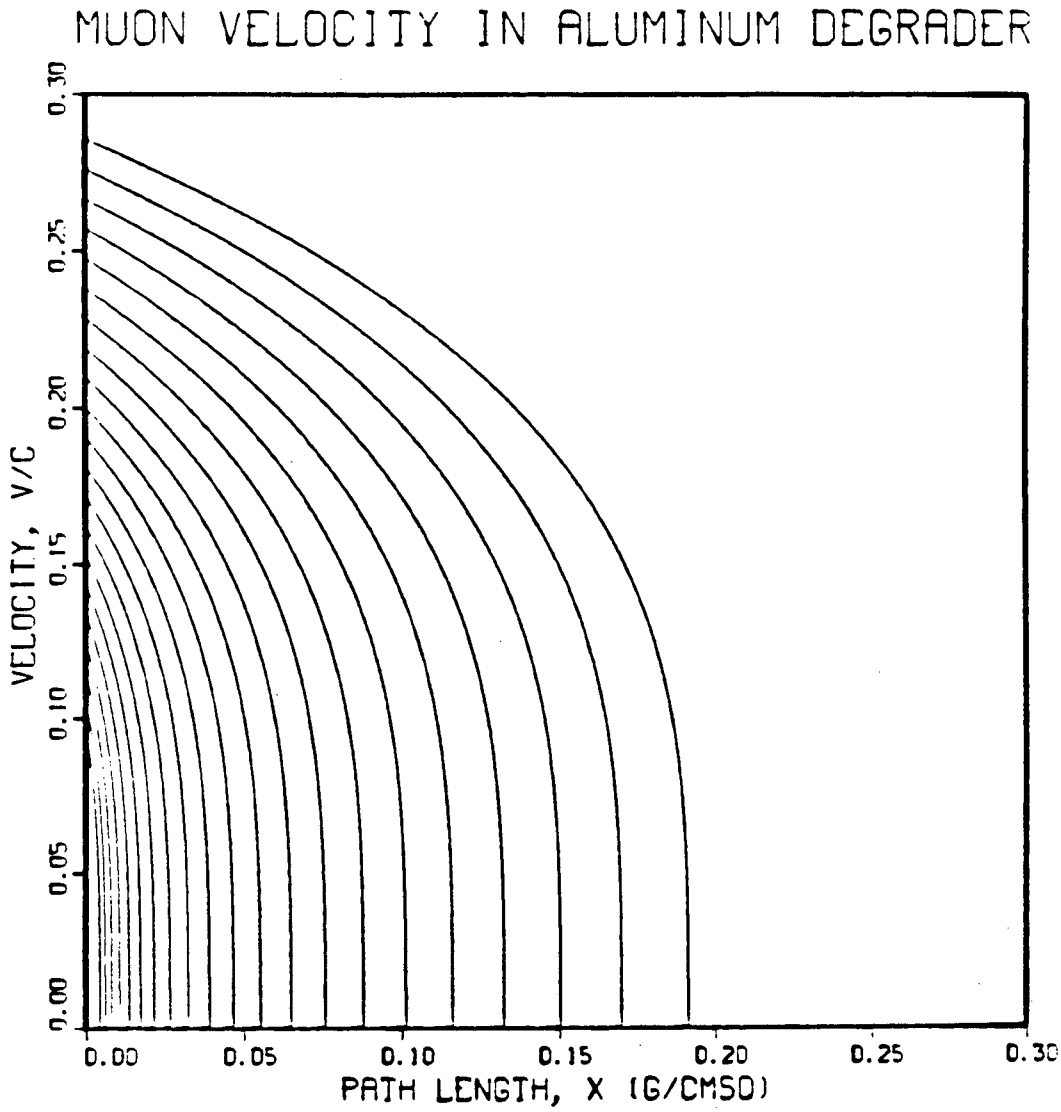

Figure 3.3: Muon velocity as a function of path length in an aluminum degrader.

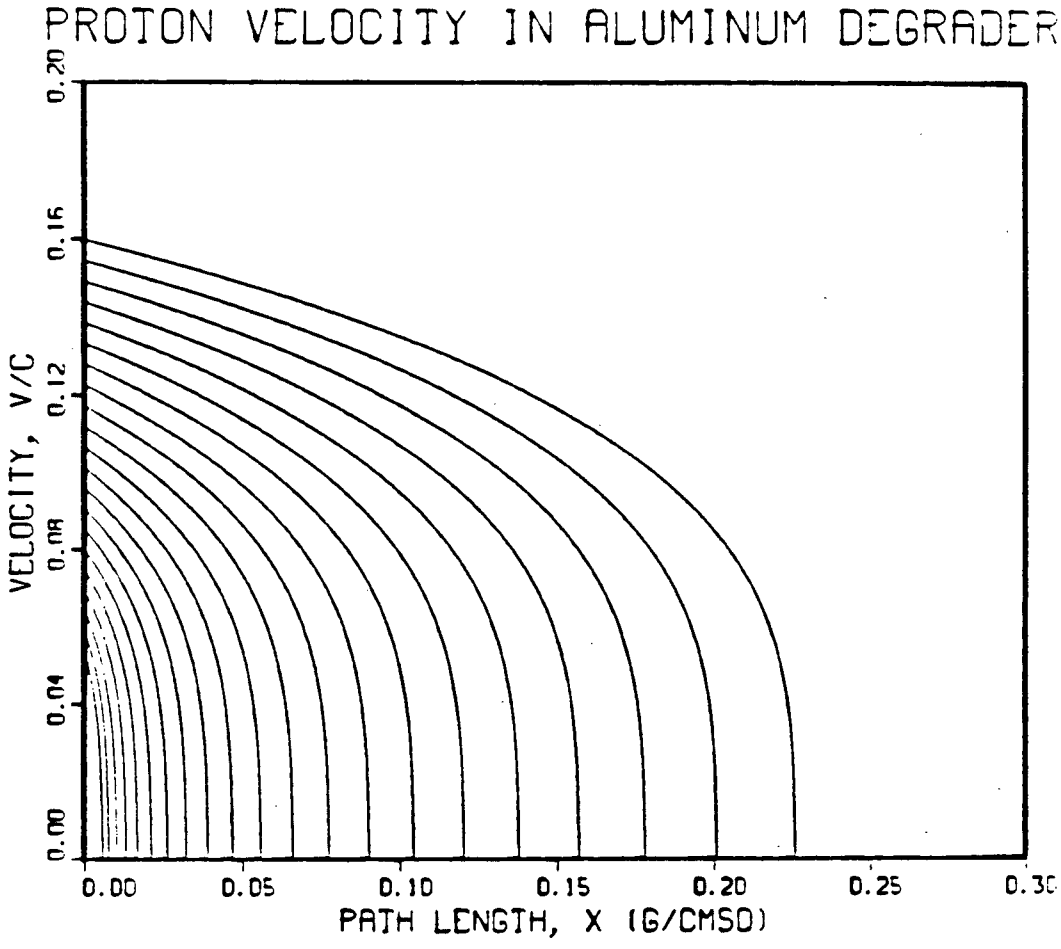

Figure 3.4: Proton velocity as a function of path length in an aluminum degrader.

$$\rho_x \simeq \begin{cases} (v/b)^{5/2}+1 \ ; \ p < p_x \\ 0 \ ; \ \text{otherwise} \end{cases}$$

...(3.10)

This is just the situation in the production target. Numerous experiments have confirmed equation 3.10. Figure 3.5 shows the results for the M13 beamline at TRIUMF (Oram, 1981b).

The secondary channel viewing the production target selects a range of momenta specified by $\Delta p_c/p_c$ where p_c is the channel momentum. Clearly, for fixed $\Delta p_c/p_c$ (see equation (3.8)) the number of muons transported will decrease as $p_c^{7/2}$.

Particles of momentum p_c from a secondary channel are incident on a degrader of thickness x. The output momenta fall in a range p_x to $p_x - \Delta p_x$ (the maximum momentum output is p_x). Even a mono-energetic beam (i.e. $\Delta p_c = 0$) would degrade to a non-zero value of Δp_x when straggling is taken into account; however, as long as random effects like straggling remove and contribute equal amounts to the range Δp_x, we can write

$$\frac{\Delta p_x}{p_x} \simeq \frac{\Delta p_c}{p_c} (p_c/p_x)^{7/2}$$

...(3.11)

Now, since $\Delta p_x/p_x$ is by defintion less than unity, we can predict the ratio p_c/p_x for which particles will begin to stop, given the value of $\Delta p_c/p_c$. Attempts to increase p_c/p_x

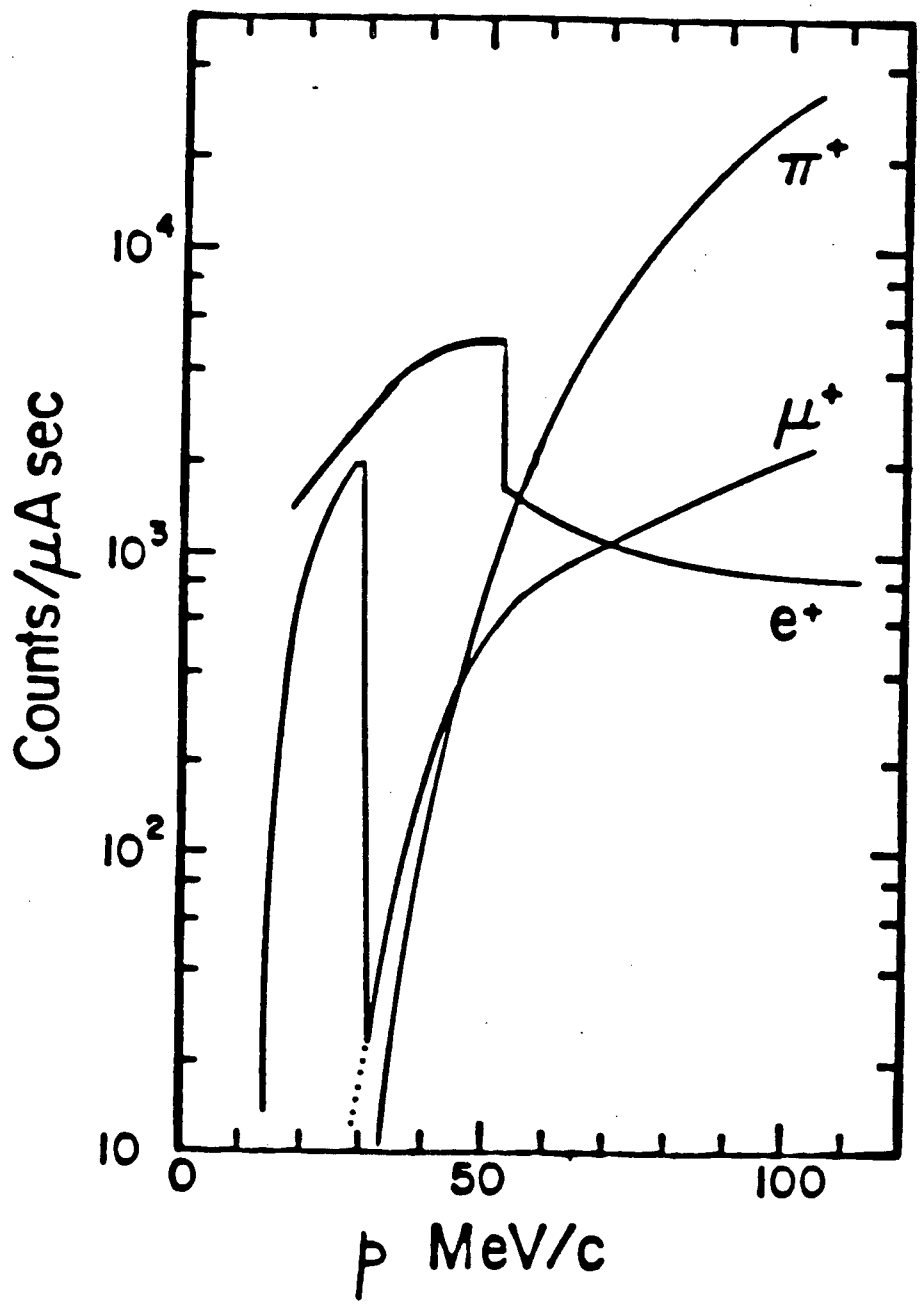

Figure 3.5: Number of particles available from the M13 beam line at TRIUMF as a function of momentum per μA of primary proton current at 500 MeV.

will result in more particles stopping in, and fewer particles emerging from, the degrader. The intensity (number of particles), I, emerging from a degrader under the condition that $\Delta p_x/p_x = 1$ is related to the intensity, I_c striking the degrader by

$$I = \frac{(2/7)v(v/b)^{5/2}+v}{\Delta v_c(v_c/b)^{5/2}} I_c \qquad \ldots(3.12)$$

Since the intensity I_c striking the degrader is proportional to $v_c^{7/2}\Delta v_c/v_c$, I is independent of the values of p_c and $\Delta p_c/p_c$. For example, in this experiment one calculates given $\Delta p_c/p_c = 7\%$ and $p_c = 15.4$ MeV/c that the number of particles emerging with $v < c/50$ is $0.012\ I_c$. It is emphasized that the result is independent of the beam line momentum interval and momentum. The "efficiency" of production, on the other hand, is 0.012 and does depend markedly on the beam line settings. Given the constraints of degrader thickness and that $v_x > c/50$ and ignoring straggling one wishes to minimize the denominator of equation 3.12 in order to maximize the efficiency.

It is interesting to calculate the ratio p_x/p_c for which half the particles stop in the degrader. The result is

$$p_x/p_c \simeq [(7/4)(\Delta p_c/p_c)]^{2/7} \qquad \ldots(3.13)$$

showing that half stop for $p_x/p_c = 1/2$ and $\Delta p_c/p_c$ equal to about 6%. If $\Delta p_c/p_c$ is zero, then initially momentum straggling will contribute an effective spread to the

momentum which in turn will be amplified by the processes discussed in this section so that half the particles will have stopped before p_x is zero.

3.5 THE STATISTICAL PROPERTIES OF A DEGRADER

The random nature of the moderation process has been ignored to this point. Monte Carlo studies of such processes are numerous but they are only as good as the underlying assumptions put into them. An understanding of at least the general features of the statisitics must precede any simulation using Monte Carlo methods.

3.5.1 MOMENTUM STRAGGLING

The primary agent which slows the surface μ^+ is collisions with electrons in the degrader. The characteristic momentum change in such a collision is

$$\Delta p = -mp/M \qquad \ldots(3.14)$$

where p is the momentum of the projectile, M is the mass of the projectile and m is the electron mass. It follows that for a momentum loss dp the mean number μ of such collisions is

$$\mu = -\frac{M}{m}\frac{dp}{p} \qquad \ldots(3.15)$$

The variance or mean squared deviation of the momentum loss

is

$$\mathrm{var}(dp) = \mu(mp/M)^2 = \frac{m}{M}\, p\,dp \qquad \ldots(3.16)$$

where Poisson statistics have been assumed for μ. If we assume independence of each dp as the particle slows down (this is only approximately true) we can get a rough idea of the magnitude of the straggling involved in slowing a particle of momentum p_0 to momentum p.

$$\mathrm{var}(p_0-p) = \frac{1}{2}\frac{m}{M}(p_0{}^2-p^2) \qquad \ldots(3.17)$$

Hence, one expects straggling on the order of $\sqrt{\{m/(2M)\}}$ = 5% for stopping muons.

3.5.2 MULTIPLE SCATTERING

The dominant source of angular deflection in degrading surface muons is Rutherford scattering by the coulomb fields of the degrader nuclei. The mean squared deviation of the deflection angle in a collision is (projected into a plane)

$$d\phi^2{}_{\mathrm{plane}} = 2\left[\frac{a\hbar c Z}{p\beta b}\right]^2 \qquad \ldots(3.18)$$

where a is the fine structure constant and Z/b is the effective value of the charge to impact parameter ratio for the collision. Taking the example of aluminum (density = 2.7g/cm^3 or $6\cdot10^{22}$ atoms/cm^3) one obtains the average

deflection per unit degrader thiskness,

$$d\phi^2_{plane} \simeq \frac{6}{(p\beta)^2} dx \qquad ...(3.19)$$

for $(Z/b)^2_{average}$ of about $1 \cdot 10^{19} cm^{-2}$, dx in g/cm^2 and p in MeV/c. These rough arguments and calculations confirm the approximate validity of the multiple scattering formula recommended for common use by the Particle Data Group (Particle Data Group, 1984) which is:

$$\phi_{plane} = \frac{14.1}{p\beta} \left[\frac{x}{x_{rad}}\right]^{1/2} \qquad ...(3.20)$$

Using the radiation length for aluminum, $x_{rad} = 24\ g/cm^2$ in equation 3.20 one obtains:

$$d\phi^2_{plane} \simeq \frac{8}{(p\beta)^2} dx \qquad ...(3.21)$$

which agrees fairly well with equation 3.19.

3.6 MONTE CARLO SIMULATION OF MODERATION OF THE MUON BEAM

In order to obtain quantitative predictions to compare with the experiment the assumptions previously outlined in this chapter were incorporated into a Monte Carlo computer program. The momentum change and angle of multiple scattering were calculated for small steps as the particle traversed the foil. For simplicity it was assumed that the total degrader thickness was 0.0180 g/cm^2 of aluminum. The

change in momentum Δp (including straggling) for a small distance Δx in the foil is given by

$$\Delta p = \Delta x \; dp/dx + \Delta S \qquad \ldots(3.22)$$

where ΔS is a random variable with a normal distribution having variance specified by

$$\mathrm{var}(\Delta S) = \frac{m}{M} \frac{dp}{dx} \Delta x \qquad \ldots(3.23)$$

The angular deflection of $\Delta\phi_{space}$ for each Δx is a random variable having a normal distribution with variance given by

$$\mathrm{var}(\Delta\phi_{space}) = 2 \frac{(14.1)^2}{(p\beta)^2} \frac{\Delta x}{x_{rad}} \qquad \ldots(3.24)$$

A muon is deemed to have stopped if its velocity is less than c/300, without having emerged from the foil (because it is of little consequence in this experiment). Figure 3.6 shows the fraction of the beam which stops for beams of small $\Delta p/p$. It is seen that the Monte Carlo simulation predicts that the transition from all μ^+ stopping to virtually all passing through the foil occurs over a small momentum change, approximately 5% of the incident momentum. Thus if a momentum interval $\Delta p/p$ much less than 5% is used in an experiment we can mimic the results shown in Figure 3.6. Figure 3.7 shows the predicted fraction of the beam which emerges from the foil with momentum less than 2 MeV/c, for various beam momenta. The result compares well

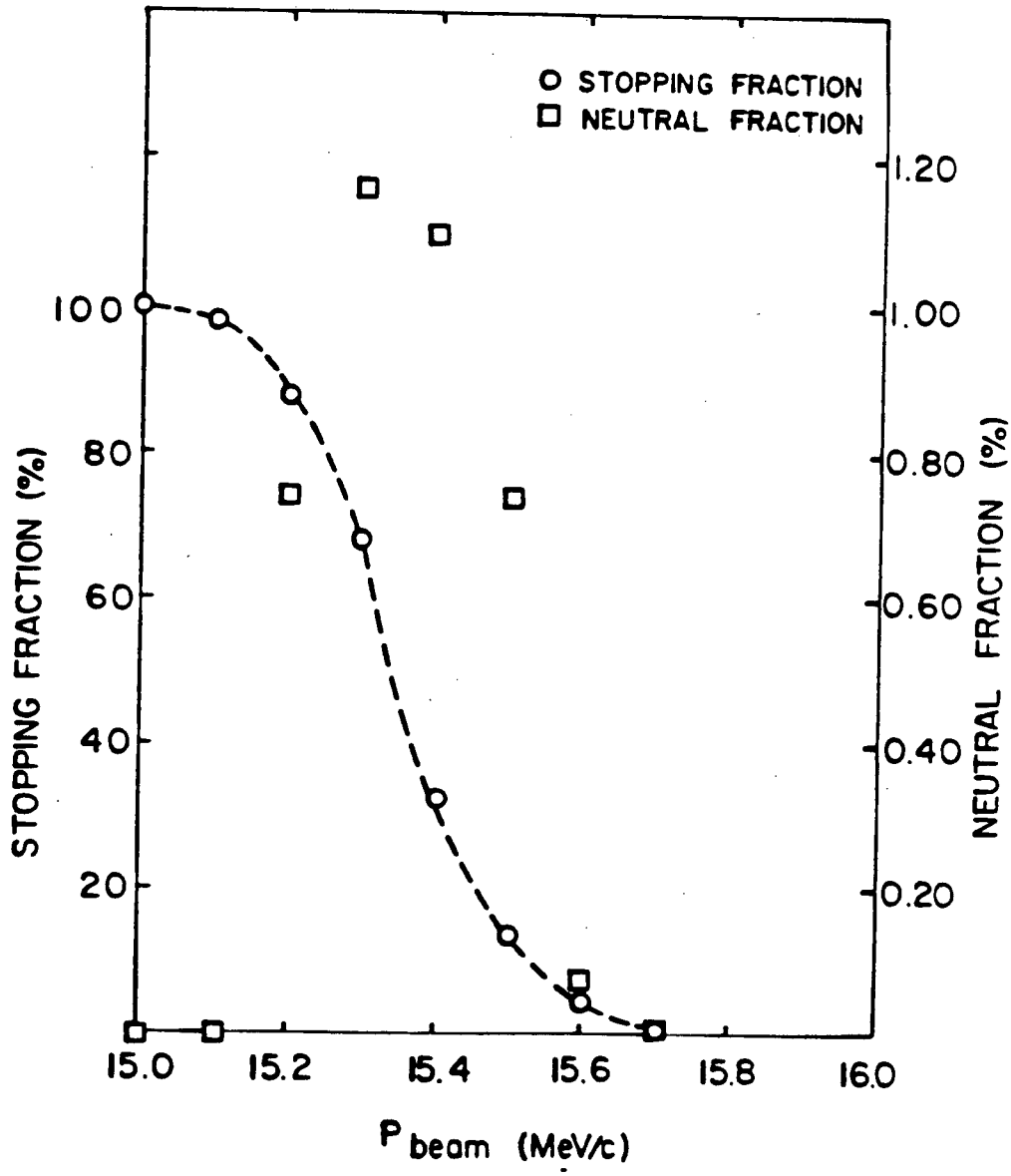

Figure 3.6: Monte Carlo results for the fraction of a muon beam stopping in an aluminum degrader and the neutral fraction as a function of incident momentum.

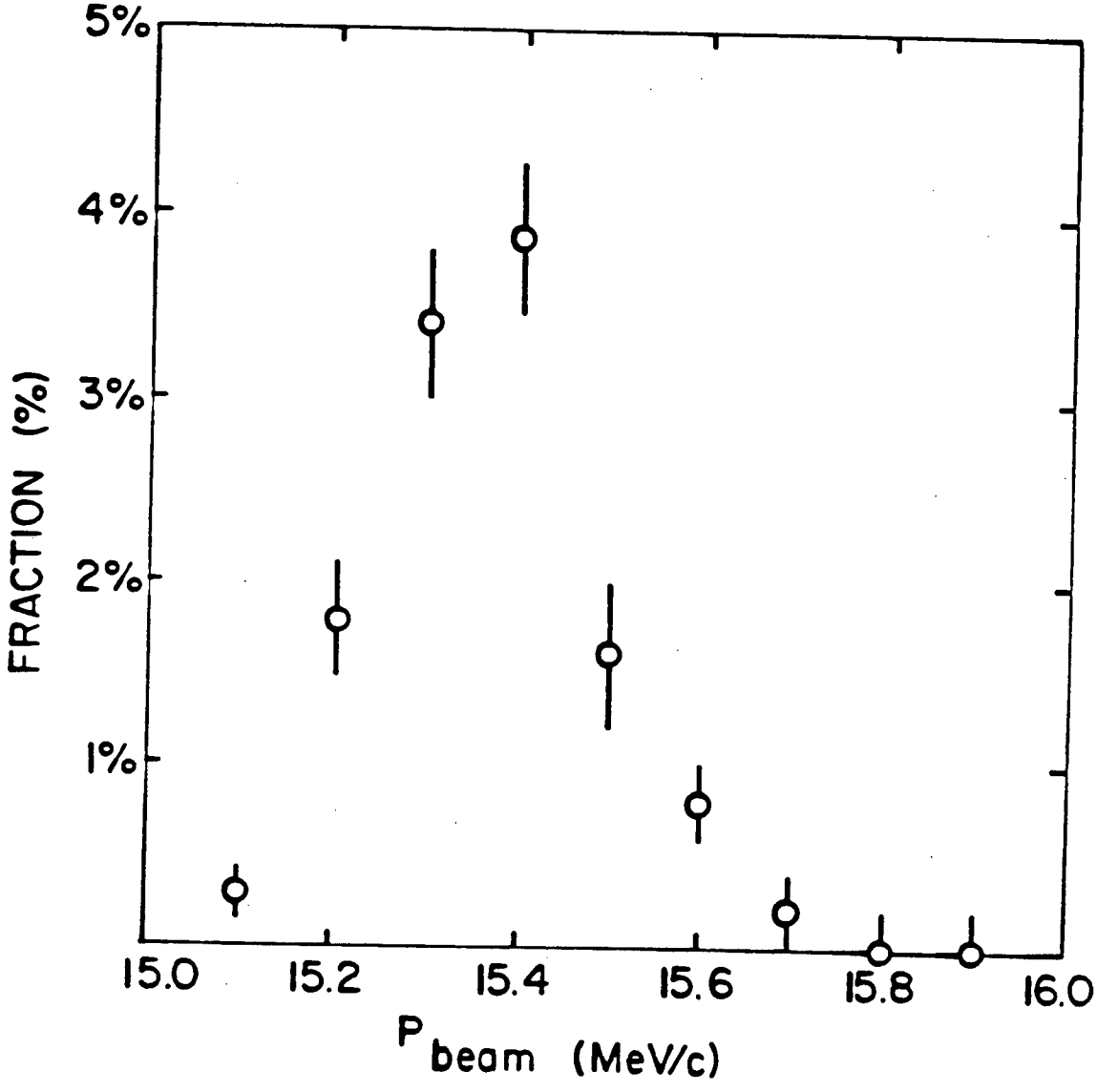

Figure 3.7: Monte Carlo results for the fraction of the beam emerging from the degrader with momentum less than 2 MeV/c as a function of the incident muon momentum.

with that of equation 3.12 which predicted for an incident momentum of 15.4 MeV/c ±3.5% that 1.2% of the beam would emerge from the degrader with $p \leq 2$ MeV/c. Figure 3.8 shows the data of Figure 3.7 compared to experimental results obtained while tuning the beam line to find the optimal momentum setting. (The comparison is not the result of any fit of the data but merely serves to illustrate the agreement visually.) Figure 3.6 also shows the neutral fraction as a function of beam momentum. The neutral fraction peaks near 15.4 MeV/c reaching a value of about 1.2% at the momentum for which half the incident beam is stopped.

The Monte Carlo results indicate that for a real beam at 15.4 MeV/c ±3.5% one expects 50% to stop. The expected fraction of the beam which emerges from the foil as neutrals is 0.34%.

Finally one can attempt to predict the number of particles which will strike MCPB (see chapter 5). This, however is quite sensitive to the multiple scattering assumed and therefore should be cautiously used in predicting rates. The predicted rate striking MCPB is about 20% of the incident beam. Most of the particles have momenta near 7 MeV/c. The number of neutrals which strike MCPB is approximately 0.06% of the incident beam. One can say something about the efficiency of the micro-channel plate MCPB to muons. The observed fraction of particles detected by MCPB was 13% of the incident beam; correcting for the

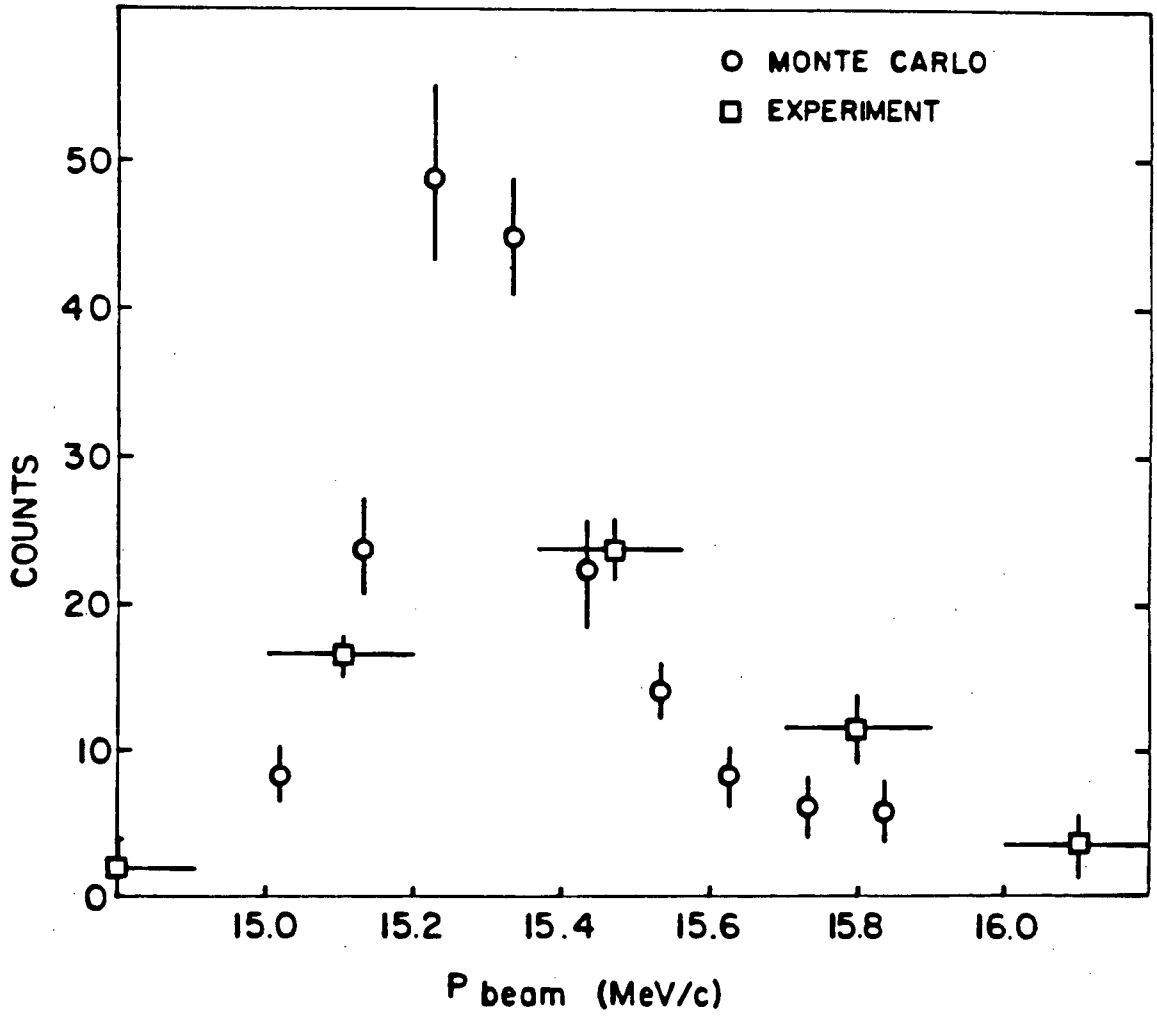

Figure 3.8: Comparison of the Monte Carlo results with experiment for the number of particles emerging from the foil with momentum less than 2 MeV/c as a function of incident momentum.

funnelled holes which cover only 70% of the MCP surface area, one obtains an efficiency of about 90% for muons in the momentum range above 4 MeV/c. The efficiency to ground-state neutrals is seen to be of the order of 15% using the observed rate of Lyman-α detection in this experiment.

3.7 SUMMARY

The production of epithermal muonium by a beam foil technique is feasible but difficult. The main problem is to degrade the muon momentum from 29.86 MeV/c (with which it is born) to something below 2 MeV/c. The non-zero momentum acceptance of a secondary channel and momentum straggling will limit the amount by which the muon beam average momentum can be usefully reduced. If the beam line is tuned so as to select as low a momentum as is possible, given the limitations of degrader thickness, then the efficiency of production of epithermal muonium is increased. In effect the degrader has been moved to the production target and the beam line selects "sub-surface" muons. The number of particles entering the experimental apparatus is thus reduced while the number of muonium atoms produced remains constant. It is optimal, in terms of signal to noise, to have as low a mass as possible in the beam at the experimental area. Eventually further reduction of the beam line momentum will introduce significant losses due to muon decay.

4. RADIO-FREQUENCY EXCITATION OF THE LAMB SHIFT TRANSITION

4.1 THE TIME DEPENDENT SCHRÖDINGER EQUATION

In this chapter analytic methods, which are of necessity approximations, are developed to deal with the evolution of a muonium atom produced in a beam foil interaction and subsequently entering a region in which transitions are induced between the $2p_{1/2}$ and $2s_{1/2}$ levels by application of an RF field. The effect of the DC electric quench field is a special case (zero frequency) of the treatment.

We start with the time dependent Schrödinger equation,

$$i\hbar\frac{\partial|\psi\rangle}{\partial t} = H|\psi\rangle \qquad \ldots(4.1)$$

The hamiltonian, H, is a sum of three terms: [1]

$$H = H_0 + H_{decay} + H_{int} \qquad \ldots(4.2)$$

H_0 is a hermitian operator, the eigenvalues and eigenstates of which describe the free muonium atom. H_{decay} is an anti-hermitian operator which accounts (phenomenologically) for the decay of the excited states of the atom. The eigenvalues of H_{decay} are $i\hbar\gamma_j/2$, where γ_j is the decay rate or inverse mean lifetime of the jth state. H_{int} is the interaction Hamiltonian for the muonium atom in the RF field. It can be written in the form

[1]This approach was suggested by S.R. Lundeen

$$H_{int} = -e\bar{E}\cdot\bar{r}$$

...(4.3)

where $\bar{r}$ is the separation of the electron and muon in the muonium atom and $\bar{E}$ is the time varying electric field vector of the RF field which we will assume to be in the $\hat{x}$ direction and to have a cosine dependence, i.e.

$$\bar{E} = E_0\cos(\omega t - \delta)\hat{x}$$

...(4.4)

where δ represents the phase of the RF field.

Experiment and calculation suggest that the beam foil interaction will prepare muonium mostly in nS states for velocities greater than c/200. The amplitude for preparation of coherent mixtures of different angular momentum states or of higher angular momentum states (e.g. np-states) is much smaller.

The solution of equation 4.1 is of the form

$$|\psi(t)\rangle = U(t)|\psi(0)\rangle$$

...(4.5)

where $|\psi(0)\rangle$ is the state at t=0 and U(t) is called the finite time evolution operator. In the case where H is time independent, or, more generally, where $\int H(t)dt$ and $H(t)$ commute, the solution of 4.1 can be written down immediately as

$$U(t) = \exp\{ -i\int H(\tau)d\tau/\hbar\}$$

...(4.6)

4.2 APPROXIMATE SOLUTION

One now makes some assumptions in order to simplify the problem. We restrict our problem to one at low RF power and at RF frequencies expected to excite the Lamb shift transitions. In particular we neglect the presence of the nearby $2p_{3/2}$ state and defer estimates of the effect of its presence. Thus we have restricted the problem to one over the subspace spanned by the basis of the $2s_{1/2}$ and $2p_{1/2}$ states. The coupling of the ground state to this subspace is included phenomenologically through H_{decay}. Appropriate choice of the basis functions for this subspace allows us to write H_{int} in such a way as to further subdivide the problem into one involving one hyperfine level from each of the p and s states, say $|s\rangle$ and $|p\rangle$. Equation 4.1 in matrix form becomes:

$$i\frac{\partial}{\partial t}\begin{bmatrix}|s\rangle \\ |p\rangle\end{bmatrix} = \begin{bmatrix}(\omega_s - i\gamma_s/2) \;, & 2V\cos(\omega t-\delta) \\ 2V\cos(\omega t-\delta), & (\omega_p - i\gamma_p/2)\end{bmatrix}\begin{bmatrix}|s\rangle \\ |p\rangle\end{bmatrix} \qquad \ldots(4.7)$$

where $V = -eE_0\langle p|x|s\rangle/2\hbar$ and $|\langle p|x|s\rangle|^2 = 3a^2$ (a is the Bohr radius of the 1s state).

Let us define a unitary transformation A,

$$A = \begin{bmatrix} e^{+i\omega t/2}, & 0 \\ 0, & e^{-i\omega t/2} \end{bmatrix}$$

...(4.8)

we also define

$$H_A = AHA^\dagger + i\hbar\partial A/\partial t\ A^\dagger$$

...(4.9)

so that $A|\psi>$ satisfies equation 4.1 when H is replaced by H_A. The transformed Hamiltonian H_A is a sum of two terms:

$$\frac{H_A}{\hbar} = \begin{bmatrix} \omega_s-\omega/2-i\gamma_s/2, & Ve^{i\delta} \\ Ve^{i\delta}, & \omega_p+\omega/2-i\gamma_p/2 \end{bmatrix} + \begin{bmatrix} 0, & Ve^{+i\delta t} \\ Ve^{-i\delta t}, & 0 \end{bmatrix}$$

...(4.10)

The first term of H_A is time independent. If its trace is small, i.e. if $\omega \approx \omega_s-\omega_p$, then the effect of the off diagonal term $Ve^{i\delta}$ will be large. We define H' equal to the first term and neglect for the time being the rapidly varying second term. This is known as the "rotating field approximation".

The solution for the time evolution operator is now simply:

$$U(t) = \exp\{ -iH't/\hbar\}$$

...(4.11)

Clearly, a transformation which diagonalizes H' will also

diagonalize U. The eigenvalues of H' are

$$\hbar\lambda_s = \{\omega_s+\omega_p-i(\gamma_s+\gamma_p)/2+$$
$$+(\omega_s-\omega_p-\omega-i\gamma_s/2+i\gamma_p/2)\sqrt{1+(4V^2/(\omega_s-\omega_p-\omega-i\gamma_s/2+i\gamma_p/2)}\}/2$$
$$\hbar\lambda_p = \{\omega_s+\omega_p-i(\gamma_s+\gamma_p)/2+$$
$$-(\omega_s-\omega_p-\omega-i\gamma_s/2+i\gamma_p/2)\sqrt{1+(4V^2/(\omega_s-\omega_p-\omega-i\gamma_s/2+i\gamma_p/2)^2}\}/2$$

...(4.12)

where λ_s corresponds to the state which is mostly an s-state and λ_p to that which is mostly a p-state.

The imaginary part of λ_s is proportional to the inverse mean lifetime, $1/\tau$ of the s-state in the RF field. Expanding the square root one obtains

$$\frac{1}{\tau} = -2\mathrm{Im}\lambda_s \simeq \gamma_s + \frac{V^2(\gamma_p-\gamma_s)}{(\omega_s-\omega_p-\omega)^2+(\gamma_s-\gamma_p)^2/4}$$

...(4.13)

We note that the expression is symmetric about $\omega = \omega_s-\omega_p$ and that there is no observable resonance unless γ_s differs from γ_p. The decay rate is a maximum for $\omega = \omega_s - \omega_p$. Of course γ_s is small for the 2s state which has a mean lifetime of about 1/7 second. Writing (4.13) in terms of the average power flux $\sigma = cE_0^2/16\pi$ instead of the electric field, neglecting γ_s we have

$$\frac{1}{\tau} = \gamma_p \cdot \frac{4\pi e^2\sigma}{\hbar^2 c} \cdot \frac{|\langle s|\hat{x}|p\rangle|^2}{(\omega_s-\omega_p-\omega)^2+\gamma_p{}^2/4}$$

...(4.14)

This is identical to the expression appearing in Lamb's original work (Lamb, 1952).

4.2.1 DC STARK EFFECT

Equations 4.12 also give the energy shift and lifetime for the case of a DC electric field. The energy shifts of the "2s" and "2p" states are equal and opposite so as to increase their separation. The changes in the decay rates are also equal and opposite such that the lifetime of the "2p" state is increased and that of the "2s" state decreased. The results for the quadratic Stark effect (from equation (4.12) in the limit of small V) are given below:

$$\Delta\gamma_s = -\Delta\gamma_p \simeq \frac{V^2(\gamma_p-\gamma_s)}{(\omega_s-\omega_p)^2}$$

$$\Delta E_s = -\Delta E_p \simeq \frac{V^2}{\omega_s-\omega_p} \qquad \ldots(4.15)$$

The values given by equation 4.12 for the DC Stark effect do not involve the "rotating field approximation" but still do neglect the presence of the $2p_{3/2}$ states.

4.2.2 AC STARK SHIFT

The second term of H_A varies rapidly. The effect of this term is similar to the DC Stark effect when averaged over all values of δ, reducing the DC result by half. We consider it as a perturbation and obtain an estimate of the AC Stark shift (from equation 4.10).

$$\Delta E_s = -\Delta E_p \simeq \frac{V^2}{2(\omega_s-\omega_p)} \qquad \ldots(4.16)$$

4.2.3 EFFECT OF THE $2P_{3/2}$ STATE

The RF field also has matrix elements between the $2s_{1/2}$ and $2p_{3/2}$ states which we have until now neglected. Considering these as perturbations and summing over the various matrix elements (one hyperfine component of the $2s_{1/2}$ level connects to two components of the $2p_{3/2}$ level) one obtains

$$\Delta E_s = -2\frac{(eE_0)^2}{2\hbar^2}\frac{|\langle p_{3/2}|x|s\rangle|^2}{\omega_s-\omega_{p3/2}} \qquad \ldots(4.17)$$

The value of $|\langle p_{3/2}|x|s\rangle|^2$ is $3a^2$.

5. DESCRIPTION OF THE APPARATUS AND EXPERIMENTAL PROCEDURE

5.1 VACUUM SYSTEM

The apparatus shown in Figure 5.1 was separated from the beam line by a 50 μm mylar window. The operating pressure of approximately 10^{-5} Torr was maintained by a 4 inch diffusion pump operating through a liquid nitrogen cold trap and gate valve assembly. The cold trap was necessary to minimize oil entering the apparatus which would have had deleterious effects on the microchannel plates. The gate valve was controlled automatically so that if the vacuum were to change by about 10^{-5} Torr it would be closed to prevent not only possible damage to the diffusion pump but more importantly, the possible flow of oil particles into the apparatus should the cold trap begin to warm up. Had there been an oil free pumping system available (e.g., a turbo molecular pump) the system would have been much simpler and more reliable.

5.2 SCINTILLATION COUNTERS

The incident scintillator (X) and collimating scintillator were mounted on sliding flanges to permit access to the foil and RF regions. The front of the box scintillator (BOX) consisted of two scintillators which entered from opposite sides of the apparatus and meshed together to form a 3.8 cm x 1.3 cm slit at the entrance to the quench region. The remaining five scintillators which formed the top, bottom,

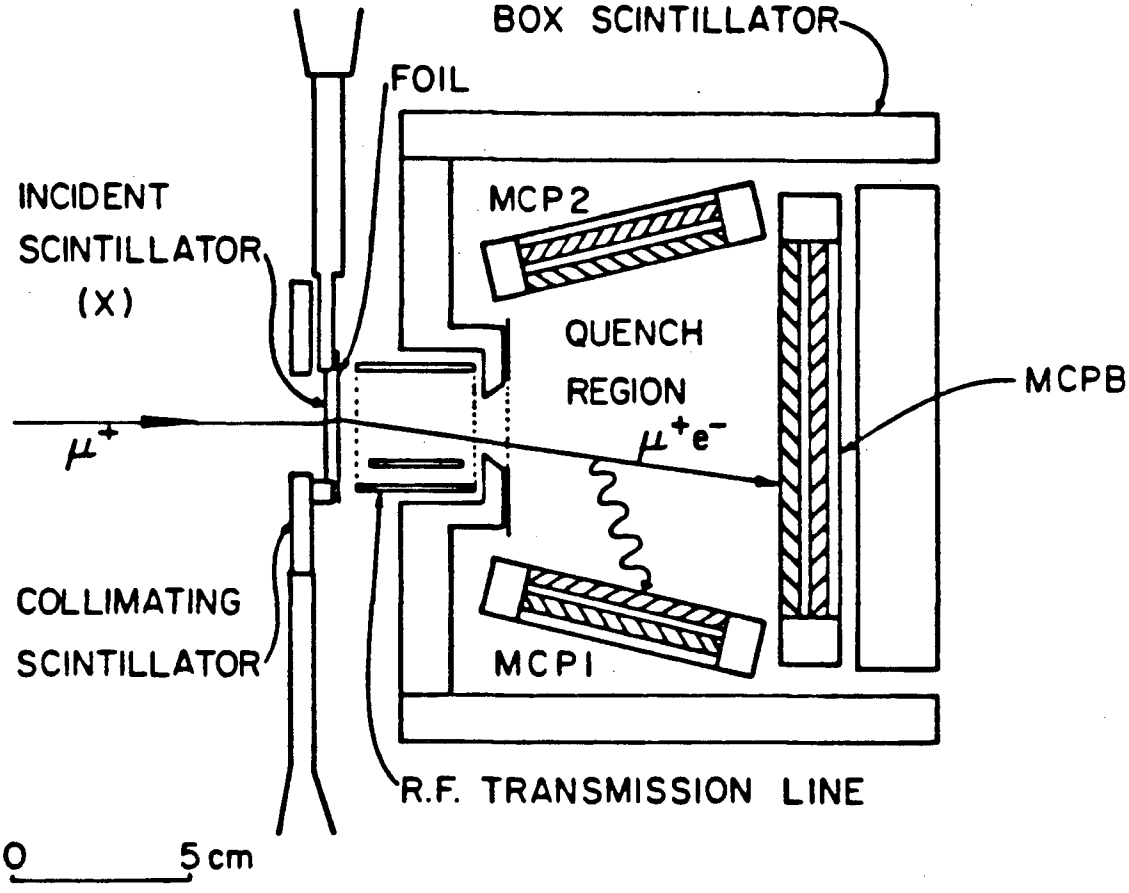

Figure 5.1: A schematic diagram of the apparatus.

sides and rear of the box scintillator were mounted on five light guides entering from the rear of the apparatus. The wrapping of the scintillators was not completely light tight so a low level of "cross talk" was observed in the various scintillators of the box. The incident counter was a 2.5 cm diameter disk, 63 μm thick. Light collection was from two opposite light guides and facilitated by a thin 0.75 μm aluminum wrapping. The voltages on the photomultipliers for each scintillator were interlocked in the same way as the gate valve (in section 5.1) so that the photomultipliers would be turned off should the apparatus be let up to atmospheric pressure and (possibly) opened, admitting light to the scintillators.

The box scintillator was used to veto copious beam positrons (see Figure 3.5), which passed through the apparatus, and decay positrons (one for every μ^+!) which exited the box triggering one of the microchannel plates. The incident counter could also be replaced by a very thin (7.5 μm) scintillator which permitted simulation of the muon beam using an ^{241}Am alpha source.

5.3 NEUTRAL PRODUCTION FOIL

The 0.75 μm Al foil used to produce neutrals was mounted on the RF transmission line assembly shown in Figure 5.2. Table 5.1 summarizes the various masses in the beam.

Table 5.1

Masses in the Beam

Material	t(μm)	ρ(g/cm²)	Mass (mg/cm²)	Equivalent Mass Al (mg/cm²)
Mylar Beam Pipe Window, ($C_5H_8O_2$)	51	1.39	7.06	7.65
Scintillator (X) $(CH)^k$	63	1.03	6.54	7.32
Scintillator Wrapping (Al)	1.50	2.70	0.40	0.40
Foil (Al)	0.75	2.70	0.20	0.20
Total Equivalent Mass (Al)				16.6

Table 5.1: Summary of materials present in the path of the muon beam.

5.4 RF REGION

The RF region was a radio frequency transmission line shown in Figure 5.2. It was based on a design by F.M. Pipkin (Pipkin, 1982). A simple calculation using the dimensions given in Figure 5.2 shows that the impedance at the centre of the line is about 50 ohms. Measurement of the impedance characteristics of the RF transmission line confirmed the calculation. If P is the power transmitted in watts, the average (rms) voltage difference between the central conductor and the grounded outer conductor is:

$$V_{rms} = \sqrt{50\ P}\ [\text{volt}] \qquad \ldots(5.1)$$

The power density in the upper part of the transmission line is:

$$0.04\ P\ [\text{w/cm}^2] \qquad \ldots(5.2)$$

The power through the transmission line was monitored and continuously regulated using the circuit shown in Figure 5.3. The frequency of the RF source was remotely set by the data acquisition computer, which switched to a different frequency every few minutes. In addition, the actual frequency transmitted was read by a frequency counter and sent back to the computer to be recorded with other data. An improvement for a subsequent experiment would be the addition of computer controlled switching and read back of the power level.

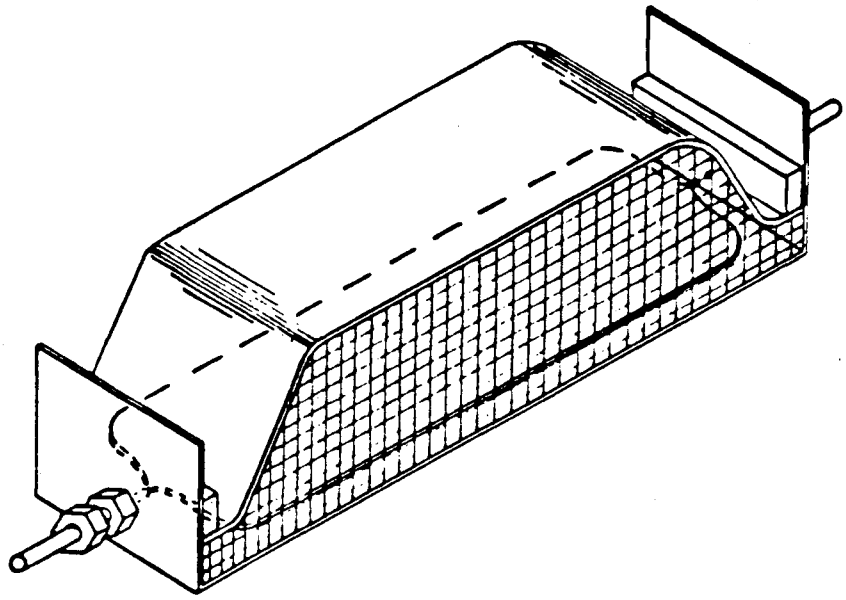

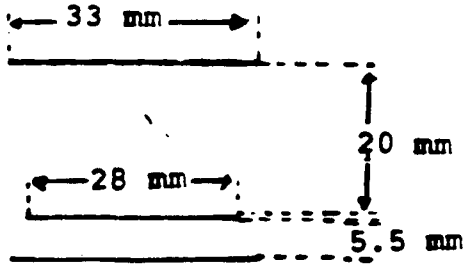

Figure 5.2: The RF transmission line arrangement.

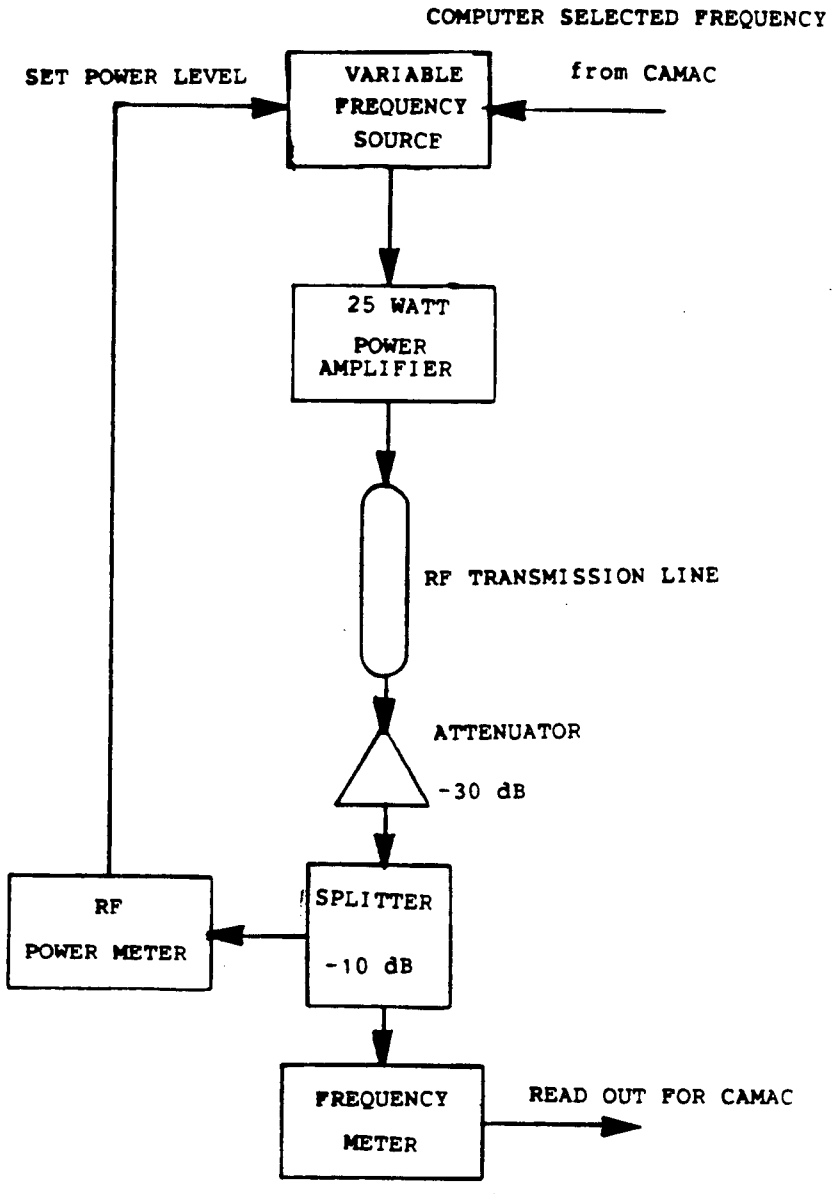

Figure 5.3: The RF system.

5.5 THE QUENCH REGION AND MICROCHANNEL PLATES

Figure 5.4 shows the potential map of the electric field in the quench region as viewed from the side at the midplane of the apparatus (computed numerically). The equipotentials (30 equal increments) show that the electric field maintained between the front faces of the three channel plates and the grid at the entrance slit was approximately parallel to the beam direction, strongest at the entrance (about 500 V/cm), and decreased linearly to about 200 V/cm at the microchannel plate labelled MCPB. The quench region electric field also served to prevent electrons ejected from the foil from reaching the microchannel plates.

Situated inside the box scintillator above and below the quench region were two 40 mm diameter microchannel plates (MCP1 and MCP2)[1]. These were used to detect Lyman-α photons (122 nm) from the stark quenching of any excited states which entered the quench region. A larger rectangular (92 mm x 75 mm) microchannel plate (MCPB) was used to stop the muonium atoms, determining the time of flight from the incident counter (X) over a minimum effective path length from the foil of 11.4 cm.

All three microchannel plates were "funneled" to increase their sensitive area to 68% from the value of 55% for unfunneled types. The front faces were coated (at the factory) with a layer of CsI to enhance their efficiency to Lyman α photons by a factor of ten (see Figure 5.5). The

[1] The three microchannel plates used in this experiment were manufactured by Galileo Corporation, Mass., USA.

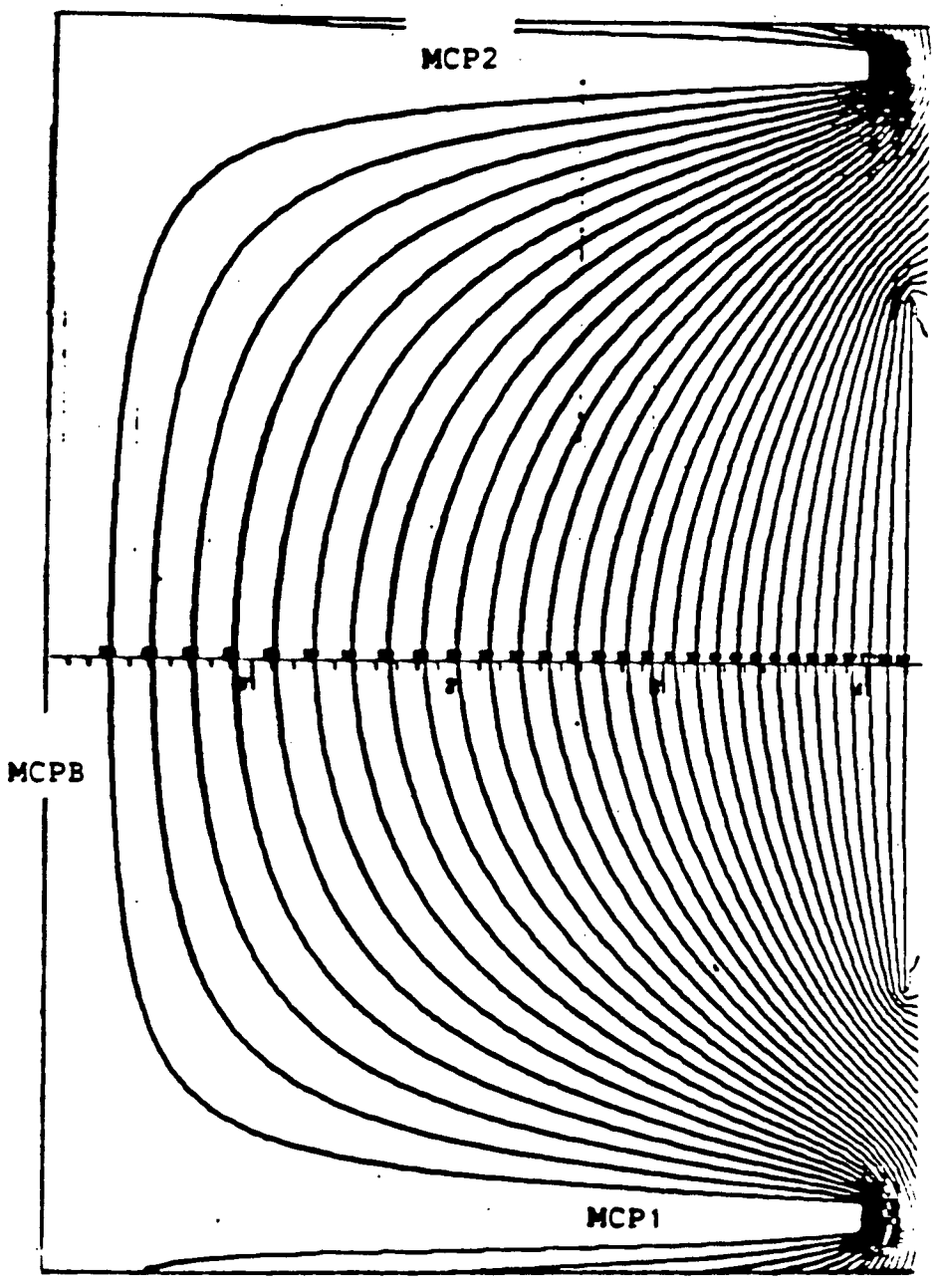

Figure 5.4: The electric field in the quench region. View is from the side at the vertical midplane.

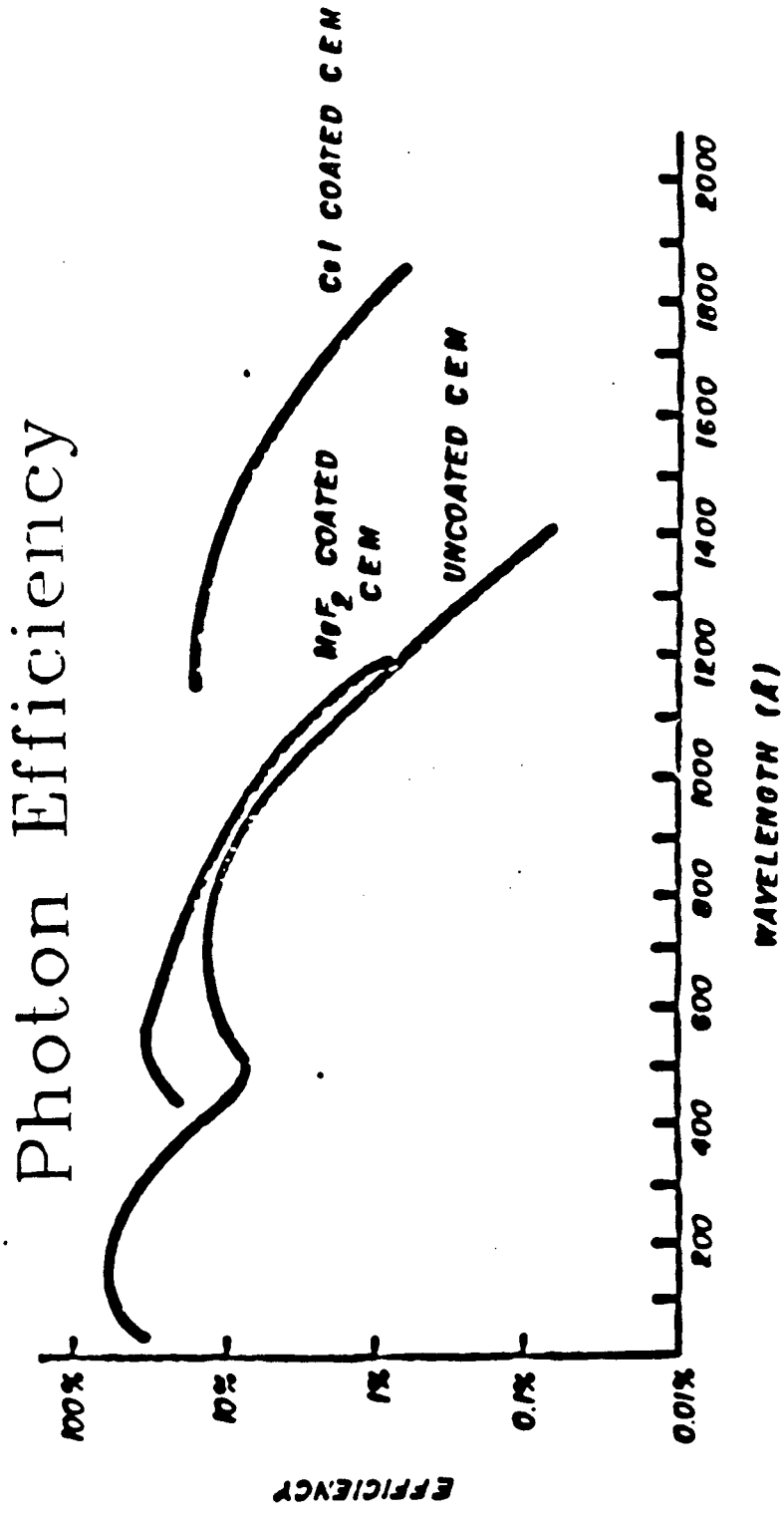

Figure 5.5: Efficiency of channel electron multipliers as a function of wave length.

enhancement is, however, difficult to maintian because CsI is hydroscopic. Even a few minutes of exposure to room air was observed to greatly decrease their efficiency. In order to rejuvenate the MCP's CsI coating, two quartz halogen 55 W bulbs[1] were installed to left and right of the entrance slit of the quench region. It was then possible to rapidly heat the front surfaces of the MCP's using these bulbs in the vacuum, causing the desorption of water from the CsI coating. It was also possible to observe the response of the MCP's to photons since at even longer wavelengths there is some small probability of detection.

Figure 5.6 shows the circuitry used to run each microchannel plate. Typically the front surface of each MCP was maintained at -2000 V, which was responsible for maintaining the quench region field described above. The high voltages supplied to the MCP's by three independent HV power supplies were each interlocked to the system that controlled the gate valve and photomultiplier voltages. As a safety measure, each supply was set so that an increase in current by about 50% would cause it to shut off.

5.6 DATA ACQUISITION AND EVENT TRIGGER

A Digital Equipment Corporation PDP-11/34 computer running the program MULTI (T. Miles, 1983) and using standard CAMAC (CAMAC, 1982) was used to control various experimental parameters and to acquire and record data. A simplified

[1] Chosen for their small size.

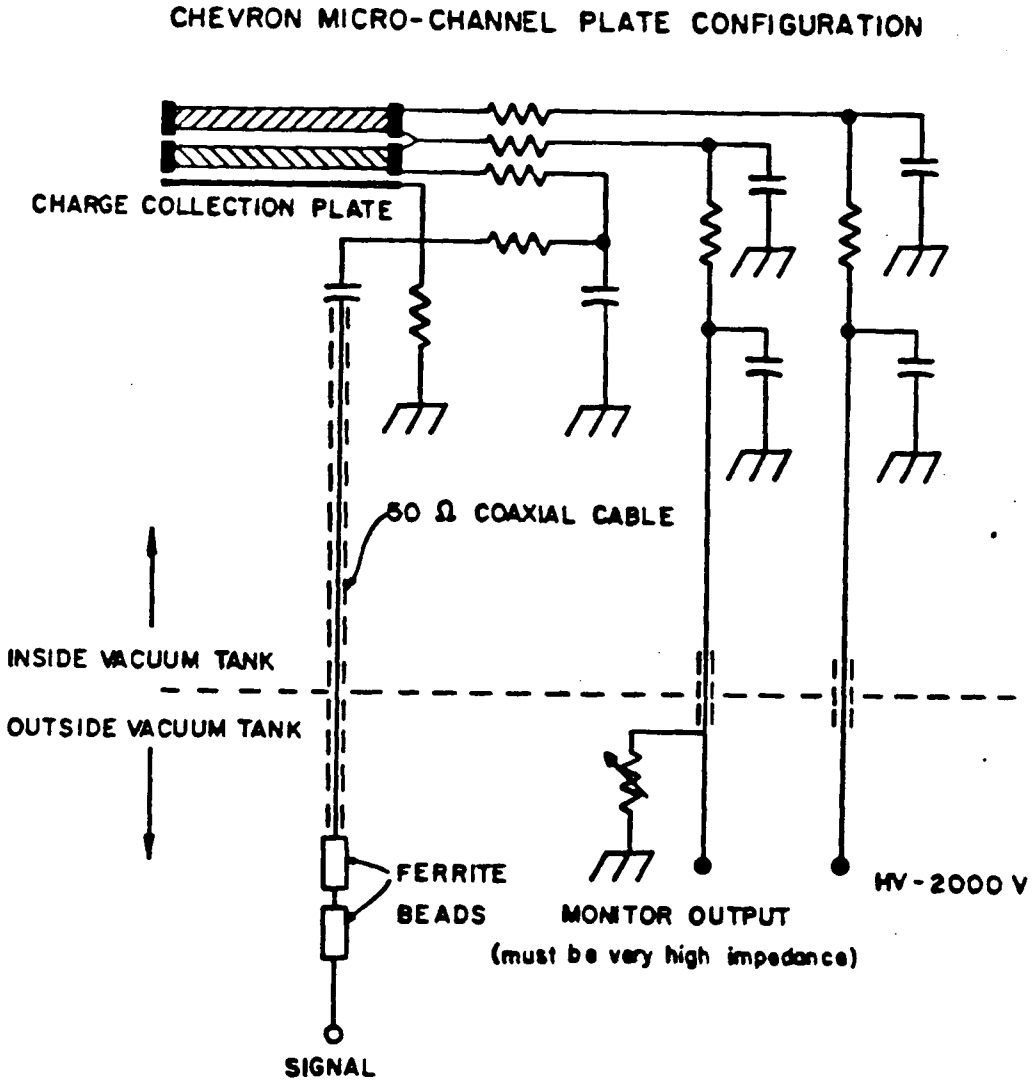

Figure 5.6: Typical circuit used to run a micro-channel plate. Specific values of the resistances and capacitances depend on the size and kind of micro-channel plates.

logic schematic is shown in Figure 5.7.

The event trigger had three requirements (see Figure 5.7). A muon detected by the incident scintillator (X) started the CAMAC TDC's as well as a 500 ns gate (WIDE X) during which a pulse from MCPB and from one or other of MCP1 or MCP2 must have been detected. This event trigger obviously accepted many more events unlikely to be due to 2s muonium quenching than those likely to be due to it. However, it was possible to select the interesting events off-line since the times of all pulses on the MCP's were recorded.

Each event recorded (on magnetic tape) had several additional pieces of information not mentioned above. The pulse heights of the four incident scintillators and three MCP's were recorded. The RF frequency was monitored and recorded as were the times (relative to the time of a pulse on the incident scintillator) of pulses on each of the scintillators of the BOX and the collimating scintillator, as well as the times of the previous and next pulses in the incident scintillator.

5.7 BEAM PARAMETERS AND EXPERIMENTAL RATES

The experiment was performed at the first doubly achromatic focus of the secondary channel M13 at TRIUMF (Oram, 1981b). Figure 5.8 is a diagram of the beam line configuration. The beam line momentum was adjusted using a relatively small $\Delta p/p$ of 0.5% in order to find the point of maximum

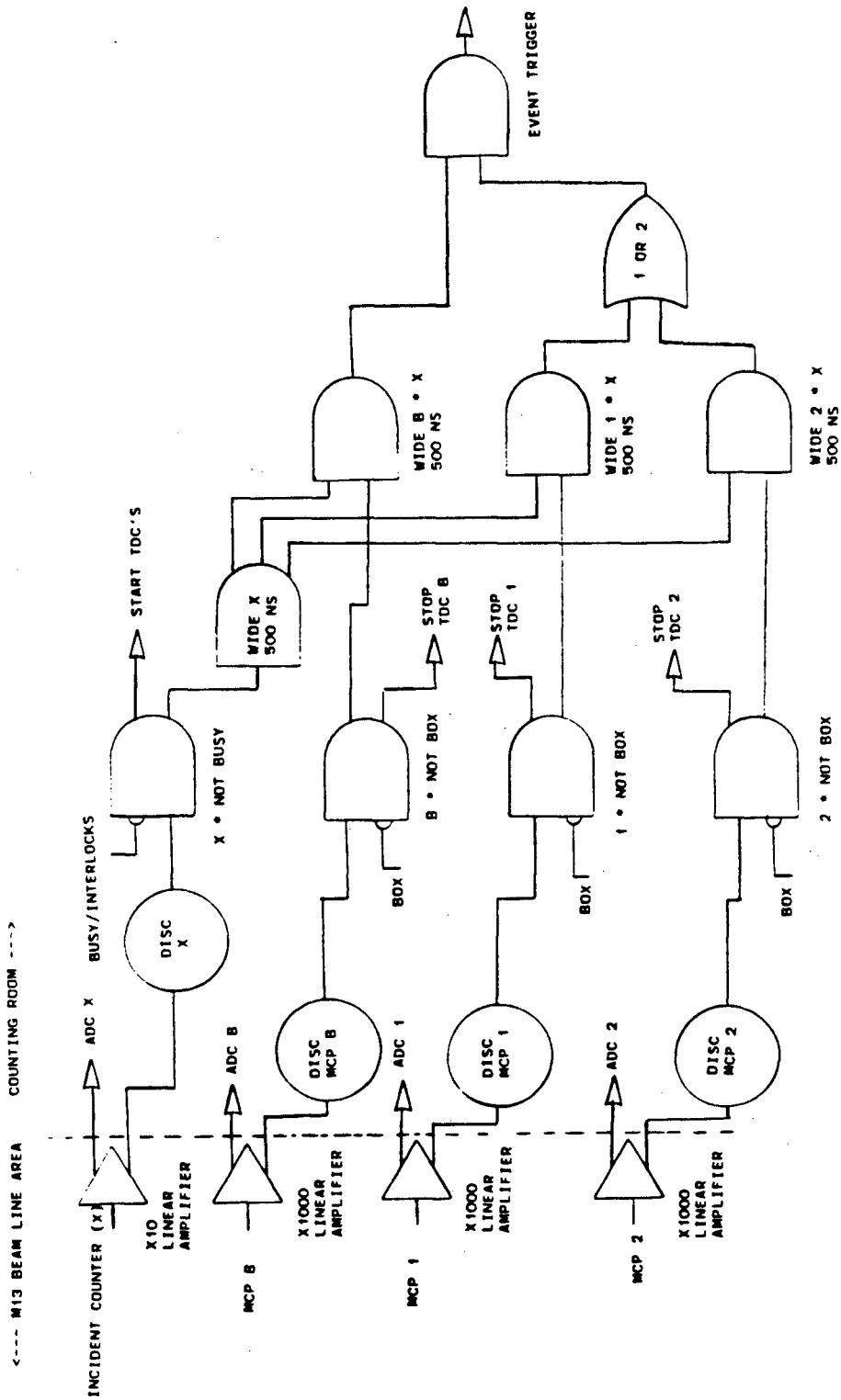

Figure 5.7: Simplified diagram of the electronic logic for data acquisition.

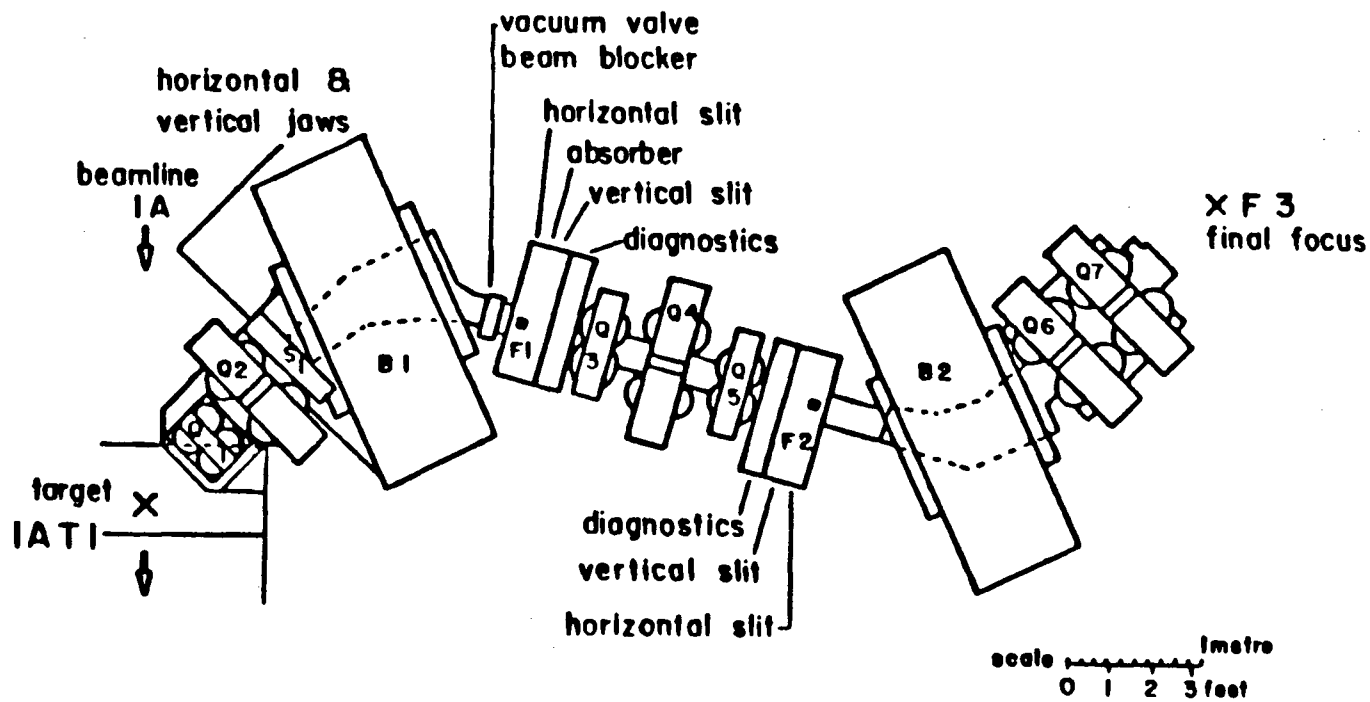

Figure 5.8: The M13 beam line at TRIUMF

production of particles with velocities between c/50 and c/100 (see Figure 3.8); i.e. particles likely to be neutral. Once the optimum momentum of 15.4 MeV/c was found, the channel momentum acceptance was increased to a $\Delta p/p$ of 7%. The available muon flux as a function of momentum is shown in Figure 3.5. At 15.4 MeV/c the incident scintillator detected approximately 36,000 muons per second for a primary proton current of 100 μA at 500 MeV striking a 10 mm graphite target. The logic of Figure 5.7 accepted about 32,000 Hz (i.e. there were 32 KHz WIDE X). Beam positrons at this momentum were much more numerous than the muons but were vetoed by the box scintillators, the collimating scintillator, and the low pulse height pulses from the incident scintillator.

The raw rate on MCPB under these conditions averaged about 80 KHz and was largely beam positrons which entered the apparatus at a rate of about 120 KHz. The BOX veto system reduced this rate to just 8.9 KHz. About half of this rate, 4.2 KHz, was correlated (within the 500 ns gate) with an incident μ^+. This corresponded to 13.1% of the muons incident on (X) being detected by MCPB. The additional trigger requirement that a pulse be present from either MCP1 or MCP2 within the same 500 ns gate reduced the trigger rate to about 15 Hz. Later analysis showed that the rate of detection of Lyman-α events was about 8 per hour, under these conditions.

6. DATA REDUCTION AND ANALYSIS

6.1 TIMING

Data reduction started with scanning of all the data on tape and generation of histograms of the timing of each MCP and scintillator. Positrons in the beam provided a definitive signature which determined the relative timing of all the detectors and associated electronics. In all cases, timing could be determined to better than 2 ns resolution.

Figure 6.1 shows a typical time-of-flight (t) histogram for particles between the incident counter and MCPB. Figure 6.2 shows a two dimensional plot of the time (relative to the time of detection of the incident muon) of putative photon detection in the Lyman-α detectors, t_α (relative to the incident counter), against the overall time-of-flight from the incident counter X to the back channel plate MCPB, t (again for a typical run). The majority of the events in Figure 6.2 are consistent with the rates expected for three random backgrounds. The diagonal enhancement labelled (a) corresponds to near simultaneous events on MCPB and one of the Lyman-α detectors ($t_\alpha = t$). The smaller enhancement labelled (b) resulted from random pulses on MCPB and a real coincidence between X and a Lyman-α detector. That is, X doesn't trigger on all of the beam positrons and therefore not all of the positrons which strike MCPB are vetoed by X. Occasionally one will manage to trigger MCPB without penetrating the scintillator box. This happens at random

times relative to muons triggering X. Finally the third enhancement labelled (c) is the result of random pulses on the Lyman-α detectors in coincidence with a real coincidence of MCPB and X. It resulted from decay positrons which stopped in the Lyman-α detectors randomly in coincidence with the passage of a muon between X and MCPB. The total time-of-flight t was used to calculate (on the basis of geometry) the fraction of time (t_{rf} = 0.289 t) spent in traversal of the RF transmission line as well as the amount of time elapsed before the particle entered the quench region. This permitted calculation of the amount of time spent by the particle in the quench region before its de-excitation photon was detected, $t_Q = t_\alpha - 0.404\ t$.

On the basis of timing, the events could be classified and the number of events worthy of further consideration as posssible 2s muonium greatly reduced. The following timing criteria are illustrated by Figures 6.2 and 6.3:

(i) The time-of-flight t between X and MCPB was required to correspond to a particle with velocity between c/55 and c/200; i.e., 21 ns < t < 76 ns [see Figure 6.3, label (i)].

(ii) The interval t_Q between entry into the quench region and detection of a Lyman-α photon was required to be such that the particle had entered the region but had spent less than 20 ns in it; i.e., 0 ns < t_Q < 20 ns or t_α - 20 ns < 0.404 t < t_α [see Figure 6.3, label (ii)].

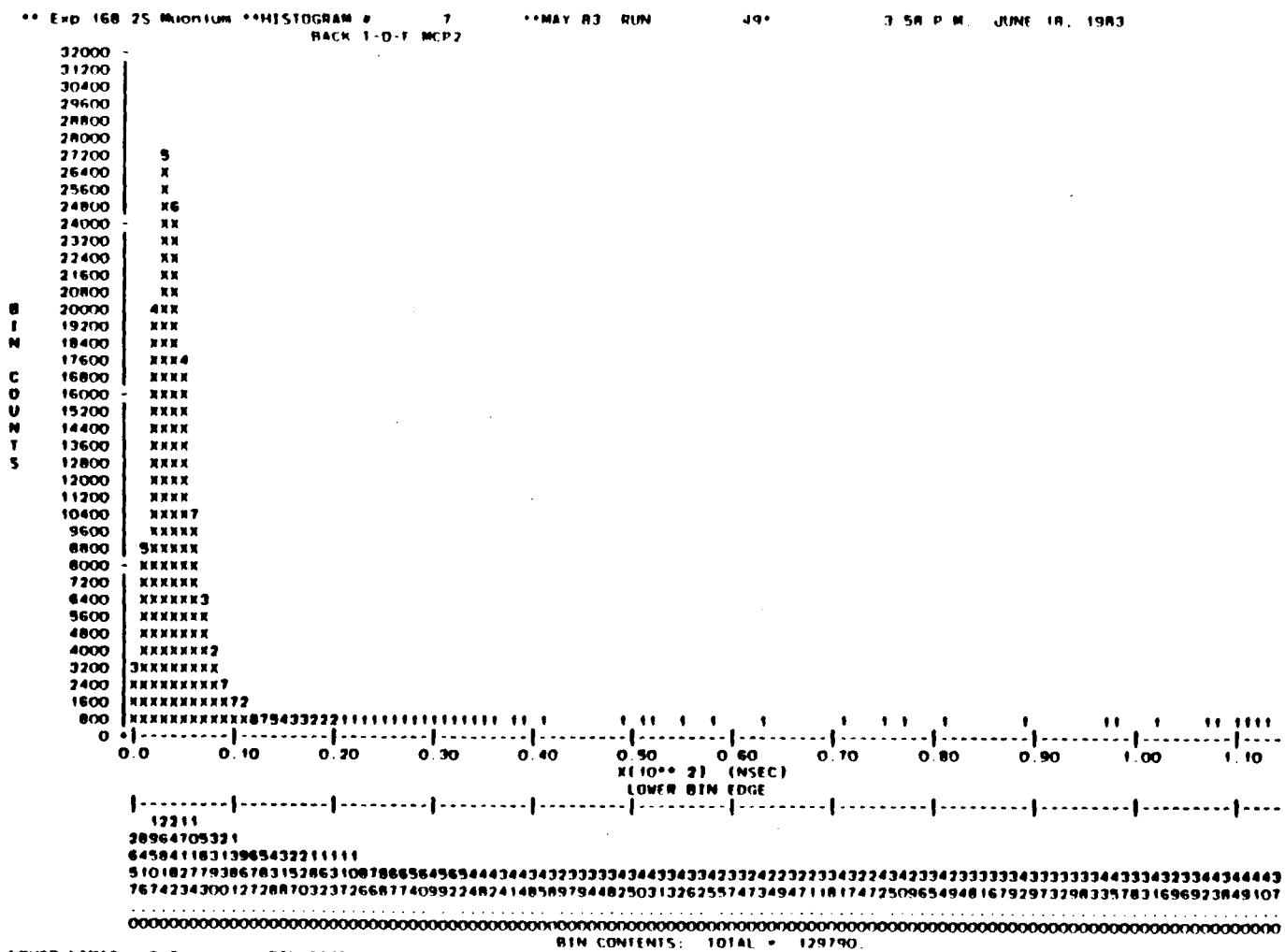

Figure 6.1: A typical time-of-flight histogram for particles travelling between the incident scintillator and MCP B.

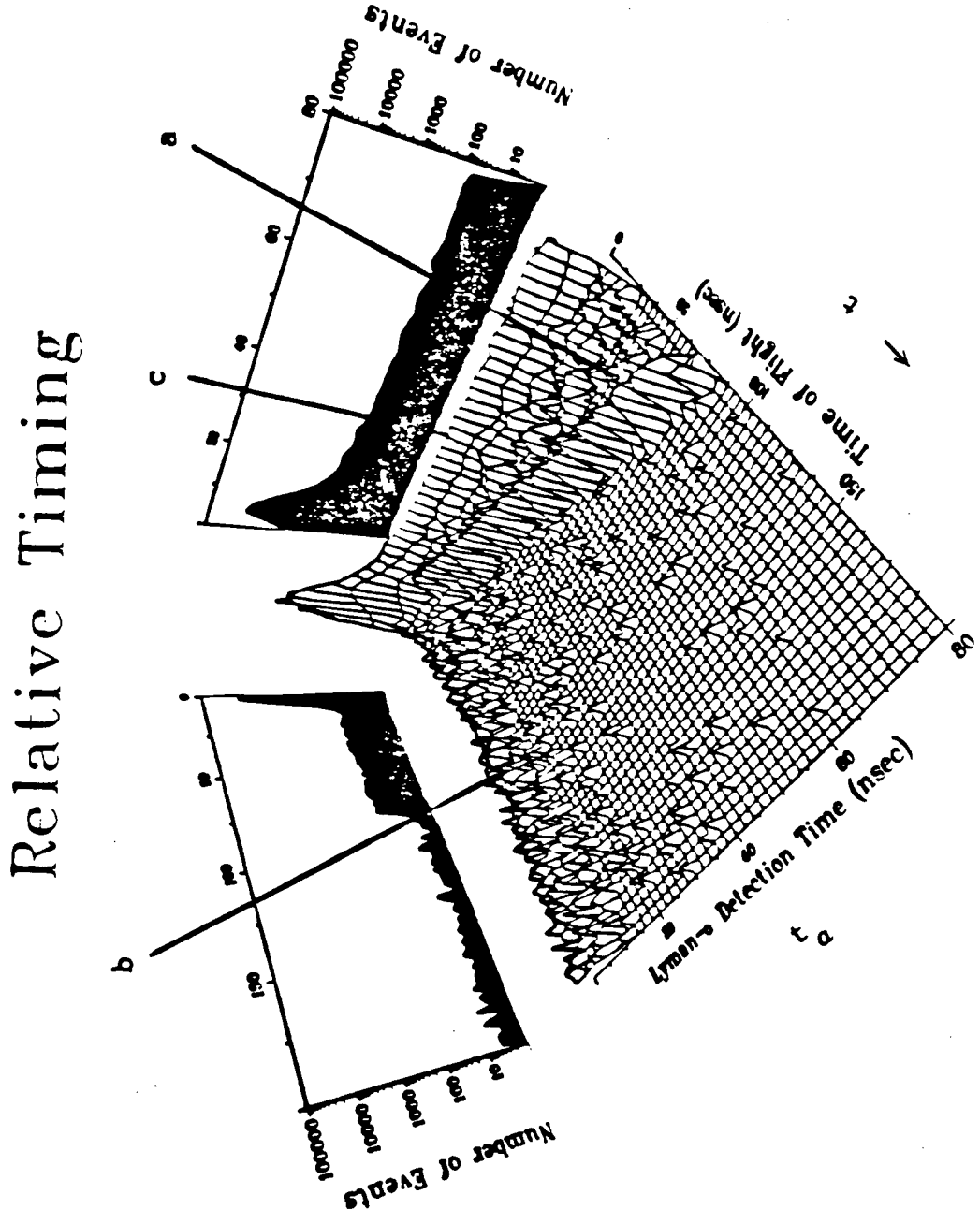

Figure 6.2: Events as a function of time-of-flight and time of detection of a Lyman-α photon. See text for meanings of a, b, c.

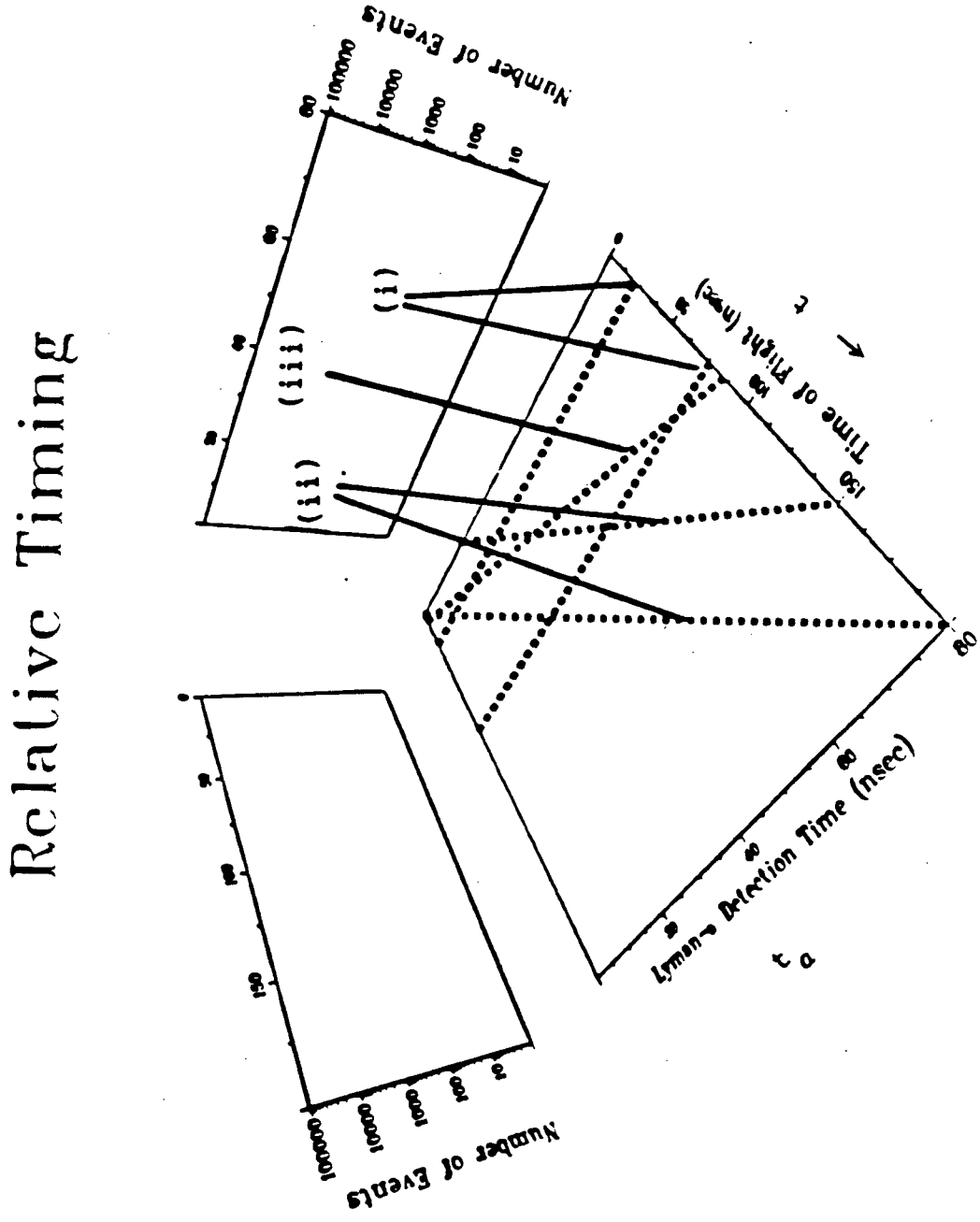

Figure 6.3: The timing cuts on the events of figure 6.2 (see text).

(iii) The time t_a of detection of a Lyman-α photon was required to be more than 5 ns prior to the time t that the particle struck MCPB; i.e., $t_a < t - 5$ ns [see Figure 6.3, label (iii)].

(iv) No second muon arrived in X, nor positron in any of the scintillators, before the muon was detected by MCPB.

Figure 6.4 shows the result of applying timing criteria somewhat looser than those listed above: -10 ns $< t_Q <$ 35 ns and 19 ns $< t <$ 95 ns. The data to be analyzed were first reduced with loose timing and then the timing was "fine-tuned" to that listed above, removing 99.98% of the raw events. Figures 6.5 and 6.6 show the effects of the velocity criteria (i) and the timing criteria (ii) and (iii).

Loose requirements on the pulse heights from the incident scintillator X and the three MCP's served to reduce the background due to positrons but eliminated only a further 20% of the events. Variation of the timing cuts and of the pulse height cuts within reasonable limits (i.e. ±2 ns in time) produced data which when fitted gave a Lamb shift value that in no instance differed by more than 1 MHz from the quoted value. The numbers of events which satisfied the above criteria for each frequency and power level are listed in Table 6.1 .

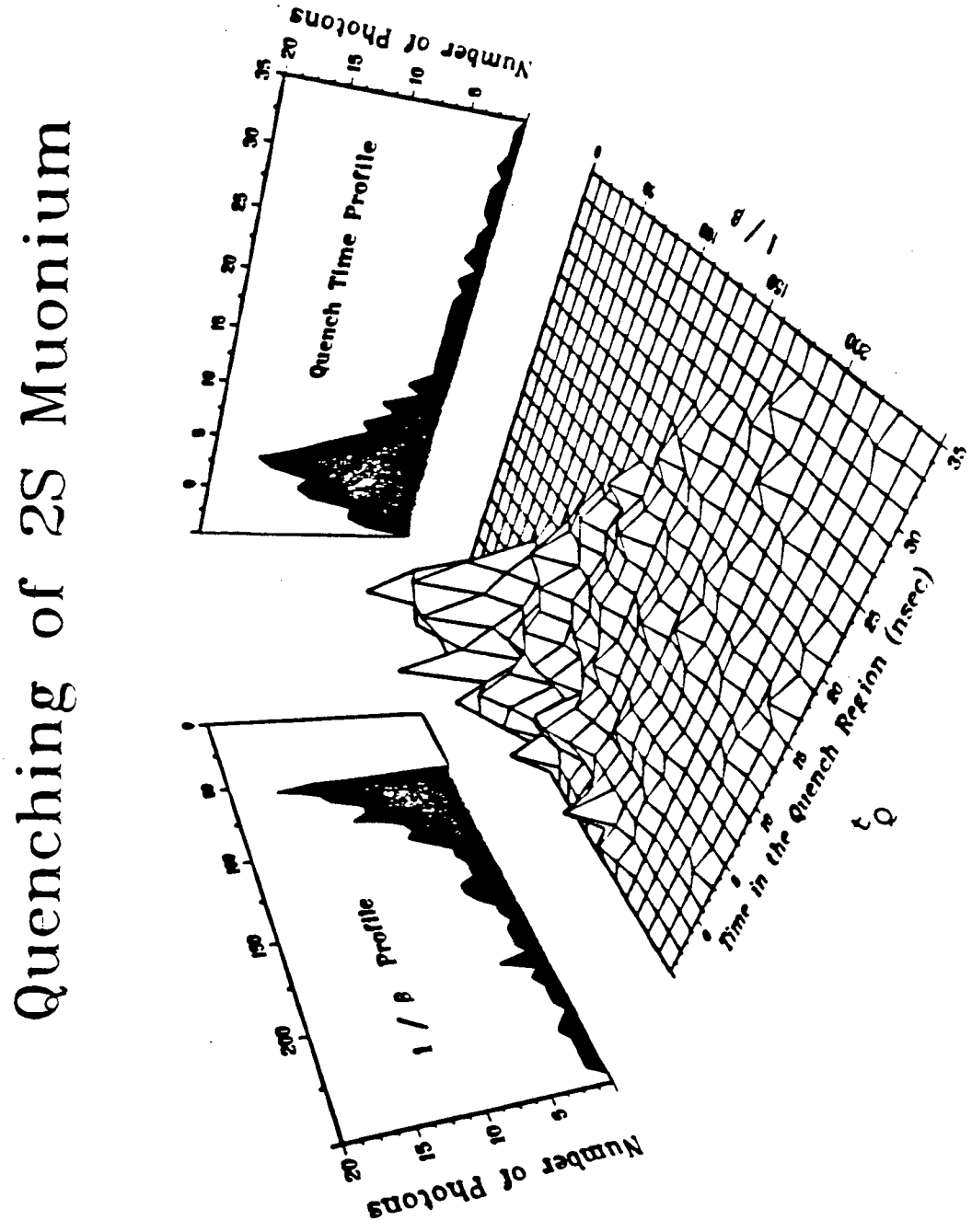

Figure 6.4: Events as a function of $1/\beta$ and time in the quench region (i.e. time of detection of the Lyman-α photon less the time of entry into the quench region).

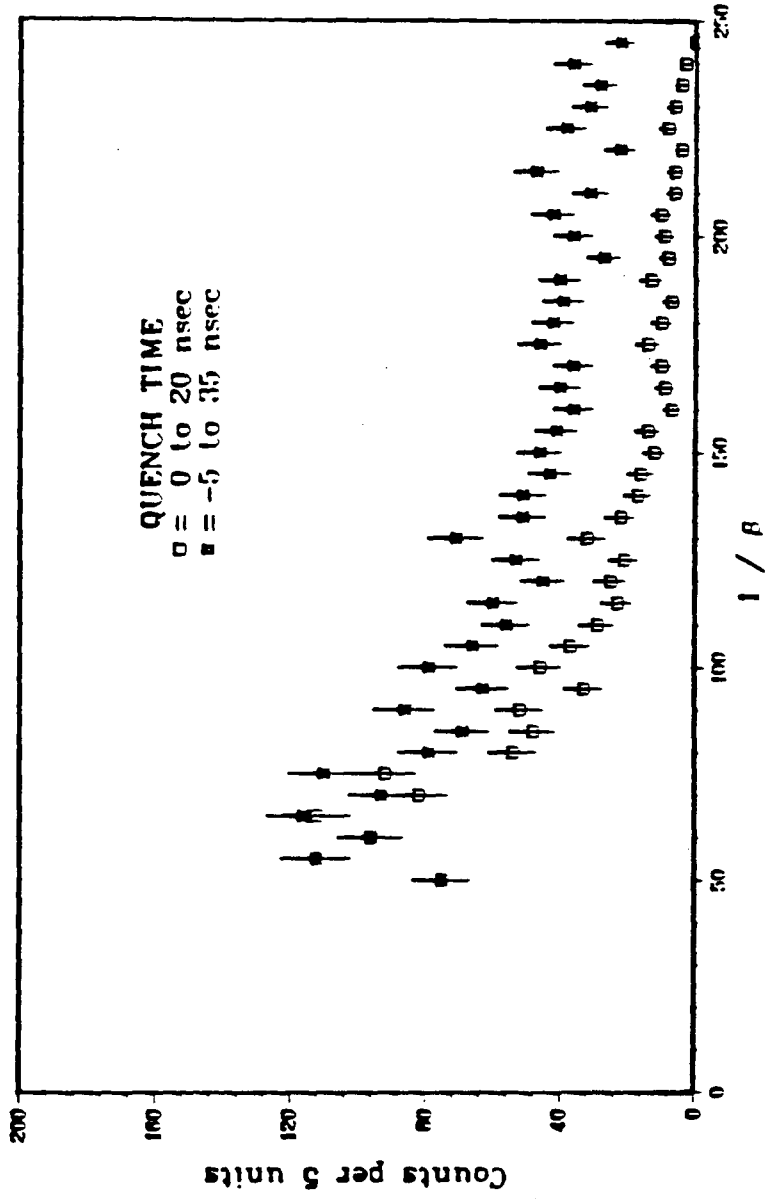

Figure 6.5: 2s muonium detected as a function of velocity. The effect of timing criteria for entry into the quench region is illustrated.

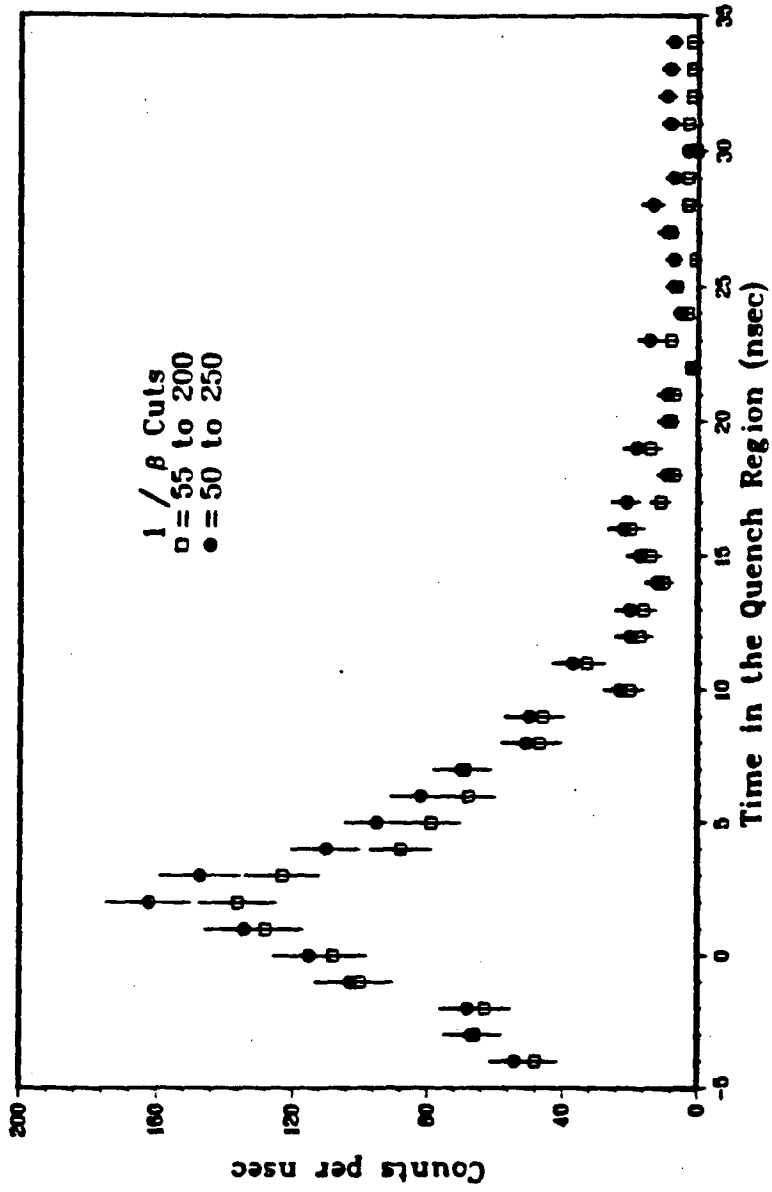

Figure 6.6: 2s muonium detected as a function of time from entry into the quench region to emit a Lyman-α photon. The effect of velocity requirements is illustrated.

2 WATT DATA SUMMARY

ν (MHz)	900	1066	1141	1221	1360	1601
COUNTS	19	18	26	20	11	16
SIGNAL	56.6	53.2	78.7	58.4	56.8	46.5

12.5 WATT DATA SUMMARY

ν (MHz)	900	1066	1141	1221	1360	1601
COUNTS	78	74	54	67	29	72
SIGNAL	57.7	55.1	40.3	50.2	40.7	53.3

25 WATT DATA SUMMARY

ν (MHz)	900	1066	1141	1221	1360	1601
COUNTS	88	82	48	67	23	92
SIGNAL	58.7	52.7	31.9	42.4	36.7	60.3

Table 6.1: The observed numbers of counts and normalized signals used to determine the Lamb shift.

6.2 NORMALIZATION

The amount of time spent acquiring data at each of the 18 points varied because it was desirable to have better statistics at some points than at others. For instance, the six points for an RF power of 2 watts contain little information to do with frequency and could be considered as a single determination of the off resonance signal with six times the statistics.

To compare the data with the expected resonance curve one must have a means of normalization. Total live time at each point was not useful as the beam current could change greatly over the course of each run and of the experiment. The number of incident muons detected by the incident scintillator and the number of events recorded on tape were found to vary consistently (i.e., the ratio was constant). The number of events at each frequency and power was used to normalize the 2s muonium signal observed. The ratio of this normalization to the number of incident muons varied by less than 2% between data points. The results of applying this normalization to the observed number of events to obtain the normalized signal are listed in Table 6.1.

6.3 FORM OF THE RESONANCE CURVE

The number of 2s muonium observed at each of the eighteen frequency and power pairs, N_i, was fitted to the predicted number F_i given by:

$$F_i = b + \alpha_i \, a \sum_{j=1}^{4} \int dv \; w_j \; f_{2s}(v) \; [1-R_{ij}(v)] \qquad \ldots(6.1)$$

where:

α_i is a normalization constant determined experimentally as previously discussed in section 6.2 for each of the eighteen data points.

w_j is the relative probablility of populating each of the four hyperfine states of the 2s level. ($\sum_{j=1}^{4} w_j = 1$)

f_{2s} is the expected probablity of formation of 2s muonium per unit velocity, v such that $\int dv \; f_{2s}(v) = 1$.

a is the intensity of the 2s signal to be determined by the fitting process.

b is a flat (frequency- and power-independent background also to be determined by the fitting process.

$R_{ij}(v)$ is the fraction of the 2s hyperfine state labelled j which quenches in the RF region.

$$R_{ij}(v) = \exp[\; -\gamma_{ij}\tau(v) \;] \qquad \ldots(6.2)$$

$\tau(v)$ is the time spent in the RF region by the atom.

γ_{ij} is the total transition rate induced by microwaves of frequency ν_i and power P_i from the $2s_{1/2}$ hyperfine level j. It is the sum of the individual rates from state j to each of the four $2p_{1/2}$ hyperfine levels labelled k:

$$\gamma_{ij} = \sum_{k=1}^{4} c_{jk} P_i \{(\nu_i - \nu_{jk})^2 + \Gamma^2 / 4\}^{-1} \qquad \ldots(6.3)$$

where:

$$c_{jk} = \frac{4\sigma_i}{c\hbar\Gamma} |\langle k|\bar{r}|j\rangle|^2$$

σ_i is the power density for the ith point.

Γ = width of the $2p_{1/2}$ level in MHz.

ν_{jk} = energy difference of the states j and k (MHz).

The frequencies ν_{jk} depend on the Lamb shift S and the hyperfine splittings of the p and s states h_{2p} and h_{2s}. If we assign an energy value of zero to the $2p_{1/2}$ level then the energy levels become:

Hyperfine level	Energy
$2^3s_{1/2}$ (F = 1)	$S + h_{2s}/4$
$2^1s_{1/2}$ (F = 0)	$S - 3h_{2s}/4$
$2^3p_{1/2}$ (F = 1)	$+ h_{2p}/4$
$2^1p_{1/2}$ (F = 0)	$- 3h_{2p}/4$

The transitions driven by the microwaves fall into two categories depending on the relative orientation of the muon beam and the RF transmission line:

(i) RF polarized parallel to the beam ($\Delta m_F = 0$)

Transition	Nominal energy (MHz)
$\|S,F=1,m_F=+1\rangle \rightarrow \|P,F=1,m_F=1\rangle$	1140
$\|S,F=1,m_F=-1\rangle \rightarrow \|P,F=1,m_F=-1\rangle$	1140
$\|S,F=1,m_F=0\rangle \rightarrow \|P,F=0,m_F=0\rangle$	1327
$\|S,F=0,m_F=0\rangle \rightarrow \|P,F=1,m_F=0\rangle$	581

The four transitions above each have $|\langle P|Z|S\rangle|^2 = 3a_0^2$.

(ii) RF polarized perpendicular to the beam direction ($\Delta m_F = \pm 1$).

Transition	Nominal Energy (MHz)
$\|S,F=1,m_F=+1\rangle \rightarrow \|P,F=1,m_F=0\rangle$	1140
$\|S,F=1,m_F=+1\rangle \rightarrow \|P,F=0,m_F=0\rangle$	1327
$\|S,F=1,m_F=-1\rangle \rightarrow \|P,F=1,m_F=0\rangle$	1140
$\|S,F=1,m_F=-1\rangle \rightarrow \|P,F=0,m_F=0\rangle$	1327
$\|S,F=1,m_F=0\rangle \rightarrow \|P,F=1,m_F=1\rangle$	1140
$\|S,F=1,m_F=0\rangle \rightarrow \|P,F=1,m_F=-1\rangle$	1140
$\|S,F=0,m_F=0\rangle \rightarrow \|P,F=1,m_F=1\rangle$	581
$\|S,F=0,m_F=0\rangle \rightarrow \|P,F=1,m_F=-1\rangle$	581

The eight transitions above have $|\langle P|X|S\rangle|^2 = 3a_0^2 / 2$.

Equation 6.1 could be simplified by assuming the velocity distribution to be a delta function centered at an average v, thus eliminating the integral over the distribution of velocities in the beam.

6.4 THE FITTING PROCEDURE

The number of counts F_i given by 6.1 was adjusted by variation of the three parameters a, b, and S. The goodness of fit criterion was that of maximum likelihood (Appendix A). The fit was found to be insensitive to the exact form of the velocity distribution so the velocity dependence was suppressed by assuming an average velocity of c / 70. Figure

6.7 shows the three dimensional nature of the resulting resonance curve as a function of RF frequency and power. Figure 6.8 shows more quantitatively the best fit resonance curve. The opend circles show the quality of the normalization (see section 6.2).

The typical number of counts N_i was of the order of 50 at each data point so that the criteria of maximum likelihood or of minimum χ^2 were indistinguishable. Table 6.2 summarizes, in terms of χ^2, the results of a variety of fits in which different parameters were allowed to vary from their nominal values.

Figures 6.9 and 6.10 show χ^2 contours for variation of various parameters in the fitting function. That is, $\chi^2=1$ contour encloses 68% of all the likelihood, $\chi^2=4$ encloses 90%, and so on.

6.5 SYSTEMATIC UNCERTAINTIES IN THE LAMB SHIFT MEASUREMENT

Although systematic uncertainties totalled less than the statistical uncertainty of the Lamb shift they were significant. In a future experiment of greater statistical accuracy they would rapidly dominate. Table 6.3 summarizes the systematic uncertainties.

6.5.1 RF POWER UNCERTAINTY

The power transmitted by the RF transmission line was monitored using a Hewlett Packard meter (Model 432A). Comparison of the readings obtained by this meter with those

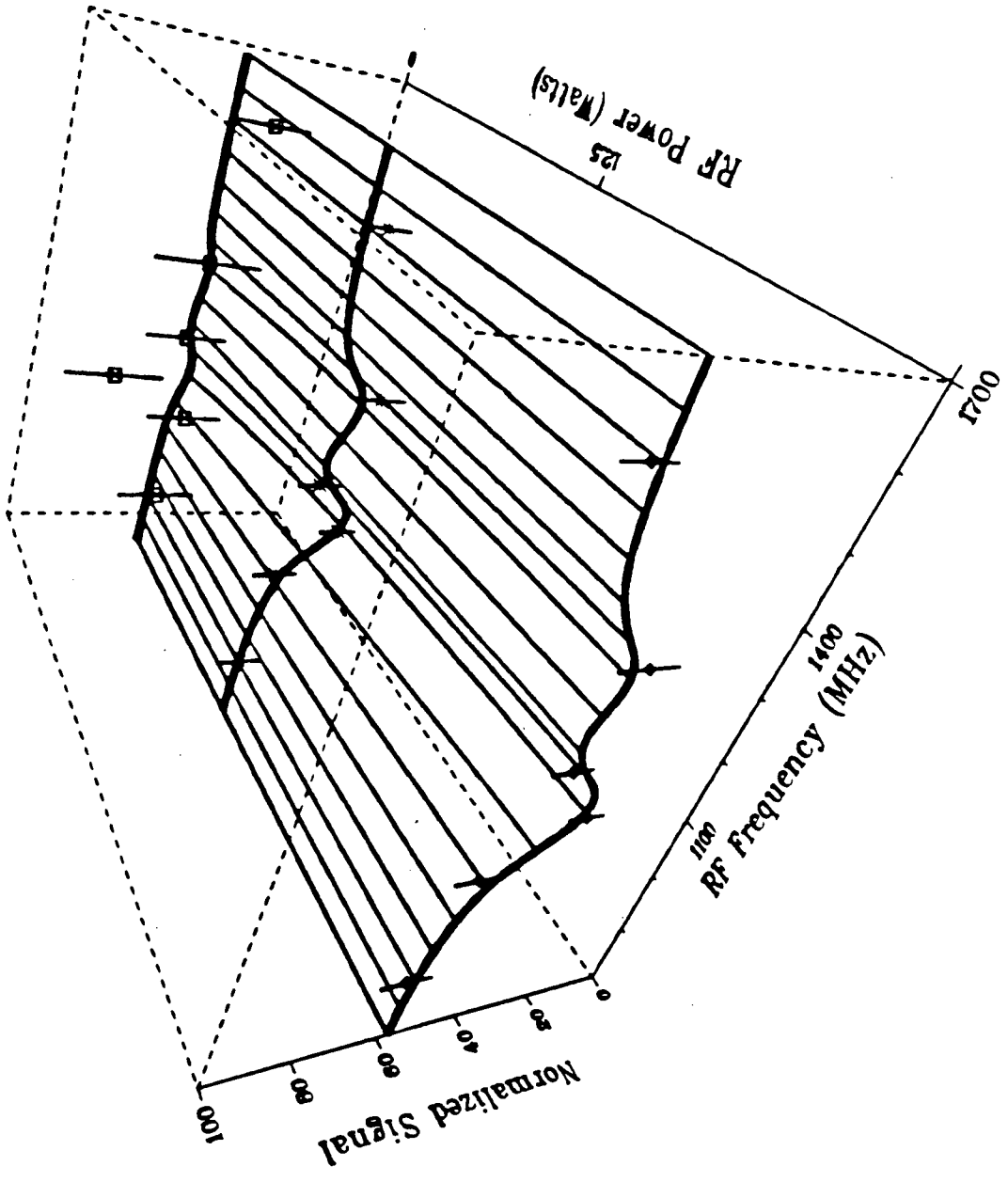

Figure 6.7: The data points and best fit resonance curve as a function of applied RF power and frequency.

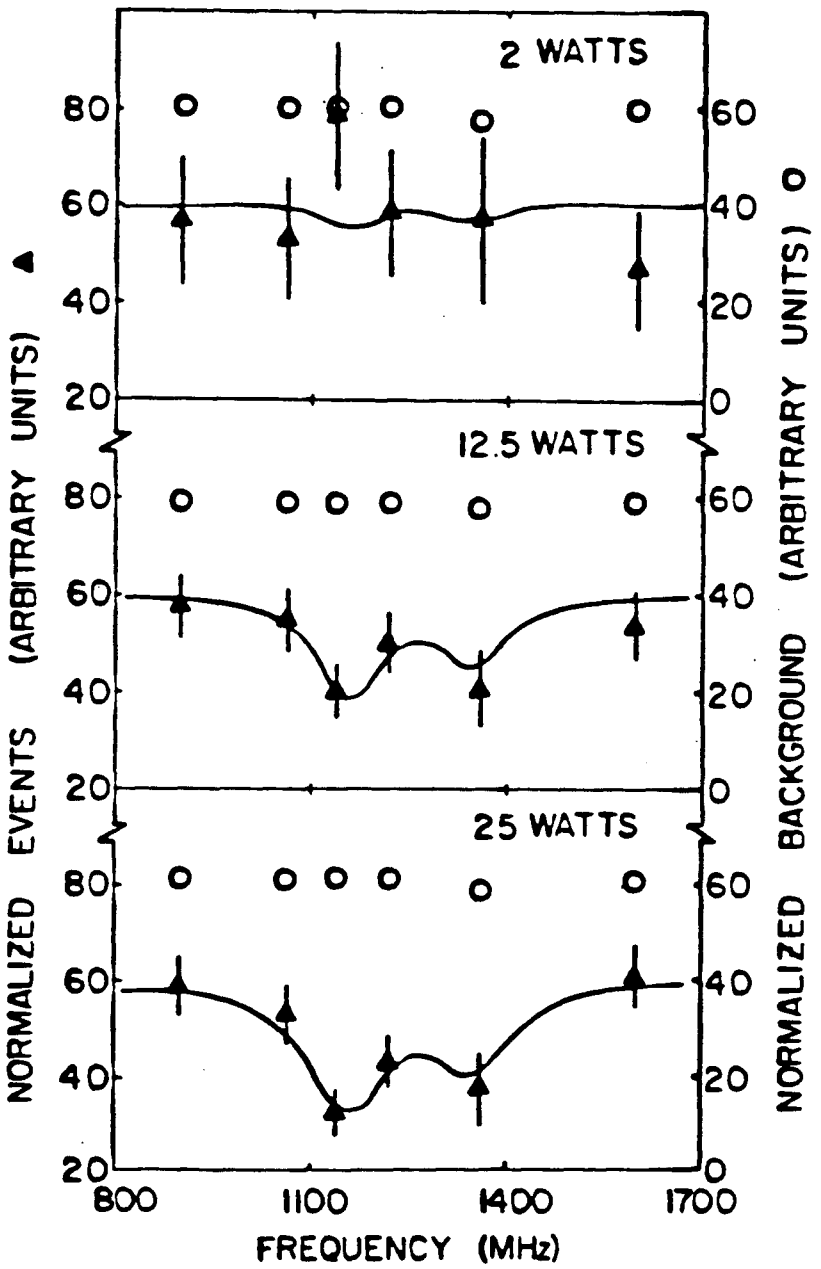

Figure 6.8: The best fit resonance curve shown for the three power levels at which data was acquired. The open circles are an independent test of the normalization (see text).

Table 6.2: The results of various fits to the resonance data, in which different parameters have been allowed to vary. Line III is the the quoted result for the Lamb shift.

Fit	Signal amplitude	Background amplitude	Lamb shift (MHz)	Hyperfine splitting $2p_{1/2}$ level (MHz)	$2P_{1/2}$ Mean life (ns)	Contributions to χ^2 2 W	12.5 W	25 W	Number of degrees of freedom
I	Fixed 0	51.1±1.7	-	-	-	5.8	6.3	20.0	17
II	40.7±8.1	19.8±6.0	1047.0[a]	187[b]	1.6[c]	4.5	2.3	3.0	16
III	43.3±8.3	17.2±6.3	1069.8 ±13.3	187[b]	1.6[c]	4.4	1.3	2.7	15
IV	43.7±8.3	17.2±6.3	1068.0 ±13.6	205 ±35	1.6[c]	4.4	1.2	1.6	14
V	41.2±11.6	19.4±10.1	1069.6 ±13.6	203 ±36	1.8 ±0.8	4.5	1.1	1.4	13

[a]Theoretical Lamb shift of muonium.

[b]Theoretical hyperfine splitting of the $2P_{1/2}$ level.

[c]Theoretical $2P_{1/2}$ mean life.

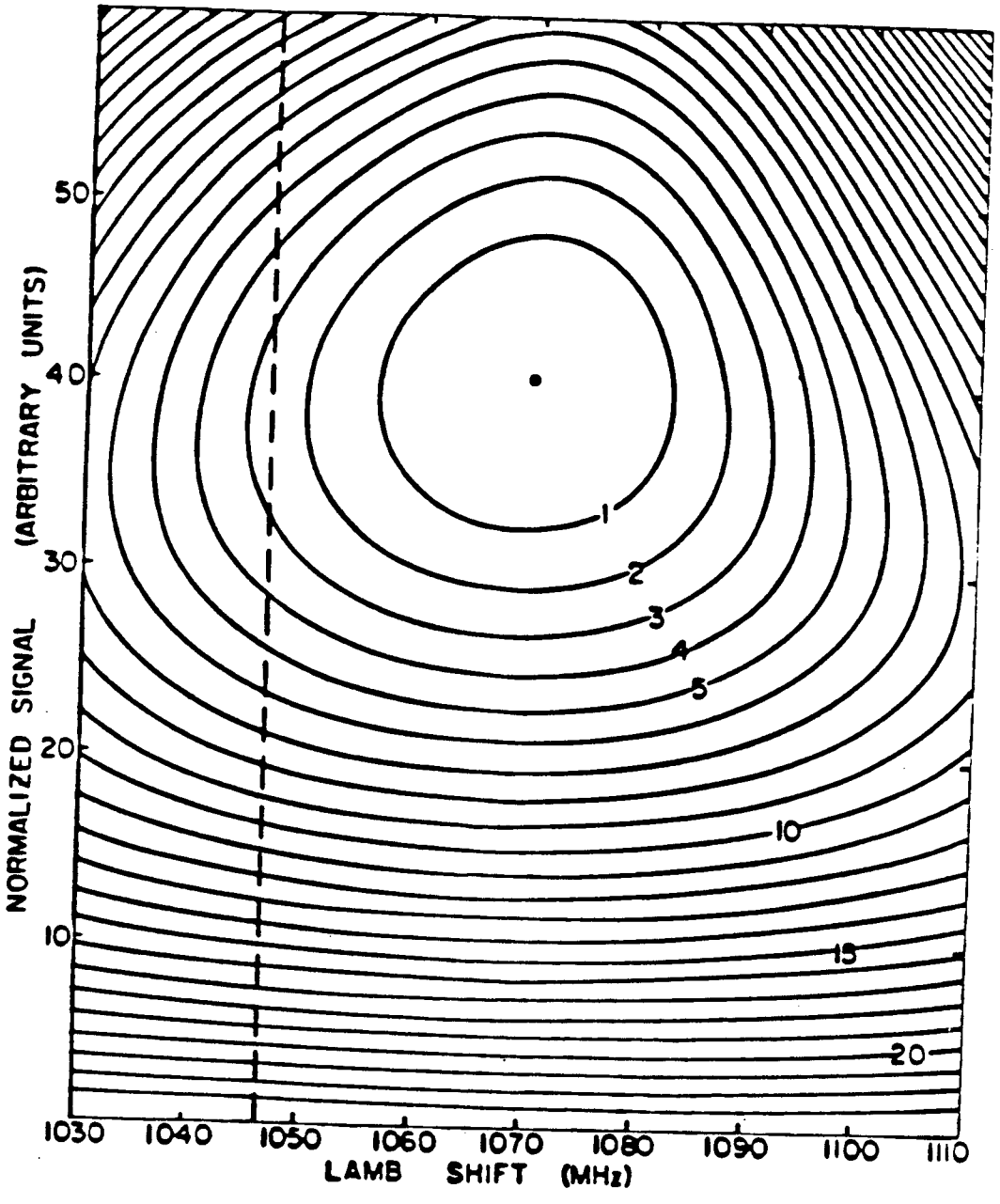

Figure 6.9: χ^2 contours for variation of the Lamb shift S and the signal intensity, a.

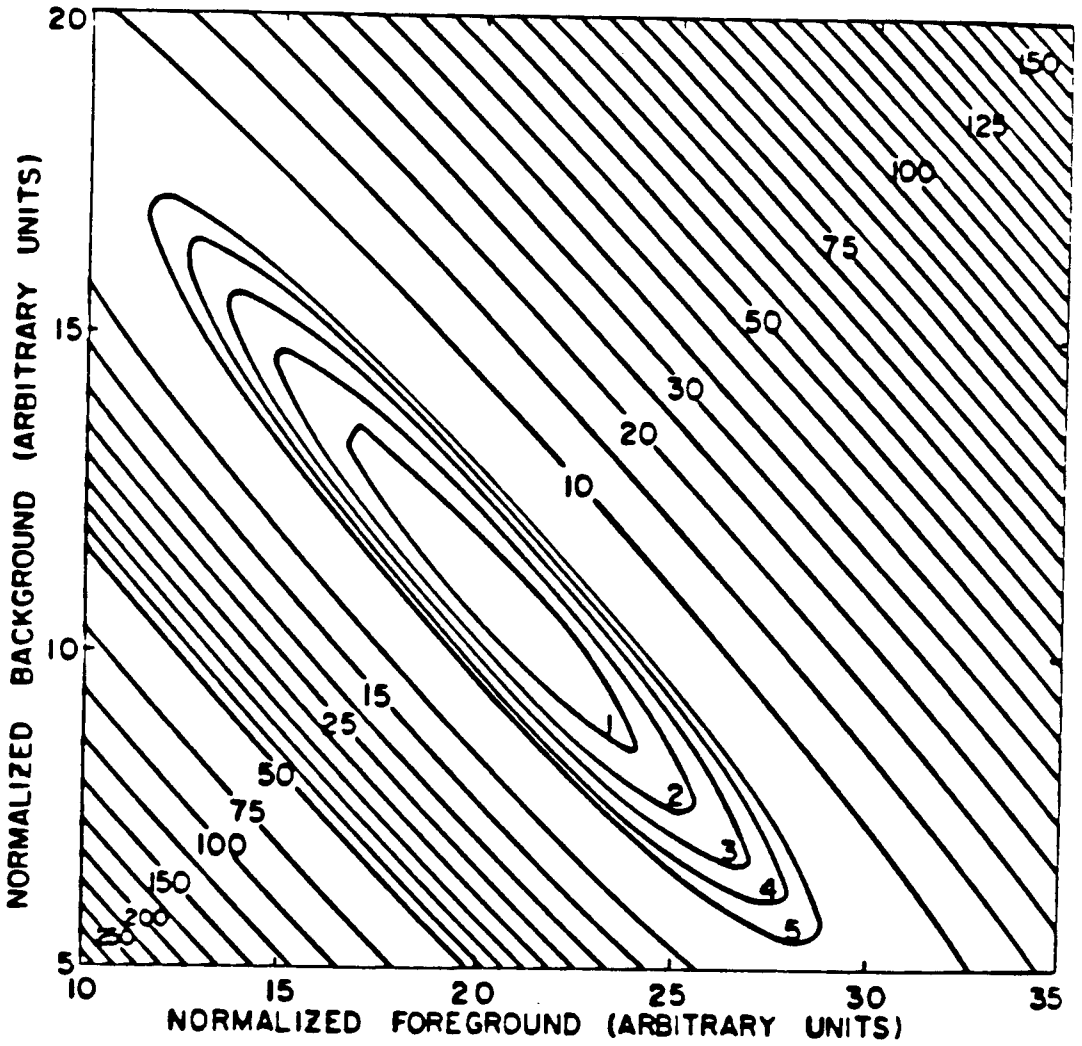

Figure 6.10: χ^2 contours for variation of the signal intensity, a and background intensity, b.

Source of systematic uncertainty	Resulting uncertainty (MHz)
25% uncertainty in RF power	1.4
1% RF power variations per 100 MHz for data at the same nominal power	0.3
5° uncertainty in alignment of μ^+ beam	1.3
Uncertainty in velocity distribution	0.1
1 G uncertainty in magnetic field	0.1
2% nonlinearity in the normalization	1.0

Table 6.3: Summary of the various contributions to the systematic uncertainty of the Lamb shift.

obtained by two other similar meters showed that the factory calibrations were identical. Additionally there were small geometrical uncertainties in the tolerances of the RF region itself. The power reflected by the transmission line was negligible. We therfore assigned, very conservatively, an uncertainty of 25 % to the RF power density seen by the muonium as it traverses the RF region.

6.5.2 NON-LINEARITY OF THE RF POWER LEVEL

The system which maintained the RF power at a constant level throughout the experiment had small variations in frequency response. According to the manufacturer's specification these non-linearities were less than 0.1% per 100 MHz. We pessimistically assumed 1% per 100 MHz. Adding deviations of this magnitude randomly to the data produced a maximum change of 0.3 MHz in the fitted value of the Lamb shift.

6.5.3 ALIGNMENT OF THE RF REGION AND THE BEAM

The alignment of the RF region so that it was perpendicular to the mean beam direction was critical. Any misalignment by, say, an angle θ, could lead to a longitudinal doppler shift $\Delta\nu$ of the frequency seen by the muonium:

$$\Delta\nu = \nu\beta\sin\theta \qquad \ldots(6.4)$$

In addition, any left to right anisotropy (i.e., in the direction of the RF transmision line) of the efficiency of detection of 2s muonium could lead to a shift as in 6.4. The divergence of the muonium entering the detection region was as great as ±22 degrees. For this reason the holes of MCPB were angled upward (neither to the left nor to the right) and the Lyman-α detectors placed above and below the beam (so that there would not be any systematic efficiency variation with θ). The simple precaution of reversing the RF transmission line periodically would have reduced any such systematic effect. The alignment of the beam, the RF region, and the Lyman-α detection system was carried out to an accuracy of ±5 degrees, thus contributing 1.3 MHz uncertainty to the experimental value of S for the mean value of β = 1/70

6.5.4 VELOCITY DISTRIBUTION

The simplifying assumption of a single velocity v of c/70 contributed only ±0.1 MHz systematic uncertainty. The effect is similar to an uncertainty in the power level since equations 6.1, 6.2 and 6.3 show that the signal depends on the product of power P_i and time in the RF region, $\tau(v)$.

6.5.5 NORMALIZATION UNCERTAINTY

The open cirlces shown in Figure 6.8 are an independent test of the normalization. Variations were less than 2% between points. Variations of this magnitude introduced

randomly into the data were found to cause a shift in the fitted Lamb shift value of at most 1 MHz. This could have been reduced by splitting the analysis into several parts, as the length of time spent acquiring data at certain frequencies was changed over the course of the experiment and hence the relative normalization of different frequencies possibly affected.

6.6 OTHER EFFECTS

6.6.1 TRANSVERSE DOPPLER SHIFT (TIME DILATION)

Time dilation for particles traveling at c/70 causes the muonium to see a slightly higher frequency than the laboratory value.

$$\nu_{atom} = \nu_{lab}/\sqrt{(1 - \beta^2)} \qquad \ldots(6.5)$$

This amounts to decreasing the measured Lamb shift by 0.2 MHz for $\beta = 1/50$, which is an overestimate since the fastest particles accepted in the analysis had $\beta = 1/55$.

6.6.2 RF STARK SHIFT

The muonium atoms experience an electric field as they traverse the RF region. The average field (r.m.s.) was

$$\sqrt{50\ P/2.0}\ [\mathrm{V/cm}] \qquad \ldots(6.6)$$

where P is the power level through the transmission line. Thus at a power level of 25 watts the average electric field

was 18 V/cm vertically in the transmission line. The change in the energy interval is seen to be (see equation 4.16)

$$|2\omega_{12}|^2/16\pi S \qquad \ldots(6.7)$$

where S is the Lamb shift in MHz and

$$\omega_{12} = -eE_0\langle 2S_{1/2}|Z|2P_{1/2}\rangle \qquad \ldots(6.8)$$

At 25 watts this effect shifts the measured energy difference upward by 0.5 MHz. The effect is proportional to the power level.

6.6.3 MAGNETIC FIELDS

The cyclotron magnet at TRIUMF caused a vertical field of approximately 1 G measured in the RF region. A field of this magnitude shifts the resonance frequencies by less than 0.1 MHz. The motional electric field seen by muonium moving at c/70 in this field is negligible:

$$\beta B = 1/70 \cdot 1\ \mathrm{G} = 0.014\ \mathrm{V/cm} \qquad \ldots(6.9)$$

6.7 SUMMARY OF UNCERTAINTIES AND SYSTEMATIC EFFECTS

The RF Stark shift and time dilation effects shift the observed resonance frequency upward by 0.3 MHz which is therefore subtracted from the fitted value. The systematic uncertainties are believed to be uncorrelated. Therefore they were added in quadrature, totalling 2 MHz. The statistical uncertainties, as given by the χ^2contours of

Figures 6.9 and 6.10, show that the Lamb shift, S, of maximum likelihood determined in this experiment is 1070^{+12}_{-15} MHz with 68% confidence and 1070^{+25}_{-30} MHz with 90% confidence.

7. CONCLUSION

7.1 COMPARISON WITH THE OTHER LAMB SHIFT MEASUREMENT

Recently, a group at LAMPF (Baderstacher, 1984) has reported their measurement of the muonium Lamb shift. Using a very similar technique and a more intense muon beam than can be extracted at TRIUMF they obtained $S = 1057^{+25}_{-30}$ MHz where the uncertainties correspond to one standard deviation (see Figure 7.1). Their muonium production rates, when corrected for differences in beam line parameters, agree with those obtained here. The main difference between the two experiments is in the solid angle accepted from the foil into the experiment, which was much higher in the TRIUMF experiment. The LAMPF result utilized a smaller fraction of the muonium produced in the beam-foil interaction. On the other hand, their Lyman-α detection system, using photomultipliers instead of MCP's, covered a larger solid angle (about 30%, three times greater). The transmission of their MgF_2 window and the quantum efficiency of the photocathode in the photomultipliers combined to produce a narrow window of sensitivity at the Lyman-α wavelength, with good efficiency (10%), at the same time reducing some of the background signal[1].

The Los Alamos experiment measured, at each frequency, the difference in the Lyman-α detection rate between RF

[1]Photomultipliers with large photcathodes and good efficiency in the Lyman-α region of the spectrum have only recently become available. They used Hamamatsu type R2050.

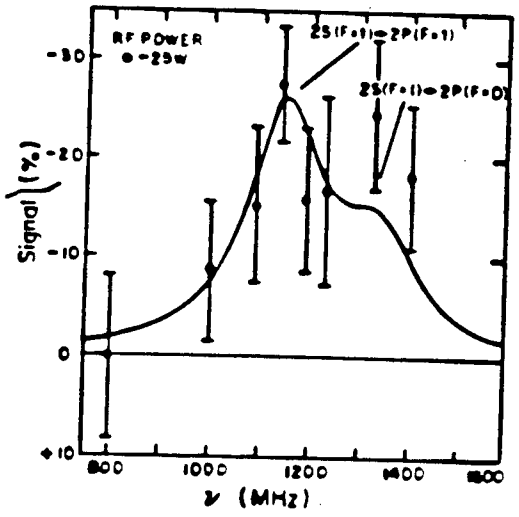

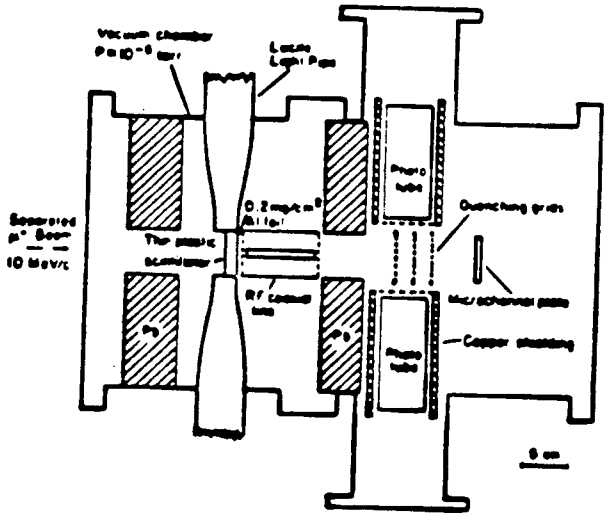

Figure 7.1: The data obtained by Baderstacher *et al.* for the Lamb shift transition and a schematic of the apparatus used.

power on and RF power off. This reduced the rate at which they could acquire useful data by a factor of two. The point is that there really is no reason *a priori* that RF power off is a true indication of the level of background anymore than simply an off resonance frequency. In fact it may be a worse indication since the Lyman-α detection system as well as the epithermal muonium detector (MCPB) may be sensitive to the RF power and operate differently at different power levels, introducing RF frequency and power dependent effects into the data. Of course, it is important to sample the "off" state, whatever it may be, frequently over the course of the measurement to reduce systematic effects. There is no frequency dependent information in simply turning the RF power down or off, therefore the total amount of time spent in this state should not much exceed the amount of time spent in acquiring data at any single frequency with power on, if one wishes to optimize the use of the muon beam.

7.2 LIMITATIONS OF THE PRESENT TECHNIQUE

The present experiments can be improved by quite simple (but of course expensive) modifications. The first of these would involve increasing the solid angle acceptance of the Lyman-α detectors. In principle the RF region could be made transparent and be moved inside the BOX scintillator. Assuming that the back channel plate could be used to detect photons as well, this would give a factor of ten increase in the detection efficiency of Lyman-α from the de-excitation

of the n=2 muonium. The detection of de-excitation photons in the RF region would give another factor of two. The possible increase in solid angle for collection of muonium from the foil has not been considered.

A second modification is required in order to use the back micro-channel plate for detection of Lyman-α photons and, at almost the same time, to detect epithermal muonium striking it. The channel plates must be segmented so that pulses from different parts can be distinguished. This is not such a difficult thing to do. Only the collection sheet behind the MCP need be segmented and the appropriate multiplication of the electronics for pulse processing installed. Segmentation of the BOX scintillator in a similar pattern would also be valuable so that decay positrons need not always veto events. In fact, under these circumstances it becomes possible with a small modification of the BOX scintillator, or by using something like drift chambers, to track the decay positron from a muon striking a particular segment of MCPB and require its presence as a further criterion in the event definition, with a corresponding reduction in the level of background events.

In all, it would be possible with little effort to increase the sensitivity of the present experiment by a factor of roughly 20. If the apparatus were moved to a higher intensity muon beam a further factor of five in the muonium production rate could be achieved. Thus for a similar amount of running time one could expect to measure

the Lamb shift to an accuracy of just under a megahertz (one assumes that more attention will have been paid to systematic effects so that they will not contribute to the uncertainty too much). Using the same apparatus and beam line adjusted for protons of equivalent range would serve as a valuable test of systematic effects.

A measurement at this level would test the recoil terms in the Lamb shift, perhaps distinguishing the calculation by Owen from that yielded by straightforward application of Erickson's method (see Table 2.2). The recoil terms are about 3 MHz; in hydrogen they are already tested to greater accuracy where they amount to about 0.4 MHz or about 50 times greater than the standard deviation of the experimental results. Further experiments of this kind should be attempted but it must be recognized that they are not likely to give results which can test the current theory. They will aid in the design and development of new and better techniques which hopefully will eventually permit a measurement to an accuracy comparable with the hydrogen measurements.

7.3 NEW METHODS FOR A MUONIUM LAMB SHIFT MEASUREMENT

In order to increase the accuracy of a new Lamb shift measurement to a level where QED can be really tested, new ideas are needed. There has been much discussion along these lines. Three avenues of attack suggest themselves.

The first is to look for an alternative method of measurement which would yield a better result without requiring the rather difficult criteria that the RF technique does of the muonium beam. Various Lamb shift measurements have been made using non-RF techniques. Notable is the experiment of Pal'chikov and Solokov who produced hydrogen in the 2S state and observed the interference pattern of the Lyman-α radiation as it passed through two separate regions of electric field. The experiment, however, required a well collimated and mono-energetic beam. Similar comments apply to methods employing Stark beats (Andrä, 1974) and methods which measure the anisotropy of the Lyman-α radiation emitted in a well known quenching electric field (Drake, 1975), deducing the Lamb shift from the implied mixing of the $2p_{3/2}$ state and the assumed value of the $2p_{3/2}$-$2p_{1/2}$ energy difference.

The second avenue is to try to improve the muon beams available. To this end there have been many suggestions, some of which will be investigated in the near future. Most of these can be loosely described as follows. One produces μ^+ in a solid, as near as possible to the surface. Whether the production is by injection of high energy protons to produce π^+ and then μ^+, or by injection of π^+, or by injection of μ^+ need not concern us here. One hopes that the muonium can be induced to diffuse to the surface of the solid. Possible methods of increasing the number of muons which reach the surface are:

(i)To heat the material, thus increasing the diffusion rate.,

(ii)To use semiconductors with a bias voltage applied to favour migration of positive charges to the surface.

(iii)To use materials in which the diffusion rate of hydrogen or muonium is know to be high, such as Vanadium (Suzuki,1983).

The muons which reach the surface may be bound to the surface in the form of muonium. However, careful choice of the material may permit the muon to be ejected and subsequently accelerated by a system of electrostatic lenses where, since the initial energy was thermal, a beam of exceptionally well defined energy, spatial extent and divergence can be delivered to an experiment. Modulation of the accelerating field can even define the timing of beam pulses.

The crux of the matter is to get the muons off the surface. Mills has suggested that LiF may have a favourable surface binding potential for muonium (Mills, 1984). Other ideas are to flash the surface with a laser tuned to remove the muons or just to raise the temperature to encourage thermal processes to do the job. Estimates of the possible efficiency of such schemes vary widely.

The third alternative is perhaps the most direct. The greatest loss of efficiency is in the utilization of the muons produced from pion decay. Slowing them down from a kinetic energy of about 4.1 MeV using a degrader is

inefficient. Using a degrader one will lose a factor of $\{(c/50)/(c/3)\}^{7/2}$ or about 20000, inescapably. Schemes have been proposed which could, in principle, circumvent this loss. One envisages some form of time dependent electric field (for example an RF field), to accomplish the deceleration of a 4.1 MeV surface muon beam. Utilizing the time-of-flight spread of a bunch of muons, which increases as they are transported down a beam line, it would be possible to selectively decelerate the fastest μ^+ the most and achieve some phase space compression. A second method envisages the use of a system of magnets to cause the muons to undergo repeated interaction with a very thin foil, situated in a field free region between them so that most of the muons will at some time form muonium at the foil, where the measurement can be performed on the neutral atom before it exits the system. Schemes such as these, if pessimistically estimated to increase the 2s muonium flux by a factor of 10 000, will increase the statistical accuracy of the experiment by a factor of 100 over the present accuracy.

7.4 POSSIBLE MEASUREMENT OF THE N=2 LAMB SHIFT IN PIONIUM

Recently, Bolton *et al.* have reported the observation of the neutral atom π^+e^- called pionium, formed in a beam-foil interaction analgous with that employed in this experiment. The pion, however, is short lived compared to the muon, decaying with a mean lifetime of about 26 ns. Also, the

mechanics of pion production preclude anything like a surface muon beam. It may be possible, however, to measure the Lamb shift in this system because there are factors which make the measurement easier. One factor is that the pion is spinless, and therefore there is no hyperfine structure to deal with so that the resonance curve would be a single resonance of full intensity. The other is that the pion decay into a low energy muon and a subsequent positron is a distinctive signature which can be employed experimentally. These should compensate for the loss of flux due to the short pion lifetime and the increased background problems due to necessity of utilizing a higher momentum pion beam to get sufficient flux.

7.5 SUMMARY OF RESULTS

The Lamb shift determined by this experiment was S = 1070 MHz. The statistical uncertainty of this result was asymmetric: +12/-15 MHz at the 68% confidence level and +25/-30 MHz at the 90 % confidence level. The total systematic uncertainty was 2 MHz. This result just barely agrees with the currently accepted theoretical value for S of 1047.03 MHz (Owen 1973). The probability of the same experiment yielding a result deviating further (than the one obtained) from Owen's value for S is about 14%. It has been shown that the present technique could be used to measure the n=2 Lamb shift in muonium to about the 1 MHz level. The present result, while it can perhaps be said to test the

correctness of the Lamb shift calculation, is of insufficient accuracy to test the validity of the QED prescriptions for the Lamb shift calculation in hydrogen-like systems. Such tests require measurement at better than the 100 ppm level (i.e., to better than 0.1 MHz). The present measurement has shown how one must proceed in order to achieve this goal. It has revealed some of the systematic effects which must be dealt with in any more accurate measurement. Finally, it has demonstrated that what would have been considered impossible a decade ago has been achieved because of technological refinement; even with a beam of 10^{+10} times lower intensity and of 10^{4} times higher velocity and a 2s detection system of 100 times less efficiency than that used by Lamb, a Lamb shift measurement in muonium is possible.

REFERENCES

S.K. Allison, Rev. Mod. Phys. **30**, (1958) 1137.

H.H. Anderson and J.F. Ziegler, *The Stopping Powers and Ranges of Ions in Matter, Volume 3: Hydrogen Stopping Powers and Ranges in All Elements*. (New York: Pergamon, 1977).

H. Andrä, Physica Scripta **9**, (1974) 257.

A. Baderstacher, V.W. Hughes, D.C. Lu, M.W. Ritter, K.A. Woodle, M. Gladisch, H. Orth, G. zu Putlitz, M. Eckhause, J. Kane, and F.G. Mariam, "The Lamb Shift in Muonium" in *ATOMIC PHYSICS 9*, editors: R. S. Van Dyck, Jr. and E. Norval Fortson, (Singapore: World Scientific Pub. Co., 1984).

A. Baderstacher, S. Dhawan, P.O. Egan, V.W. Hughes, D.C. Lu, M.W. Ritter, K.A. Woodle, M. Gladisch, H. Orth, G. zu Putlitz, M. Eckhause, J. Kane, F.G. Mariam, and J. Reidy, Phys. Rev. Lett. **52**, (1984) 914.

J. Bailey, K. Borer, F. Combley, H. Drumm, F.J.M. Farley, J.H. Field, W. Flegel, P.M. Hattersley, F. Krienen, F. Lange, E. Picasso and W. von Rüden, Phys. Lett. **68B**, (1977) 191.

M. Baranger, F.J. Dyson, and E.E. Salpeter, Phys. Rev. **88**, (1952) 680.

M. Baranger, H.A. Bethe, and R.P. Feynman, Phys. Rev. **92**, (1953) 482.

W.A. Barker and F.N. Glover, Phys. Rev. **99**, (1955) 317.

H.A. Bethe, Phys. Rev. **72**, (1947) 339.

H.A. Bethe and E.E. Salpeter, *The Quantum Mechanics of One- and Two-Electron Atoms* (New York: Plenum, 1977).

J.D. Bjorken and S.D. Drell, *Relativistic Quantum Mechanics*, (New York: McGraw Hill, 1964).

N. Bohr, Phil. Mag. **26**, (1913) 1.

N. Bohr, Phil. Mag. **27**, (1914), 506.

P.R. Bolton, A. Badertscher, P.O. Egan, C.J. Gardner, M. Gladisch, V.W. Hughes, D.C. Lu, M. Ritter, and P.A. Souder, Phys. Rev. Lett., **47** (1981) 1441.

P.R. Bolton *et al.*, unpublished proceedings of the Ninth International Conference on Atomic Physics, (1984).

E. Borie, "The Anomalous Magnetic Moment of the Leptons: Theory and Status" in *Proceedings, Present Status and Aims of Quantum Electrodynamics*. (Mainz: 1980)

E. Borie, Phys. Rev. Lett. **47**, (1981) 568.

CAMAC Instrumentation and Interface Standards, (IEEE, 1982).

D.E. Casperson, T.W. Crane, V.W. Hughes, P.A. Souder, R.D. Stambaugli, P.A. Thompson, H. Orth, G. zu Putlitz, H.F. Kaspar, H.W. Reist, A.B. Denison, Phys. Lett., **59B** (1975) 397.

S. Chu and A.P. Mills, Phys. Rev. **148**, (1982) 1337.

W.E. Cleland, J.M. Bailey, M. Eckhause, V.W. Hughes, R. Prepost, J.E. Rothberg, and R.M. Mobley, Phys. Rev., **A5** (1972)

E. S. Dayhoff, S. Triebwasser, and W.E. Lamb Jr., Phys. Rev. **106**, (1953) 106.

P.A.M. Dirac, Proc. R. Soc. London Ser. A **114**, (1927) 243.

G.W.F. Drake, P.S. Farago and A. van Wijngaarden, Phys. Rev. **A11**, (1975) 1621.

G.W.F. Drake,"RELATIVISTIC AND QED EFFECTS IN HIGHLY IONIZED SYSTEMS" in *ATOMIC PHYSICS OF HIGHLY IONIZED ATOMS* , edited by Richard Marrus. (Plenum, 1983)

G.W. Erickson and D.R. Yennie, Annals of Physics **35**, (1965) 271.

G.W. Erickson, J. Phys. Chem. Ref. Data **6**, (1977) 831.

L.L. Foldy, Phys. Rev. **83**, (1951) 688.

C.A. Fry, J.B. Warren, R.F. Kiefl, C.J. Oram, G.A. Ludgate, P.W. Schmor, A. Olin, G.M. Marshall, B. Erickson, G. Morris, Hyp. Int., **17-19** (1984) 691.

T. Fulton and P.C. Martin, Phys. Rev. **99**, (1954) 811.

H. Grotch and D.R. Yennie, Rev. Mod. Phys. **41**, (1969) 350.

R. Karplus and N.M. Kroll, Phys. Rev. **77**, (1949) 536.

R. Karplus, A. Klein, and J. Schwinger, Phys. Rev. **84**, (1951a) 597.

R. Karplus, A. Klein, and J. Schwinger, Phys. Rev. **86**, (1951b) 288.

T. Kinoshita, B. Nizic, and Y. Okamoto, Phys. Rev. Lett., **32**

(1984) 717.

T. Kinoshita and J. Sapirstein, "New Developments in QED" in *ATOMIC PHYSICS 9*, editors: R. S. Van Dyck, Jr. and E. Norval Fortson, (Singapore: World Scientific Pub. Co., 1984).

Z. Koba, Prog. Theor. Phys. **4**, (1949) 319.

N.M. Kroll and W.E. Lamb, Jr., Phys. Rev. **75**, (1949) 388.

W.E. Lamb, Jr. and R.C. Retherford, Phys. Rev. **72**, (1947) 241.

W.E. Lamb, Jr. and R.C. Retherford, Phys. Rev. **75**, (1949) 1325.

W.E. Lamb, Jr. and R.C. Retherford, Phys. Rev. **79**, (1950) 549.

W.E. Lamb, Jr. and R.C. Retherford, Phys. Rev. **81**, (1951) 222.

W.E. Lamb, Jr. and R.C. Retherford, Phys. Rev. **86**, (1952) 1014.

B.E. Lautrup, A. Peterman, and E. de Rafael, Phys. Lett. **3C**, (1972) 193.

A.R. Lee, D.G. Williams and E.C. Butcher, Phys. Lett. **107A**, (1985) 218.

G.P. Lepage, D.R. Yennie and G.W. Erickson, Phys. Rev. Lett. **47**, (1981) 1680C.

S.R. Lundeen and F.M. Pipkin, Phys. Rev. Lett. **46**, (1981) 232.

G. Mezzorani, V. Pisano, P. Quarati, L. Sulis, and G. Puddu, Z. Phys. A **308**, (1982) 195.

T. Miles and A. Satanove, IEEE Trans. Nucl. Sci. **NS-30**, (1983) 3746.

E.A. Miller, private communication, (1980).

A.P. Mills, S. Berko, and K.F. Canter, Phys. Rev. Lett. **34**, (1975) 1541.

A.P. Mills, Jr., private communication (1984).

P.J. Mohr, Phys. Rev. Lett. **34**, (1975a) 1050.

P.J. Mohr,"The Lamb Shift in Hydrogen-like Ions" in *Beam-foil Spectroscopy: Volume I, Atomic Structure and*

Lifetimes, edited by I.A. Sellin and D.J. Pegg (New York: Plenum, 1975b).

C.J. Oram, J.B. Warren, J.H. Brewer, C.A. Fry, R.F. Kiefl, and G.M. Marshall, TRIUMF research proposal no. 181, (TRIUMF; Vancouver, 1981a).

C.J. Oram, J.B. Warren, G. Marshall, and J. Doornbus, Nucl. Instr. and Meth. **179**, (1981b) 95.

C.J. Oram, C.A. Fry, J.B. Warren, R.F. Kiefl, and J.H.Brewer, J. Phys **B14**, (1981c) L789.

C.J. Oram, J.M. Bailey, P.W. Schmor, C.A. Fry, R.F. Kiefl, J.B. Warren, G.M. Marshall, and A. Olin, Phys. Rev. Lett. **52**, (1984) 910.

D.A. Owen, Phys. Lett. **44B**, (1973) 199.

D.A. Owen, Phys. Rev. **29A**, (1984) 3411.

V.G. Pal'chikov, Y.L. Solokov and V.P. Yakovlev, JETP Lett. **38**, (1983) 418.

Particle Data Group, Rev. Mod. Phys. **56**, (1984) 1.

S. Pasternack, Phys. Rev. **54**, (1938) 1113.

F.M. Pipkin, private communication, (1982).

M.W. Ritter, P.O. Egan, V.W. Hughes and K.A. Woodle, Phys. Rev. **A30**, (1984) 1331.

E.E. Salpeter, Phys. Rev. **87**, (1952) 328.

E.E. Salpeter, Phys. Rev. **89**, (1953) 92.

J. Sapirstein, Phys. Rev. Lett. **47**, (1981) 1723.

E. Schrödinger, Annal. Phys. **79**, (1926) 489.

G.G. Simon, F. Borkowski, Ch. Schmitt and V.W. Walther, Z. Naturforsch. **35A**, (1980) 1.
G. Simon et al., Nuclear Physics **A333**, (1980) 381.

T. Suzuki, H. Namazue, and H. Hayakawa, Phys. Rev. Lett. **51**, (1983) 798.

D. Taqqu, *Phase Space Compression of Muon Beams*, SIN Internal Report TM-30-25, 1984.

M. Tinkham, *Group Theory and Quantum Mechanics*, (New York: McGraw Hill, 1964)

S.Triebwasser, E. S. Dayhoff and W. E. Lamb Jr., Phys. Rev.

89, (1953) 98.

E.A. Ühling, Phys. Rev. **48**, (1935) 55.

C. Varelas and J. Biersack, Nucl. Instr. and Meth. **79**, (1970) 213.

T. A. Welton, Phys. Rev. **74**, (1948) 1157.

E.H. Wichmann and N.M. Kroll, Phys. Rev. **101**, (1956) 843.

APPENDIX A: THE MAXIMUM LIKELIHOOD TECHNIQUE FOR A POISSON PROCESS

The counts observed at each data point follow a probability law. Let $P_i[x]$ be the probability of observing x counts at the ith point. If the process obeys Poisson statistics

$$P_i[x] = (\mu^x/x!)e^{-\mu} \qquad \ldots(A.1)$$

where μ is the mean number of counts observed, called the intensity of the process. If we have n datapoints, then the total probability of the experimental results is

$$P = \prod_{i=1}^{n} (\mu_i^{x_i}/x_i!)e^{-\mu_i} \qquad \ldots(A.2)$$

where μ_i may vary from point to point. One parameterizes the μ_i according to some theory to predict the values for each i as a function of the independent variables of the experiment. One varies the parameters until the set of values which maximizes the total probability P in equation A.2 is found. It is convenient for numerical reasons to minimize the quantity

$$-\ln P = -\sum_{i=1}^{n} \{x_i \ln\mu_i - \sum_{k=1}^{x_i} \ln k - \mu_i\} \qquad \ldots(A.3)$$

A change in -lnP of 0.5 from its minimum value by variation of the parameters corresponds to one standard deviation if one has an approximately Gaussian probability law, i.e. if the number of counts observed is greater than about 7 or 8 at each data point. More generally in this situation one has the relation that

$$-2 \ln P = \chi^2 + \text{constant} \qquad \ldots(A.4)$$

PUBLICATIONS

C.A. Fry, R.F. Kiefl, J.B. Warren, G.A. Ludgate, C.J. Oram, P.W. Schmor, G.M. Marshall and A. Olin, The Muonium Lamb Shift Experiment, presented at the Canadian Association of Physicists Congress, Victoria, (1983).

C.J. Oram, J.M. Bailey, P.W. Schmor, C.A. Fry, R.F. Kiefl, J.B. Warren, B.M. Marshall and A. Olin, Measurement of the Lamb Shift in Muonium, Physical Review Letters, 52 (1983) 910.

C.J. Oram et al., Measurement of the Lamb Shift in Muonium, published in the proceedings of PANIC (Particles and Nuclei-Tenth International Conference), Heidelberg, July 30-August 3, (1984).

C.A. Fry, G.A. Beer, G.R. Mason, R.M. Pearce, P.R. Poffenberger, and C.I. Sayre, Pionic X-rays from $^{12,13}C$, Nuclear Physics, A375 (1982) 325.

A. Olin et al., Strong Interaction Shifts and Widths in Pionic $^{10,11}B$ and $^{12,13}C$, Proceedings of the 8th ICOHEPANS, Vancouver, August 1979.

B.H. Olaniyi, G.A. Beer, C.A. Fry, J.A. MacDonald, G.R. Mason, A. Olin, R.M. Pearce and P.R. Poffenberger, Pionic KαX-ray Energy and Linewidth in ^{20}Ne and ^{22}Ne, Nuclear Physics, A384 (1982) 345.

C.J. Oram, C.A. Fry, J.B. Warren, R.F. Kiefl and J.H. Brewer, Observation of the 2S State of Muonium in a Vacuum, Journal of Physics B: Atomic and Molecular Physics, 14 (1981) L789.

C.A. Fry, J.B. Warren, R.F. Kiefl, C.J. Oram, G.A. Ludgate, P.W. Schmor A. Olin, G.M. Marshall, B. Erickson and G. Morris, Observation of Epithermal 2S Muonium, Hyperfine Interactions, 17-19 (1984) 691.